An investigation of the diffraction of detonation waves around single cylinders

by

Michel Kamel

A thesis submitted to the
Faculty of Graduate Studies and Research
in partial fulfillment of the requirements for the degree of
Master of Engineering

Department of Mechanical Engineering
McGill University
Montréal, Québec
June 1993

Abstract

An experimental and theoretical investigation of detonation diffraction around single cylinders is performed. Four cylinder diameters: 1", 1.25", 2.35", and 4", along with three different mixtures: stoichiometric, equimolar, and 40% argon diluted oxyacetylene, are used interchangeably. The initial pressure is varied from 20 to 90 torr in order to determine the critical parameters governing the diffraction pattern. Experiments are performed in a two dimensional rectangular channel with a test section 1085 mm long, 101 mm wide, and 25.4 mm thick. High speed framing Schlieren photographs of the diffraction phenomena are taken. Smoke foils are also used to provide a record of the change in cell size during the diffraction process. The distance of re-initiation behind the cylinder is found to be inversely proportional to the ratio of cylinder diameter to cell size, D/λ. Also, for low D/λ values, a region is formed in the cylinder's wake and prior to re-initiation where the cell structure fails. However, for large D/λ values, the diffraction has little effect on the cell structure.

Two mechanisms of re-initiation are observed. For low D/λ, re-initiation is triggered by the collision of transverse waves downstream the cylinder in the region where no cell structure exists. For high values of D/λ, re-initiation is a result of the transition from regular to strong reflection of the two diffracted waves colliding with each other downstream the cylinder. The diffraction pattern becomes independent of cell size.

In the theoretical investigation, the problem is divided into two cases: diffraction along the upstream half of the cylinder, and that along the downstream half. The first case deals with detonation propagation in converging channels and an approach similar to Whitham's can be used. The second case deals with detonation propagation in diverging channels, and a theory is developed based on Murray's equation relating velocity deficit to area increase between the shock and CJ plane. The theory is implemented in a computer code based on a code for shock wave propagation. The numerical results are good qualitatively, and have to verified experimentally.

Résumé

Une étude expérimentale et théorique de la diffraction d'une détonation autour d'un cylindre a été entreprise. Quatre cylindres de differents diamètres ont été utilisés (1",1.25",2.35", et 4"), ainsi que trois différents mélanges: oxyacétylène stoéchiométrique, équimolaire, et dilués à 40% d'argon. La pression initiale été variée de 20 à 90 torr, afin de déterminer les paramètres critiques qui gouvernent la diffraction. Les expériences ont été réalisées dans une chambre de combustion parallélipipédique (1085 mm de long, 101 mm de large, et 25.4 mm d'épaisseur). Des techniques de photographie par la méthode Schlieren, ainsi que des smoked foils ont été utilisés pour suivre le développement des cellules pendant la diffraction. La distance de réinitiation en aval du cylindre est inversement proportionelle à la valeur de D/λ, où D est le diamètre du cylindre et λ la largeur moyenne des cellules de détonation. Pour des valeurs de D/λ petites, une zone se forme en arrière du cylindre où les cellules n'existent pas. A l'oppose, pour les grandes valeurs de D/λ, la diffraction a un effet minime sur la forme des cellules.
Deux mécanismes de ré-initiation ont été ainsi observés. Pour des petites valeurs de D/λ, la re-initiation est amorcée lors de l'interaction des ondes transversales en aval du cylindre, dans la région où la forme cellulaire n'existe plus. Pour les grandes valeurs de D/λ, la ré-initiation est le résultat de la réflection régulière des deux parties de la détonation derrière le cylindre, générant une onde de réflection forte. La diffraction est alors indépendante des dimensions des cellules.

L'étude théorique comprenait deux parties: la diffraction le long de la face avant du cylindre, et celle de la face arrière. La première n'est en faite qu'un problème de détonation se propageant dans un canal à section décroissante, où la méthode de Whitham peut être utilisée. La seconde est le cas d'une détonation se propageant dans un canal à section croissante. Une théorie a été developpée à partir de l'équation de Murray qui lie le déficit de vitesse de détonation, à la différence d'aire entre le plan de l'onde de choc et celle du plan CJ. Cette théorie a été incorporée dans un programme d'informatique dérivant d'un code sur la propagation des ondes de choc. Les résultats numériques ont une valeur qualitative, et auront besoin d'être vérifiés avec d'autres expériences.

Acknowledgments

I am grateful to my supervisor Professor John Lee for offering me the opportunity of undertaking graduate studies with him, and for his support and invaluable guidance throughout the course of my work. I extend my sincere gratitude to Professor Rom Knystautas for his encouragement, and assistance in preparing the Schlieren set-up, and in various aspects of my experimental work. Special thanks are also due to Professor David Frost for his unselfishness in allowing me the use of his personal computational facilities.

I would also like to acknowledge Dr. D. Schwendeman for allowing me the use of his code. I am also indebted to Dr. Fan Zhang for his stimulating and enlightening discussions on the computational aspects of my work.

The assistance, encouragement, and friendship of the members of the Shock Wave Physics Group, during my stay at McGill, have proved to be indispensable and is gratefully acknowledged. Specifically, I would like to thank Dr. Olivier Peraldi for his patience and availability in recurring consultations, (future Dr.) Randy Chue for all his time spent introducing me to the world of UNIX and in solving computer related problems. Also, very special thanks go to Julian Lee for his devotion in helping me solve the problems related with the ignition systems, scopes, electronic circuits, etc. . Last but not least, my stay would not have been the same if it weren't for (another future Dr.) Aris Makris, his unique joyful character, help and support in all aspects of my work.

Finally, I would like to thank all my friends: Chiko, Ibrahim, Fadi N., Joseph, Alain, Fadi A-J, Ziad, and the others, whom by their numerous calls have made my long overnights spent at McGill seem short.

The greatest thanks are due to my parents, brothers, and family for their utmost support during all my years of existence, and to Marie-Gabrielle for having stood by me for the past three years.

Table Of Contents

List of Figures

Chapter 1
Introduction

The diffraction of a detonation wave is an important fundamental problem. For example, the critical tube diameter problem is essentially determined by the failure of the diffracted detonation to reinitiate upon exiting the tube. The detailed propagation of detonations in heterogeneous systems (i.e. porous media, detonation in obstacle filled tubes, detonation with particles and microballoon additives) are all centered on the fundamental problem of detonation diffraction around obstacles creating hot spots for reignition. Even in a normal cellular detonation, the mechanism of propagation is a continuous Mach interaction of the transverse waves with the leading shock front as in a diffraction process.

From a practical point of view, the detonation diffraction problem arises in the evaluation of the pressure loads on a structure from the interaction with a detonation wave. Thus in estimating risks in accidental vapor cloud explosions in the chemical and nuclear industry, detailed understanding and ability to obtain good quantitative prediction of the diffraction process is important. In hypersonic ramjet (detonation engines) the diffraction and reflection of detonation also arises in analyzing the geometry and detailed flow structure inside the engine.

The objective of this thesis is to investigate the diffraction of detonation waves around single cylinders, and to determine the critical parameters governing the diffraction

Among the earliest theoretical and experimental work done on diffraction of detonation waves was the study of R.S. Ong (1955), who investigated the interaction of planar CJ detonation waves incident on a wedge. Ong derived a method to determine the critical wedge angle which would give rise to a Mach reflection for an incident CJ detonation. His analysis is essentially identical to the Von Newman theory for Mach reflection of shock waves. As in the case of non-reacting shock waves, Ong found that there exists a unique angle of incidence beyond which regular reflections cannot occur, and Mach reflections take place.

Ong developed an approximate method of determining the configuration of the reflected shock wave. To do so, he transformed the problem from the physical plane to the pseudo-stationary plane, thus reducing the problem to a time independent boundary value problem. He used the independent variables x/t and y/t where x and y are rectangular Cartesian coordinates, and t is the time from the instant the detonation wave struck the corner.

Ong also did a series of experiments to check the validity of his theoretical analyses. Using Schlieren photography, he determined the critical wedge angle for a mixture of 50% by volume H_2-O_2 for initial pressures of 20 psia. He then varied the wedge angle from 0 to 30° and recorded the angle between the Mach triple-point trajectory and the horizontal. The experimental angle compared well (to within 1°) with the predicted theoretical value. Also the actual configuration of the reflected wave was very close to the calculated one for wedge angles less than 15 degrees. Ong proved that it is possible to determine an approximate configuration of the reflected shock wave, as well as the triple point trajectory of Mach reflections of CJ detonations. Ong's work showed that for sensitive mixtures, the diffraction of detonation waves can be successfully treated by assuming that the detonation is essentially a discontinuity. The effect of the complex three dimensional cellular structure of the detonation does not appear to influence the Mach reflection problem when the mixture is sensitive. It should be noted that in Ong's experiments, the initial pressure is high, and the H_2-O_2 mixture is also highly sensitive.

Diffractions of detonation waves were also studied by Bergeron (1978) who investigated the focusing of detonation waves in a convergent area channel. He applied Whitham's ray-shock theory for the propagation of non-reactive shock waves to describe the amplification of the detonation in the converging channel. Bergeron substituted Chester's equation relating the change in Mach number to a change in area of the shock front with a similar relation applicable to detonation waves, given by Lee and Lee (1965). As in Ong's study, Bergeron also modelled the detonation wave as a discontinuity, thus neglecting the complex 3-D structure of the detonation wave and its cellular structure. This is valid provided that the cell size of the detonation wave is much smaller than any characteristic length scale of the problem. In the limit of highly overdriven

detonation waves, the area Mach number relation for detonations approaches the one for shock waves.

Bergeron considered the cases of detonation amplification through conical sections of different overall area ratios, 64 and 144, and three different half-angles, 5,10,and 20°. In his theoretical analysis of the problem, he applied the 1-D CCW theory and the 2-D Whitham theory. To test his theoretical analyses, he carried out experiments using converging conical sections with the specifications as given above. Based on Whitham's ray-shock theory, he also designed an axisymmetric focusing channel in which an initially planar wave was made to converge without the formation of discontinuities in its front. He build the special wall-shaped channel with an inlet diameter of 5 cm and carried out experiments in it. In his experiments he used equimolar and stoichiometric oxyacetylene mixtures at initial pressures of 1 atm. The strength of the detonation was monitored by pressure transducers placed along the channel walls. The CCW theory turned out to apply very well to the convergence of detonations in conical channels of not too large vertex angles. Whitham's theory gave an accurate description of the qualitative behavior for a detonation wave in his conical sections. In the case of the special wall-shaped channel, the experimental pressure rise was also accurately described qualitatively by the ray-shock theory, although it was lower in magnitude than expected. The high pressure rise expected was to be due to the hot gases moving along the specially shaped wall behind the detonation. In these experiments, the pressure transducers were placed at the end of the special channel, where the high and low pressure gases have already mixed.The high pressure hot gases had a smaller mass in proportion to the lower pressure gases moving along the channel axis. Hence, their contribution to the total pressure registered by the transducers was diluted by the lower pressure gases along the axis which had not yet been affected by the area convergence. To avoid that problem, Bergeron suggested to experiment on a larger scale special wall-shaped channel.

Bergeron recommended that future work include working on a modified ray-shock theory which would use the three-shock theory to give a more accurate description of the shock-shock propagation. He also suggested the use of a specific heat more representative of the actual

situation, such as to take into account the change in specific heat due to the increase in Mach number, as was done by Russel D.A. (1967) for shock wave focusing.

A thorough experimental investigation on the diffraction of detonations at an abrupt area change was undertaken by Edwards et al. (1979) They aimed at obtaining a more detailed description of the mechanism of reinitiation at criticality. Using a fixed channel width, they varied the initial pressure of a stoichiometric oxyacetylene mixture and made detailed observations of the wave's reinitiation upon exiting the channel. They took Schlieren photographs of the diffraction process and used smoke foil records to monitor the change in cell size. Their findings confirmed previous observations of Mitrovanov and Soloukhin that the critical width of a flat channel is about ten times the initial cell size, for detonation waves in oxyacetylene mixtures. When the ratio of channel width to cell size is much higher than 10, the problem is in the supercritical case and there is continuous transition of the detonation from the confined to the unconfined area. For ratios less than ten, the wave is subcritical, and upon diffraction there is a complete separation between the shock and reaction zone all along the wave front. Shock and reaction zone separations were attributed mainly to the following two reasons. Firstly, the transverse waves moving through the head of the expansion do not meet an opposite family of transverse waves. Second, exothermic reactions behind the transverse shock cease to exist due to the weakening of the frontal shock by the expansion.

It should be noted that unlike the works of Ong and Bergeron, Edwards et al. deal with large initial cell size such that the detonation front cannot be considered a thin discontinuity. Even though they look at failure of detonation waves, their work sheds insight into the mechanism of propagation of detonation waves, which is useful for studies of detonation diffractions.

Based on Schelkin's instability criterion, Edwards et al. established that the onset of decoupling in a decaying wavefront should occur when $\Delta M_{CJ}/M_{CJ} \leq -0.1$. They expressed the criteria for criticality for reignition in a diffracted wavefront as $\partial M_S/\partial y_S \leq \Delta M_{CJ}/L_C$, where $L_C=1.67\lambda$ and used $0.1 \leq \Delta M_{CJ}/M_{CJ} \leq 0.2$. To find values for the gradient of Mach number along the vertical, $\partial M_S/\partial y_S$, they described the decoupled detonation wave there as a non-reactive shock

and used Whitham's theory to get the gradient's value. The agreement between the theoretical values for the distance of reinitiation and the experimental ones was judged very satisfactory.

A later study of detonation refraction by Thomas et al. (1985) investigated the parameters that control the transition of a detonation wave in 2-D diverging channels. Channels with two different aspect ratios were used (L/W=0.1, 11) and the divergence angle was varied from 0° to 90° for each channel. Their study demonstrated that a detonation requires an ever-increasing number of cells to propagate successfully from a straight channel into a diverging one, as the divergence angle increases. Their work also dealt with failure of detonation waves as they propagate through diverging channels. However, it showed that criticality conditions exist for detonation waves propagating in diverging channels, above which the detonation will transmit successfully without any decoupling along its front.

Gavrilenko and Prokhorov (1983) also studied overdriven detonations generated by the interaction of a detonation with a wedge in a flat channel, and a conical insert in a tube. They performed experiments with stoichiometric oxyacetylene and hydrogen-oxygen mixtures at initial pressures varying from 0.05 to 1 atm. The critical wedge angle for the mixtures used was found to be 40±1° for a wedge, and 45±1° for a cone. The maximum degree of overdrive of the Mach stem ($D_{Mach\ stem}/D_{CJ}$) was 1.3 in a flat channel at a wedge angle of 38°, as measured by streak photography. From the smoke foil records of their experiments, it was determined that the locus of triple points in the flat channel was not self-similar. The non self-similarity was attributed to the complex interaction between the large scale cells of the incident wave and the triple points. The degree of overdrive was related to the ratio of cell size of the overdriven wave over the cell size of the incident wave. Their experiments also showed that when the reflected Mach stem in turn underwent a Mach reflection, the resulting wave had a degree of overdrive between 1.5 and 1.7, and no observable cells.

Other relevant observations made by Gavrilenko and Prokhorov is that the smoke foil records of Mach reflections were identical when the cell size of the mixture used was the same. Also, the triple point trajectories for the same wedge angles when non-dimensionalized with the cell size of

the incident wave, were coincident with a roughness curve not exceeding the initial cell size. That observation was true for different mixtures and at different initial pressures. Finally, they also deduced that the initial cell size in these processes can be regarded as a scale which determines geometrical dimensions and other important characteristics. These observations are interesting to note so that it can be verified later whether they also apply for cases of detonation diffractions resulting in detonation waves travelling at less than CJ velocity.

Later, Bartlmä and Schröider (1986) made a study on the diffraction of planar CJ detonations at a convex corner. They used a channel with a 25x25 mm^2 cross-section before the convex corner, and a 25x100 mm^2 after the expansion, where the wall angle was varied from 15° to 135° in steps of 15°. Two gas mixtures were used, 8.1% propane-40.3% oxygen-51.6% argon, and 6.2% propane-31.2% oxygen-62.2% nitrogen, at initial pressures between 0.8 and 1.0 bar. They claimed that for the argon diluted mixture, the channel dimensions were well above the critical value (supercritical) while the nitrogen diluted one had certainly less than ten cells across the channel's cross-section. Single and multispark Schlieren photography was used to observe the detonation wave. It is important to note that no smoke foils were used to determine whether decoupling occurs or not, and to determine the number of cells across the channel. Schlieren photographs for wall angles of 30°, 90°, and 135° are presented in their paper for both mixtures. They claim that upon expansion, the detonation wave structure ceases to exist, and the reaction zone separates from the leading shock. However, from the pictures presented the supercritical mixture (argon diluted one) does not seem to decouple at an angle of 30°, while the decoupling along the wall is clear for the other cases of severe diffraction (90°,135°). The decoupling of detonation waves for nitrogen diluted mixture is not limited to the regions close to the walls. Furthermore, the nitrogen diluted mixture (subcritical) does not reinitiate behind the convex angle, while the argon diluted one always reinitiates.

These observations agree with the ones by Edwards et al. and Thomas et al.. They do indicate that Bartlmä and Schröider are indeed dealing with the cases of failing detonation waves, since in their experiments the severe diffraction leads to rapid decoupling of the detonation front (even for

supercritical waves). The nitrogen mixture is subcritical and therefore completely decouples upon exiting the channel at convex angles of 90° and more. The maximum divergence possible for successful transmission of the nitrogen diluted mixture can be approximately determined from Thomas et al., should the number of cells across the channel be known. This would be possible with the use of smoke foils. Hence Bartlmä and Schröider's experiments deal with the failure and reinitiation of detonation waves, rather than the diffraction process of detonation waves as discontinuities.

In the same study, Bartlmä and Schröider calculated the shape of a detonation wave diffracting at a convex corner. They assumed that since a detonation is decelerated upon diffraction, the reaction zone and shock front depart. Whitham's ray shock theory for non reacting shocks was thus used to determine the diffraction process of the decoupled detonation.

They ploted the non-dimensionalized (with respect to time) shape of the diffracting detonation's leading wave front obtained from the Schlieren photographs. The theoretical results for the inert shock and the experimentally observed decoupled detonation front for the 135° case, were superimposed and presented. They stated that the agreement between the two plots was fairly good, and that the shape of the decoupled detonation front was still self-similar. However, no self-similarity was found for the trailing reaction zone behind the shock front.

Upon analyses of the plots they presented, it can be noticed that the leading shock of the subcritical mixture where the whole wavefront decouples shows much better self-similarity than the supercritical one, where the decoupling occurs only very close to the convex wall only. The fact that the agreement between the inert shock and the detonation's leading shock is good, especially for the subcritical case, is an indication that when the leading shock is separated from the burning zone, it can be approximated as an inert shock wave. Hence their analyses applies for fully decoupled detonations, and not for the general case of detonation diffractions

In a later paper on 1-D detonation propagation in channels of varying cross-section, Bartlmä (1990) distinguished between the two cases of propagation in a converging channel, and

that in a diverging channel. For the converging channel, he modelled the detonation as a single front, and applied Whitham's theory to detonation propagation. Similar to Bergeron, he substituted Chester's relation with an area-Mach number relation applicable to detonations. He claimed that since the shock is dominant in a detonation, he expects equally good agreement between experiments and Whitham's theory for converging detonations as is the case for inert shocks.
For the diverging case, he suggested that the diminishing temperatures behind the weakening shock front causes a rapid increase in induction time, which eventually lead to the decoupling of the wave. He modeled the detonation in such cases as a shock front followed some induction time later by a reaction zone. When the post shock temperatures are lower than the self-ignition one, then the velocity of the reaction zone is governed by the laws of flame propagation. Based on his previous work (Bartlmä and Schröider), he declared that for detached reaction zones, the leading shock behaves as if the chemical reaction were not present. For 1-D shock propagation in diverging channels, he used Chisnell's formula to calculate the shock position at any time. Knowing the shock strength, he then calculated the post shock state and gas velocity. An empirical relation given by Burcat et al. is used to give the values of the induction time,τ, for the mixture in use. Knowing τ, the post shock state and gas velocity, the position of the burning zone is determined.

Again, Bartlmä's analyses of decelerated detonations only apply to cases where there is a rapid decoupling of the detonation wave. There exist many cases however, where detonations diffract in diverging channels or around obstacles without any decoupling. The detonation slows down and its curvature increases, but the shock and burning zone remain coupled. Such cases cannot be solved using Bartlmä's approximation.

More recently, Akbar and Shepherd (1993) investigated the use of Whitham's theory in the problem of a detonation interacting with a ramp. The angle of the trajectory of the triple point was obtained theoretically for various ramp angles, and were then compared to experimental results and showed poor agreement. The experiments were done with stoichiometric H_2-O_2 at initial pressures

of 200 mbar. The corresponding cell size was about 8 mm while the tube width was 76 mm. The poor agreement was stated to be partly due to the inaccuracy in the technique used to measure the triple point trajectory angle, i.e. large experimental errors. However, Akbar and Shepherd believed that the primary reason for the discrepancy was the effect of the transverse waves which contributed loss terms. They stated that the inclusion of the loss terms will modify the deviation of the area-Mach number relation for both Whitham's theory and the three-shock theory. It is important to note that their experiments used insensitive mixtures with large cell size. Whereas the approximation of detonation waves as discontinuities was judged satisfactory in the studies of Ong and Bergeron, it does not apply for Akbar and Shepherd. Ong and Bergeron had used sensitive mixtures at high initial pressures, resulting in a very small cell size for the incident wave. The experiments refered to by Akbar and Shepherd had a large cell size, comparable to the characteristic geometric dimensions of their problem, the tube width.

Therefore in the study of detonation diffractions it is important to distinguish two cases: diffractions leading to overdriven detonations, e.g., in converging channels, and those leading to attenuated detonations, e.g., diverging channels. The first case has received the most attention so far and has been successfully modelled using an approach similar to Witham's ray-shock theory. However, even in such cases the single front approximation seems to only hold true when the cell size is very small relative to relevant geometrical dimensions. Experiments with cell size of the order of the channel width do not agree with the theory (Akbar).

The case of a detonation wave in diverging channels is different since Witham's approach cannot be used. Some experimental work has been done on diffraction by wedges, but it appears that only one theoretical model has been presented so far, that by Bartlmä The applicability of the model is debatable, and it is believed that it is limited to cases of complete separation between shock and reaction zone. For cases close to criticality, it is believed that the cellular structure plays an important role. It would be very complicated to model such cases, since the model would have to account for the cellular structure of the wave front. Finally, for sub-critical cases, the separation of

the leading shock and chemical reaction zone occurs rapidly, and an approach similar to Bartlmä's may be justifiable.

Since most detonation diffraction problems treated previously dealt with diffraction by wedges and ramps, the diffraction by single cylinders is examined here. A series of experimental results is presented first, which leads to the establishment of the parameters which govern the diffraction of detonations around cylinders. Schlieren photographs of the diffraction process are necessary to visualize the diffraction pattern and the wave front shape at different times. Smoke foil records are also taken to determine the conditions below which the cellular structure ceases to exist behind the cylinder, thus implying the separation of the reaction zone from the leading shock. The experiments performed are diffraction around cylinders of different radii and around quarter cylinders. Initial pressures, and gas mixtures are varied to obtain different D/l ratios, where D stands for the cylinder's diameter. The experimental investigation leads to the understanding of the diffraction process and the reinitiation mechanism behind the cylinder. Also, a value for D/λ is established, beyond which the detonation wave behaves as a discontinuity.

In the theoretical investigation, it is revealed that two different approaches have to be used for detonation propagation along the upstream and downstream half of the cylinder. As the detonation diffracts along the upstream half, it experiences an area convergence until it reaches the vertical center line. For this case an approach based on Whitham's ray shock theory similar to that of Bartlmä and Akbar can be used. The detonation wave then goes through an expansion along the downstream half of the cylinder. A theory for 2-D detonation diffractions is then developped which again neglects the 3-D cellular structure of the detonation. The theory is based on velocity deficit theory of Fay (1959) and Murray (1984), where flow divergence between the shock and the reaction zone provides the mechanism for the deficit. A computer code for solving detonation propagation in diverging channels is then outlined. The code is based on Dr. D. Schwendamen's (1986) code for shock wave propagation.

Chapter 2:
Experimental Investigation

The aim of the experimental investigation is to investigate the mechanism of detonation wave diffraction around cylinders. The ratio of the cylinder's diameter over the cell size of the mixture used is varied, to determine the effects of the cell size on the diffraction process.

In the first part of the experimental investigation, Schlieren photographs of the diffraction process are taken. In the second part, smoke foil records are used. The tests using smoke foils are devided into two sets. The first set is for cases where the cylinder diameter is of the order of one cell size and less. The effect of the cylinder is expected to be very local to the cells involved. The second set is for D/λ values up to over 65. The diffraction pattern is observed, and the re-initiation distance of the diffracted wave downstream the cylinder is plotted for various D/λ values.

2.1 Experimental Set Up

The experiments are made in a two dimensional rectangular channel with a test section 1085 mm long, 101 mm wide, and 25.4 mm thick. The channel consists of a rectangular Aluminum piece with an empty core of the test section's dimensions. The central piece is bound by two rectangular optical quality glass enclosed in a metallic frame, acting as the channel's walls. Initiation of detonation is effected at one end of the channel by a high voltage discharge across two electrodes. Two 0.1 μf capacitors connected in parallel and charged to 32 KV are used as the high voltage source for the electrodes. The cylinders are installed between 600 and 800 mm from the ignition point, halfway between the side walls. A total of four cylinder diameters are used: 1",1.25",2.35", and 4". Three mixtures are used: 40% Argon diluted oxyacetylene, equimolar and stoichiometric oxyacetylene. A 75% Argon dilluted mixture with a 1/2" diameter cylinder is also used for some qualitative tests. The initial pressures used vary from 8 to 100 torr.

A Bar and Stroud high speed framing camera, running typically at 550,000 frames per second, is used to take Schlieren pictures of the diffraction process. The Schlieren system is of a double pass type. The light provided by a 2.5 KV Xenon flash tube is focused to a point at a distance of $2f$ from a concave mirror, where f=focal length of the mirror. That point then acts as a light source sending light through the test section, reflecting off the concave mirror, and back through the test section. The reflected rays are intercepted by a planar mirror which deflects them towards the objective of the Bar and Stroud camera. The rays converge to a plane, the cut-off plane, somewhere before the camera's objective. A sharp blade is installed at the cut-off plane to produce the Schlieren effect, and the light which bypasses the blade finally makes it to the objective.

Carbon foil traces of the diffraction pattern are also obtained by placing carbon foils around the cylinders before each test. The foils are made by depositing soot produced by an oil lamp onto acetates designed for laser printers. The traces are then printed and the pictures scanned onto a Macintosh computer. Using the *Enhance* software, the distance of reinitiation of the detonation behind the cylinder is accurately determined and the loci of the triple points behind the cylinder is reproduced.

Details of the experimental set up and the Schlieren system used are given in Appendix I.

2.2 Procedure Of Experiments

To verify the influence of initial cell size on the diffraction pattern, tests are made keeping initially the cylinder diameter fixed, and using one mixture at various initial pressures. The nominal cell size of the incident wave can be determined experimentally using the smoke foil records. For consistency however, the values of the nominal cell size λ for different mixtures and at different initial pressures are obtained from Knystaustas et al. (1982). Their values compare well with the average cell size obtained experimentally using smoke foils.

The use of smoke foil records is necessary to observe the change in cell size during the diffraction process, and whether the cellular structure ceases to exist. The distance of reinitiation

and the locus of triple points are accurately determined from these records. The second set of Loci of triple points can be traced off the records from the point of reinitiation until the cell size of the reinitiated wave becomes of the order of the incident wave's nominal cell size.

From an initial inspection of the problem, the critical parameters governing the diffraction pattern are believed to be the mixture's cell size λ, the cylinder diameter D, and the channel width. The channel width comes into effect when the channel walls are regarded as planes of symmetry. If any of the walls is replaced by such a plane, and another cylinder of same diameter is placed such that both cylinders are equidistant from the plane of symmetry, then the characteristics of the flow should not change. At the limit, the flow area between cylinders can be compared to a confined area, and the expansion which follows is compared to a transition to an unconfined area. The critical conditions for transition from a confined to an unconfined area for flat channels ($W/\lambda = 10$) will then apply to the problem. If P is the hypothetical transverse pitch between cylinders, then keeping $P/\lambda > 10$ should reduce the effect of the limited channel width on our problem. In fact, the values of P/λ in the experiments vary from a low of about 10 to a high of about 90. Further confidence in the reduced effect of the channel width in these experiments is acquired from the Schlieren photographs, where the wave close to the wall is noticed to remain straight.

Experiments are first done using a cylinder diameter of 1.25", and the three different mixtures. The 40% Argon diluted mixture is used at initial pressures of 30, 50, 70, and 90 torr to obtain low values of D/λ. The stoichiometric and equimolar mixtures are used at initial pressures of 30, 50, 90 and 20, 60, 70 torr respectively. The initial pressures are chosen such as to provide a range of values for D/λ for each mixture, as well as the same value of D/λ but for different mixtures. Different cylinder diameters are then used, namely 1" and 2.35", and the same procedure is repeated. Only stoichiometric and equimolar oxyacetylene mixtures are used for the 2.35" diameter cylinder, such as to obtain high values of D/λ. The choice of mixtures to be used is made based on the sensitivity and regularity of the mixture. Both stoichiometric and equimolar oxyacetylene are known to be highly sensitive and regular, allowing us to obtain very small cells at initial pressures not exceeding 100 torr. That limit of initial pressures is imposed by the glass

channel walls. These mixtures are also easy to detonate and the resulting wave is fully developed and planar by the time it reaches the cylinders. Moving the position of the cylinders from 600 to 800 mm from the point of initiation does not change the results obtained. The cellular pattern of the incident waves recorded on the smoke foils are identical in both cases, thus proving that the detonation is fully established at both locations. Schlieren photographs of the wavefront at 600 mm from initiation show a planar wavefront, further confirming our hypothesis that the detonation is fully developed and planar by the time it reaches the cylinder.

The cell size in the above tests ranges from about 0.8 mm for the stoichiometric mixture at 90 torr, to about 8.9 mm for the argon diluted mixture at 30 torr. The D/λ vary from 3.56 (Argon diluted at 30 torr) to 54.3 (equimolar, 70 torr, D=2.35"). Restrictions apply on the initial pressure allowed to be used in the channel, hence higher values of D/λ are obtained using a larger diameter cylinder. A cylinder of diameter 4" is used for that purpose. Since the channel width is 4", the full cylinder cannot be used. The cylinder is cut in two, and half of it is fixed flush onto the lower wall, which acts as a plane of symmetry. Values of D/λ as high as 127 are obtained by this method.

In the analyses of the smoke foil records of the above tests, the distance from the front end of the cylinder to the point of reinitiation downstream of the cylinder is denoted by S. Values for S are recorded for all the tests made. Since the values of S are measured quite accurately, they are used in the initial analysis of the smoke foil records. The trend in the variation of S with the variation of the initial parameters λ and D is observed. The results are presented in the next section. The locus of triple points of the reinitiated wave is also plotted for various tests. Schlieren photography is used to monitor the wave shape and any noticeable variation in the wave's thickness during the diffraction process, as well as to have an approximate measure of the wavefront velocities. Since this method is more expensive and time consuming than the use of smoke foils, it was used for selected test conditions only.

2.3 Experimental Results

The experimental observation consisted of two parts: In the first part, Schlieren photography is used to observe the diffraction process. Smoke foil records are then used in the second part, to observe the change in cell size of the diffracted wave, and accurately determine the distance of reinitiation of the wave behind the cylinder.

2.3.1 *Description of Schlieren photographs*

A very sensitive and regular mixture is used initially to provide a smooth and planar detonation wave. The initial pressure of the mixture was gradually lowered making the mixture less sensitive and increasing the cell size of the incident detonation. Figures 2.5 and 2.6 show framing Schlieren pictures of the detonation in stoichiometric oxyacetylene mixtures at two different initial pressures, as it diffracts around a cylinder of diameter 1 inch.

The initial pressure of the mixture in figure 2.5 is 90 torr, giving an initial cell size of 1.2mm. The interval between frames is about 1.82 μs. Frame 1 shows the planar incident detonation front when it has just impinged on the cylinder. In frame 3, the resulting bow shock is seen. The bow shock, which is a reflected shock wave, is strongest along the axis of the channel, where it is close in strength to a normal shock. The front stagnation point of the cylinder acts at the limit as a vertical wall to the local detonation front, hence the reflection is normal at that point. As the wave contours the cylinder, the reflection is at first regular as seen in frames 1 and 2. In frame 3, a small Mach stem is noticed, indicating that the reflection of the incident wave off the cylinder wall becomes a strong one somewhere between frames 2 and 3. Note that the flow is symmetric with respect to the channel axis. Other tests also show that for planar detonations, a Mach stem is generated between 45 and 55° from the forward stagnation point.

Frame 4 shows the Mach stem more clearly. The foot of the Mach stem along the cylinder wall is just beyond the 90° mark (the top of the cylinder). Consider the triple point configurations seen in

frame 4, they are the intersection of three waves: the Mach stem, the incident detonation wave, and the reflected shock wave. The Mach stem is in fact an overdriven detonation wave which is caused by the compression of the incident detonation by the front end of the cylinder. The wave front between the triple point and the channel wall is the part of the incident wave which remains unchanged, non of the disturbances from the cylinder having reached it yet. Finally, the reflected shock is an inert shock wave which propagates back into the detonation products. Up to that point the effects of the cylinder on the incident detonation are similar to that of a converging convex ramp.

In frame 5, the Mach stem is past the top of the cylinder, and the wave is now diffracting along the rear end of the cylinder. The Mach stem is now undergoing an expansion, thus its velocity is expected to drop. Frames 6 and 8 confirm our expectations. The foot of the Mach stem along the cylinder wall appears darker than the rest of the wave front. This increased darkness can be attributed to a slowing down of the local wavefront, and a thicker burning zone relative to the incident wavefront. Furthermore, the triple points can no longer be distinguished, indicating that their intensity decreased. Upon diffracting past the top of the cylinder, an expansion fan is generated. The part of the Mach stem between the cylinder wall and the expansion head is weakened by the expansion. The part between the expansion head and the triple point does not feel the expansion yet. The last part of the wave between the triple point and the channel wall is an unchanged segment of the incident wave. In frame 8 the diffracted waves along the cylinder wall are heading for a frontal collision with each other. Since both waves are perpendicular to the cylinder, and the flow is symmetric with respect to the channel axis, they should both get to the rear endpoint of the cylinder at the same time. Thus the two parts of the wave which will first meet will be parallel to each other, and a normal reflection should result.

This is seen in frames 9 and 10. The waves reflect off each other along the plane of symmetry of the flow. The plane of symmetry thus acts as a wall for each part of the wave. Inspection of the shape of the reflected shock in frame 10 reveals that it is almost horizontal close to the cylinder, and then curves towards the axis of symmetry to meet the reflection point. Thus the reflection is

initially a normal reflection which gradually becomes a regular reflection as the curved parts of the wave front collide with each other. Frames 12 and 13 show the regular reflection turning into a strong one with a new Mach stem generated. Two triple point configurations are thus generated on both sides of the plane of symmetry. The wave between the two triple points is an overdriven detonation wave which slowly spreads transversely into the diffracted wave front.

In frames 15 and 17, the overdriven detonation is seen propagating froward along with the whole wavefront. The fact that it does not speed ahead of the detonation, and it does not grow into it very fast, is an indication that the diffracted wavefront has not been weakened much by the diffraction. Note the beginning of the formation of vortices in the cylinder's wake, due to the flow of the detonation products around the cylinder.

In frames 19 and 21, the scenario is the same along the wavefront. However, it can be noticed that the part of the wave front between the two triple points is very planar, as opposed to the curved fronts of the diffracted wave. Also, the reflected bow shock has now reached the channel walls and the regular reflection of these shocks with the walls can be seen. Finally, the vortices are growing into a lambda shaped wave behind the cylinder.

Not much change is seen in Frame 27 with the planar reinitiated wave still slightly distinguishable from the rest of the wavefront. The lambda shaped wave behind the cylinder is now larger, and dark vortices still exist in the cylinder's wake. The symmetry of the flow with respect to the horizontal axis of the channel is nicely illustrated in this last picture.

For the test shown in figure 2.5, the ratio of cylinder diameter to cell size is larger than 21. The wave front appears as a smooth planar discontinuity and individual cells cannot be distinguished even in the diffracted wavefront. The whole process is identical to the one for inert shock waves described by Bryson and Gross (1961). They obtained the same loci of triple points, and same configuration of diffracted wave and reflected shocks.

An analogy can be made between the Mach reflection along the upstream half of the cylinder and the interaction of a planar wave with a wedge. As the angle between a planar wave

and a wall increases from zero, a critical angle is reached beyond which Mach reflection occur, as illustrated in figure 2.1.

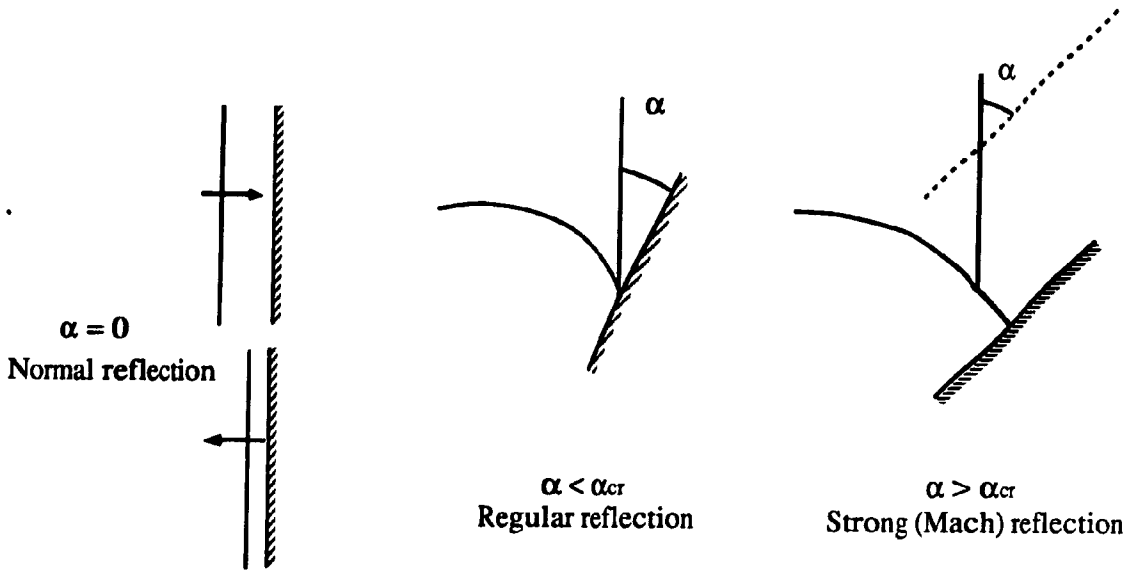

Figure 2.1. Transition from regular to strong reflection

The above is true for both shock waves and detonation waves. Recall from chapter 1 that R.S. Ong derived a method to determine the critical wedge angle for a 50% by volume H_2-O_2 mixture. Let ß denote the angle between the planar wave and the instantaneous tangent to the cylinder at the point of reflection, O (figure 2.2).

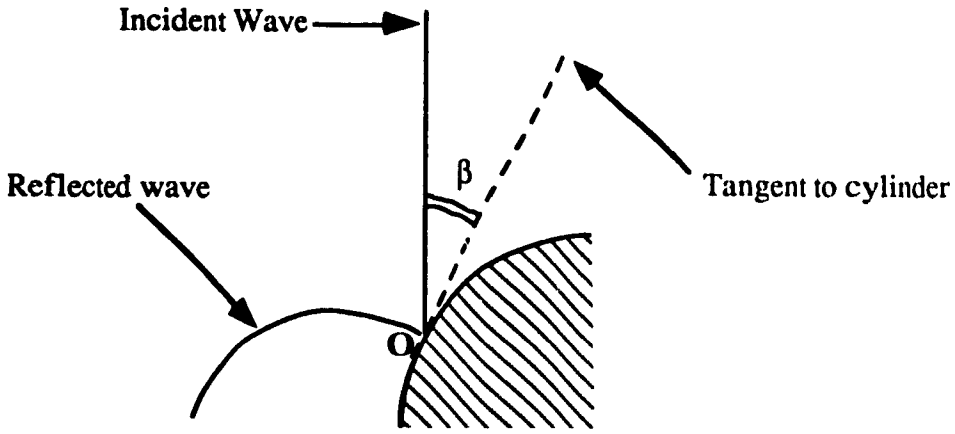

Figure 2.2. Reflection off the cylinder's upstream half

When a planar wave first impinges on a cylinder, $\beta = 0°$ and the reflection is normal. As the wave propagates along the cylinder's upstream half, the angle β increases until some critical angle β_{cr} beyond which Mach reflection occurs. Hence the analogy between β_{cr} and α_{cr} for wedges. A similar analogy can be made for the Mach reflection downstream of the cylinder.

Consider the diffracted wavefront downstream of the cylinder. The plane of symmetry of the flow acts as a solid wall for the wave on either side of it. Denote by θ the angle between the plane of symmetry and the instantaneous tangent to the diffracted wavefront at the point of reflection. Again, when the diffracted wavefront first reaches the plane of symmetry, $\theta = 0°$ and the reflection is normal.

As the wave propagates further downstream, the angle θ increases until it reaches a critical value θ_{cr}. Beyond that point, the reflection becomes a strong one, as seen in figure 2.3 For the cases of detonation waves, the above description holds true when the scale of the cellular structure is negligible relative to geometrical dimensions of the flow (high D/λ), as in figure 2.5. The detonation wave can then be approximated as a discontinuity and the diffraction pattern is governed by geometrical considerations. Whether this is true for cases of low D/λ is investigated next.

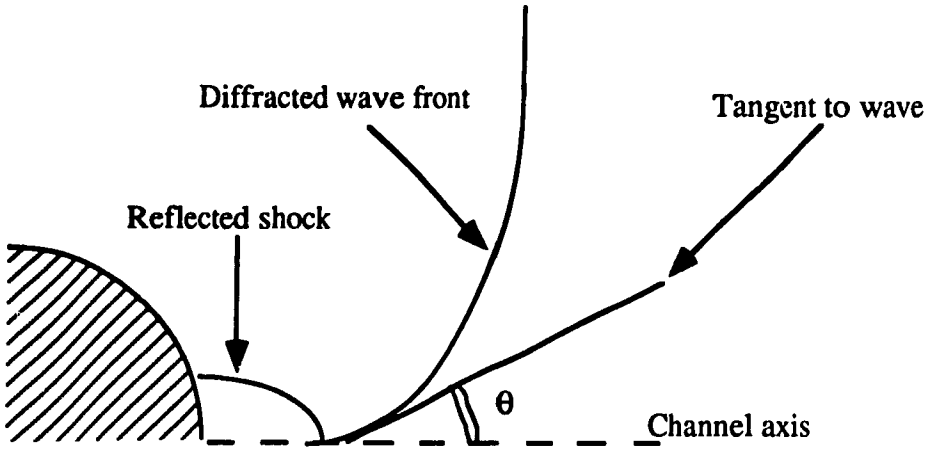

Regular reflection downstream the cylinder, $\theta < \theta_{cr}$

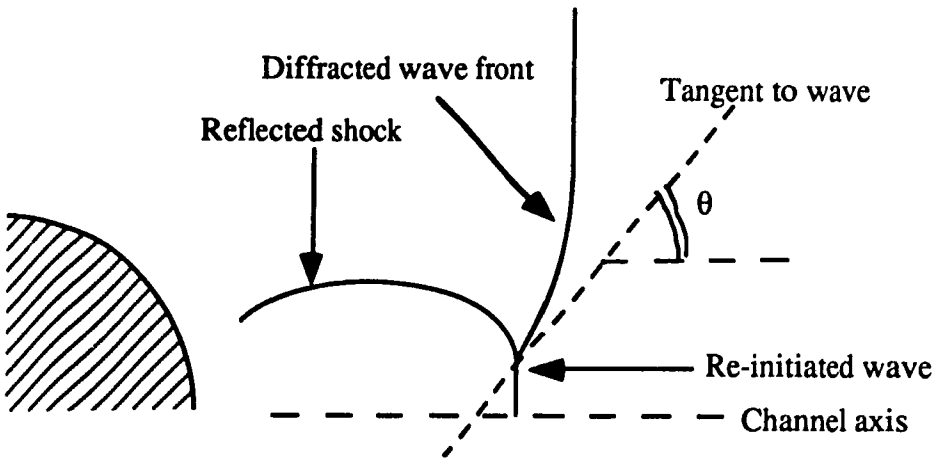

Mach reflection downstream the cylinder, $\theta > \theta_{cr}$

Figure 2.3. Reflection downstream of cylinder

As the initial pressure of the mixture is decreased, its sensitivity decreases and the nominal cell size of the incident wave increases, hence the D/λ ratio decreases.

Figure 2.6 shows a sequence of framing Shclieren photographs for a stoichiometric oxyacetylene mixture at an initial pressure of 10 torr. The corresponding nominal cell size is about 12 mm , yielding a D/λ ratio of about 2. The time interval between frames is about 3 μs.

The detonation front is first seen approaching the cylinder. It does not appear as a smooth planar discontinuity anymore. Rather, the wave front looks like a multitude of small wavelets cascaded on top of each other. Transverse waves can be seen as individual small extensions behind the wavefront.

The cylinder is indeed in the order of a few cells. In frame 11, the wave's reflection off the cylinder is again regular before it becomes a Mach reflection as shown in frame 12. However, The triple points are not very intense and fade away in frames 13 and 14. Frames 14 and 15 show the diffracted parts of the wave curving as it propagates past the cylinder. An interesting phenomena is observed in frames 15 and onwards. A local explosion is noticed in frame 15 at a distance of about half a cylinder diameter above the cylinder. The explosion itself could be due to the intersection of two transverse waves thus leading to the generation of a new cell. In frame 16, the new wavelet generated by the explosion has grown considerably and is expanding transversely into the rest of the wave. Note that the wavefront between that wavelet and the cylinder appears homogeneously thicker. That thick segment of the wave is probably so, because it has been weakened by the expansion, and no transverse cells are propagating along it. In frame 17, the wavelet is still expanding into the diffracted segment but it is now weakening. In frame 19, the transverse wave almost reached the axis of symmetry and in frame 21, the whole diffracted segment has been swept by the transverse wave. Other successive waves can be seen traveling transversely on the upper part of the wave. Note that no reflected shocks are noticed upon the collision of the two diffracted parts of the wave downstream the cylinder in frames 19 and 21. This is an indication that the leading shock has been weakened considerably by the diffraction. In frames 22 and 23, more transverse waves coming from the upper and lower parts of the wavefront collide around the

channel's axis. Between frames 22 and 23, an explosion occurs about that axis and a new wave is generated. In the next two frames, 24 and 25, the thin re-initiated wave is seen to grow rapidly into the thicker diffracted wave front and two transverse waves can be distinguished on each side of it. The spreading of that wave is not uniform, as seen in the subsequent pictures. By frame 30, the re-initiated wave has grown considerably and has taken over almost the whole wavefront. The newly initiated wave is much thinner than the previous one, indicating that it has a smaller induction length. Also in frame 23, at its point of re-initiation, the initiated wave lags a considerable distance behind the part of the wavefront along the wall. However, in frame 30 it has caught up with the wave along the wall and is bypassing it. Thus it has a higher speed than the wavefront along the wall which was originally at CJ velocity. Finally, looking at frame 30 it can be seen that the diffraction pattern although being qualitatively symmetrical with respect to the channel axis, it is not quantitatively so. In the lower part, the newly initiated wave has swept transversely to a scaled down distance of 1/2" from the channel wall. In the upper part it has expanded to about twice that distance from the lower channel wall.

It is believed that the transverse waves influence the diffraction process when the cylinder diameter is of the order of a few cell sizes. This is clearly demonstrated in figure 2.6, where the incident wave does not appear smooth and the resulting diffraction is not exactly symmetrical. Such is not the case in figure 2.5, where the cell size is much smaller than the cylinder diameter and thus does not influence the diffraction pattern.

Furthermore, the curvature of the diffracted wave behind the cylinder is much larger for the lower pressure wave indicating that it has been weakened more by the diffraction. The distance between the leading wavefront (along the channel walls) and the rear end of the cylinder at the time the two diffracted parts collide there is much larger for the case of $D/\lambda = 2$, than for the case $D/\lambda > 20$. This indicates that for lower D/λ values, the velocity of the diffracted part relative to that of the wavefront is smaller than in the case of the high D/λ value. Also the point of re-initiation behind the cylinder is farther downstream in the low D/λ case than in the higher one. The exact distance of re-initiation cannot be pinpointed accurately from these pictures, and smoke foil records are used

for that purpose. The analogy made earlier between the Mach reflection downstream of the cylinder and Mach reflections along wedges do not apply well for figure 2, where the re-initiation mechanisim might be different. When the scale of the cylinder diameter is of the order of cell size, the transverse waves affect the diffraction pattern. The re-initiation might be due to consecutive collisions of transverse waves along the axis rather than the transformation from regular to Mach reflection of the detonation front. The nonexistence, or at least the weakness of reflected shocks when the two diffracted parts meet might indicate the attenuation of the leading shock wave of the diffracted detonation. Hence the re-initiation might not be triggered by the reflection of the leading shock front of the diffracted waves, but rather by repetitive collisions of transverse waves along the channel axis. This can only be confirmed or denied by further investigation using smoke foil records.

Finally, it is noticed that once re-initiated, the new wave seems to be confined and does not spread much in the case of high D/λ values. As for the case of low D/λ, the re-initiated wave grows into almost the whole wavefront within the camera's field of view. The influence of the D/λ ratio is more apparent in the analyses of the smoke foil records which is presented next.

2.3.2 *Description Of Smoke Foil Records*

In this second part of the experimental investigation. experiments are made varying both the initial pressure of the mixture and the cylinder's diameter. Figures of the smoke foil records are divided in two sets. The first sets presents cases with D/λ values less or equal to one. The second set consists of figures for the cases of D/λ ranging from about 5 to more than 65. The effects of the cylinder are noticeably different in the two sets.

I) $D/\lambda \leq 1$

Figure 2.7 shows the smoke foil records of a detonation in a mixture of 75% argon diluted oxyacetylene mixture at an intial pressure of 50 torr, diffracting around a 1/2" cylinder. The cell size observed is about 14-16 mm, yielding a D/λ ratio slightly less than one. A weak expansion wave is noticed downstream the cylinder, and on both sides of it. In the region downstream of the cylinder, and for a distance of about three diameter lengths, no new cells are generated. However, cells originating along and upstream the expansion head send transverse waves propagating into that region from both sides (above and below) of the cylinder. The traces of these transverse waves are clearly noticed in figure 2.7. It is observed that the paths of the first of these transverse waves on both sides of the cylinder if extended will meet at a distance of about three cylinder diameters behind the cylinder's downstream stagnation point. The intersection of the transverse waves with each other create a local hot spot which re-initiates the combustion behind the diffracted wavefront at that point. From that point two traces are seen propagating forward and expanding transversely on both sides of the plane of symmetry. When these traces collide with traces of the transverse waves crossing the expansion head, a new explosion is set off, which in turn sends two traces forward in a similar horizontal V-shaped manner. Subsequently every time two traces collide with each other, another explosion is triggered. At a distance of about 9D behind the cylinder, what has started off as the initiation of one cell 6D lengths earlier, is now a well developed cellular pattern spreading across the channel's cross-section. All four tests made at the same initial pressure show a pattern similar to the one described above and shown in figure 2.7. However, the distance of re-initiation behind the cylinder varied randomly between 1D and 3D lengths. Figure 2.4 idealizes the mechanism of diffraction observed for $D/\lambda \approx 1$.

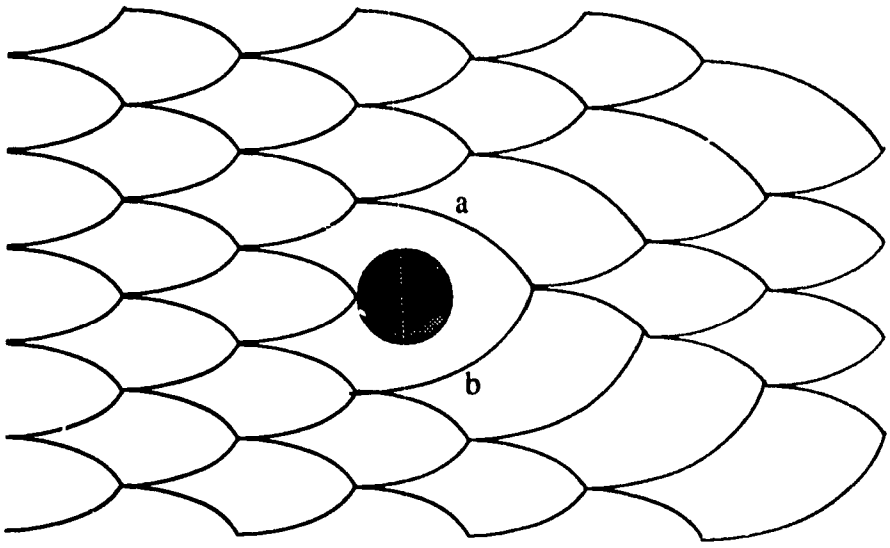

Figure 2.4. Ideal diffraction pattern for $D/\lambda \approx 1$.

The initiation of cells is due to the collision of two transverse waves with each other. Hence, the insertion of an obstacle of the order of one cell size blocks the path of the cell's transverse waves and prevents re-initiation, as illustrated in figure 2.4. The delay in the re-initiation of a cell affects the adjacent cells. The transverse waves a and b, seen in figure 2.4, now travel a longer distance unopposed until they collide with each other. Their collision creates a hot spot causing the initiation of a new cell.

So in the range of $D/\lambda \approx 1$, the cellular pattern does exhibit the characteristics of an expansion head generated on both sides of the cylinder, and a re-initiated wave downstream of the cylinder. However, these characteristics are not attributed to geometrical shock dynamics, but rather to the distortion of the cellular pattern of the wavefront. Also, the re-initiated wave has the features of one large cell which breaks up into a multitude of smaller cells upon successive collisions with transverse waves coming from the undisturbed part of the wavefront.

As is explained in the next section, when the D/λ ratio is increased, the diffraction pattern is governed more by the geometry of the flow and the process becomes almost independent of cell size. As the D/λ ratio is decreased below one, the effect of the cylinder on adjacent cells becomes

minimal. In the limit, only the individual cell is distorted, with adjacent cells suffering almost no deformation.

Figure 2.8 shows the smoke foil record of a test with 75% argon diluted oxyacetylene at an initial pressure of 30 torr. The corresponding D/λ ratio is about 1/2. The cylinder seems to have been inserted at the center of a cell. The cells just above and below the cylinder do not seem to be affected by the presence of the cylinder. Along the centerline, a new cell is initiated about 1D length downstream of the cylinder. The cellular structure resumes almost to normal from there on. This pattern is the same for all experiments made at that initial pressure. Again the distance of re-initiation of the cell is not exactly the same in all tests, but it does not exceed one cell's length behind the cylinder ($\approx$ 2D). This randomness is attributed to the fact that the cellular pattern just behind the cylinder is related to the stage at which the cell is in its development when it collides with the cylinder. Recall that in the cell size scale, the detonation wave appears like a pulsating front. It is the strongest at the initiation where it starts off with velocities of about 1.2Mcj and decays down to 0.8 Mcj at the end of the cell (Edwards et al),

Even lower D/λ ratios were attempted, but only for qualitative information. Figure 2.9 shows the smoke foil records of an experiment with the same mixture but at 20 torr. The cells are too large to be clearly distinguished within the channel width, but it appears that there are two cells across the channel width. The interesting observation made is that at about 0.4D downstream of the cylinder, a horizontal V shaped weak trace is noticed. It does not seem to be the initiation of a new cell, since these are more clearly marked further downstream of the cylinder. That V shaped trace is believed to be that of triple points along the front of an individual cell, which denote the onset of Mach reflection upon the diffraction of the cell's front around the cylinder. The hot spots created by these triple points are probably not strong enough to initiate a new cell and the Mach stem initiated just merges with the rest of the cell's front as noticed in figure 5.

The validity of this hypothesis has to be checked by building a larger channel and obtaining smoke foil records of experiments with $D/\lambda \leq 1/4$.

In summary, for cases where $D/\lambda \leq 1$, it has been shown above that the effect of the cylinder is limited to the local cells. The transverse waves of cells adjacent to the cylinder play an important part in the re-initiation of the wave downstream the cylinder. The re-initiated wave itself is nothing more than a new cell. Hence the continuity in the cellular structure is maintained. For $D/\lambda \approx 1$, the cylinder had a more pronounced effect on the cellular structure of the wavefront for more than five to six cell lengths downstream of the cylinder. That effect was the elongation of one row of cells on both sides of the line of symmetry. The cylinder in that case caused one cell cycle to be skipped as illustrated in figure 2.4.

II) $D/\lambda > 1$

In this part, the D/λ ratio is increased from about 4 to more than 65, and the change in the cellular pattern of the wavefront is described. Reference is made to the Schlieren pictures of figures 2.5 and 2.6, to interpret the traces obtained on the smoke foil records.

Figure 2.10 is a picture of the smoke foil record of a detonation diffracting around a 1.25" diameter cylinder. The mixture is 40% Argon diluted oxyacetylene at an initial pressure of 30 torr. The predicted value for D/λ is 3.6, however, the actual value in the experiments varied between 4 and 6. The initial set of triple points (seen in the Schlieren pictures of figures 1) originating between 45 and 55° from the forward stagnation point is not detectable in the figure. Recall that in figure 2.6, where $D/\lambda \approx 2$, the triple points are not distinguishable. As the detonation diffracts along the upstream half of the cylinder, no major change in the cellular structure is noticed. Beyond the top of the cylinder, the cellular structure ceases to exist and a line can be drawn downstream of which no cells exist. That line is the head of the expansion fan. Along the centerline behind the cylinder, a thick line is traced in the soot deposit. This line traces the path of the intersection of the diffracted waves behind the cylinder.

In the wake of the cylinder, no cells are noticed except for individual traces originating close to the expansion head on both sides of the cylinder. These traces are those of triple points, or transverse waves, which do not meet their opposite and hence propagate along the diffracted shock front.

Eventually they weaken out and fade away before they reach the centerline. At about 1 1/8" downstream of the cylinder, one of these traces reaches the centerline and detonation re-initiation occurs. The second locus of triple points seen in the Schlieren pictures can be clearly distinguished hereon. The trajectory traced by the triple points is not self-similar. Initially, no cells can be detected in the re-initiated wave, and the soot rather looks like it has been brushed. However, tiny cells progressively start appearing, and their size grows as the re-initiated wave propagates further downstream. Careful analyses of the transverse expansion of the re-initiated wave into the region where no cellular structure exists reveals the following. The divergence of the triple point trajectory on both sides of the axis of symmetry is increasing initially. However, every time a triple point trajectory meets a transverse wave coming from the wavefront along the channel wall, it is slightly deflected inwards towards the axis of symmetry. The triple point trajectory then diverges back out towards the channel wall until it collides with another transverse wave and is again pushed back slightly inwards. Since the distance between the successive unopposed transverse waves travelling from the region upstream the expansion head towards the centerline is large, the crookedness of the triple point trajectory is noticeable.

Further downstream of the channel, and in the region close to the walls, a cellular structure starts to appear. The cell size is however larger than the nominal one. This reappearance of a cellular structure in a region outside the boundary of the re-initiated wave, is attributed to mainly two reasons. Firstly, the expansion head is weakening allowing more of the unopposed transverse waves to pass through. Second, as the re-initiated wave propagates downstream it spreads more transversely and hence the transverse waves have to travel a shorter distance before reflecting off the triple points (i.e. the boundary of the re-initiated wave).

At the right end of the cylinder, the cells of the re-initiated wave have grown to about 50 to 60 % of their nominal size and the re-initiated wave occupies almost all the channel's cross-section. Also, note that the expansion heads and the trajectories of the triple points are not quantitatively symmetrical. This observation agrees with the one made upon analyses of the Schlieren pictures for low D/λ values (figure 2.6).

Figure 2.11 shows the smoke foil record of a detonation in an equi-molar oxyacetylene mixture with an initial pressure of 20 torr diffracting around a 1.25" diameter cylinder. The nominal cell size of the mixture at that pressure is 4.8 mm giving a D/λ ratio of about 7. Experimentally, that ratio varied between 8 and 10. Again a uniform cellular structure is noticed upstream of the cylinder. The first locus of triple points is still not detectable, and the expansion head can be distinguished for only a small distance behind the cylinder. Note that the expansion head does not reach the channel walls, as in figure 2.10, and the cellular structure ceases to exist only beyond about the 100° mark from the forward stagnation point. A first thick line is traced in the smoke foil from the expansion head and intersects the cylinder wall at about 170°. Another one is seen leaving the expansion head and colliding with the centerline behind the cylinder at about 1/4" from the cylinder's rear endpoint. These lines are the traces of the unopposed transverse waves originating in the unaffected detonation front and crossing the expansion head. Thinner, thus weaker waves, also extend from the expansion head but fade away before reaching the centerline. When a third wave traveling down from above the centerline collides with the centerline about 3/4" downstream of the cylinder, re-initiation occurs. The same pattern is observed as in figure 2.10, with no cells being distinguishable at re-initiation, and tiny cells starting to appear further downstream. Also note that the frequency of the successive transverse waves crossing the expansion head and reflecting off the re-initiated wave increases with increasing distance behind the cylinder. This is an indication that the expansion head is weakening. Note that the cell size of the initiated wave grows back to the nominal cell size and the cellular pattern of the re-initiated wave merges with the one of the wave along the wall. An inspection of the cellular structure at the right end of the picture does not indicate that any perturbations occurs to the flow.

In figure 2.12, the same mixture at the same initial pressure is used as in the previous figure, but a larger cylinder of diameter 2.35" is placed instead of the 1.25" one. The experimental value of D/λ is around 16, while it was predicted to be around 13. Upon inspection of the picture, it is noticed that the expansion head is very weak and only in the region close to the rear end of the cylinder is the cellular structure nonexistent. The cells along the cylinder wall gradually increase in size

beyond the 90° mark, until about the 130° mark where the last cell can be distinguished. Between 130° and 180° no cells exist and only two transverse waves reach the cylinder wall. Re-initiation occurs about 1" behind the cylinder. Note that on both sides of the re-initiated wave, the cells of the diffracted wave gradually reappear, and their size decreases back to the nominal value. At about 3 1/2" downstream of the cylinder, the re-initiated wave cannot be distinguished anymore from the rest of the wavefront, although the cell size is not uniform along the channel's cross-section at that distance. Around the centerline (or plane of symmetry) the cells are the smallest, but their is no distinct line separating the small cells of the re-initiated wave from the larger ones of the diffracted wave.

In figure 2.13 the same mixture is used but at a higher initial pressure of 60 torr and with the 1.25" diameter cylinder. The D/λ ratio is now more than 25. No expansion wave can be distinguished, and the cells along the cylinder's downstream half increase in size but never fail. Also note that the cellular structure of the diffracted wave along the centerline is almost back to its nominal size before re-initiation occurs.

The re-initiated wave is confined by the almost regular cellular structure of the diffracted wave, and does not expand much transversely. Beyond 3" downstream of the cylinder, the re-initiated wave is not distinguishable, and the cellular structure of the wavefront is homogeneous throughout the cross-section.

In figure 2.14, the equi-molar oxyacetylene mixture is at an initial pressure of 70 torr, and the 2.35" diameter is used. The D/λ ratio is thus more than 55. At that high D/λ value, the cellular structure throughout the process never fails. It just slightly increases in size along the cylinder's rear end. Along the plane of symmetry, the cellular structure always exist on both sides of it. Re-initiation nevertheless still occurs at about 1/2" downstream of the cylinder. The re-initiated wave seems to be confined to a very narrow strip on both sides of the plane of symmetry.

An interesting observation is made upon going to higher D/λ values. Figure 2.15 shows a stoichiometric oxyacetylene mixture at an initial pressure of 70 torr and a cylinder of 4" diameter is used. The resulting D/λ value is higher than 65. Because the channel width is only 4", half a

cylinder is used and fixed flush on a long thin plate with wedged ends. The flat plate is used to simulate a plane of symmetry instead of the channel wall itself, because the smoke foils could not be placed flush to the channel walls.

Beyond the 90° mark, the general pattern is the same as in figure 2.14. However, along the upstream half of the cylinder, the first locus of triple points can now be noticed. At about 45° from the forward stagnation point, the soot along the cylinder wall appears to have been brushed, and at about 55° tiny cells start to appear close to the cylinder wall. This pattern is a characteristic of overdriven detonations and is a consequence of the Mach reflection which arises as the detonation is converging along the upstream half of the cylinder. Hence, the behaviour of the detonation approaches more that of a discontinuity as the D/λ ratio is increased. Also note that the path traced by the locii of triple points of the reinitiated wave is now smooth and self-similar.

Some manipulations of the measurements obtained from the smoke foil records are given next.

2.4 Analyses of Results

In the analyses of the smoke foil records, S denotes the distance of reinitiation behind the cylinder. The value of S measured are plotted vs D/λ, since the ratio D/λ is believed to be a critical parameter. From the plot shown in figure 2.16a, separate point distributions are noticed. Each distribution corresponds to a different cylinder diameter. All set of points show the same trend, with the results scattered for low D/λ values, and better repeatability for high D/λ values. The values of S for each diameter value, seem to drop as D/λ increases, meaning the detonation is reinitiating closer to the cylinder. For D=2.35", S ranges between 75 and 84 mm for D/λ values of about 12, while S is about 73 mm for D/λ equal 54. The value of 73 mm is about 1.22 times the cylinder diameter. For D=1.25", S ranges between 45 and 55 mm for D/λ less than 10, and at D/λ equal to 40, the tests collapse at the value S=39mm. Note that 39mm is about 1.23 times the cylinder diameter. Based on these results an attempt is made to collapse the different set of points.

Since they are noticed to reach a terminal value of S/D about 1.22, the normalization of S with respect to D is made for all tests and S/D vs D/λ is plotted, the plot is shown in figure 2.16b. Both set of points do indeed collapse on each other. The values for S/D are very scattered for D/λ less than 20, where they get as high as about 2 for D/λ = 4. They tend to decrease and converge as D/λ is increased. For D/λ greater than 40, the values of S/D seem to reach an asymptotic value of S/D = 1.2 .

In another manipulation of the data at hand, the reinitiation distance S is normalized with respect to the cell size λ of the incident wave. The values of S/λ are then plotted versus D/λ and the plot is shown in figure 2.17a. All the test results collapse around one straight line, showing a linear relation between S/λ and D/λ. The linear relation is obvious, and the following equation is obtained:

$$S/D = 1.2 + 2.3\ \lambda/D\ .$$

This relation is in total agreement with the results of the plot of S/D vs D/λ, where it was noticed that S/D reaches an asymptotic value of 1.2 as D/λ > 40. From the above equation, it is noticed that as D/λ increases, i.e. λ/D decreases, the constant 1.2 becomes the dominant term in the relation.

The relevance of the cylinder diameter D is further illustrated in the plot of S/λ vs 1/λ presented in figure 2.17b. It is seen that if the cylinder diameter is kept constant, then the plot of S/λ vs 1/λ is still linear for each diameter value. The slopes of the lines are not the same however. The lines diverge as the values of λ decrease, and converge for large values of λ. Again this is to be expected based on the plot of figure 13a. The equation of that line can be rewritten as :

$$S/\lambda = (1.2D)*(1/\lambda) + 2.3\ .$$

Therefore when S/λ is plotted vs 1/λ the slope of each line would be 1.2D . For large values of λ, 1/λ is small and all curves get close to the value S/λ = 2.3. For small values of λ, then 1/λ is very large and (1.2D)*(1/λ) is the dominant term. Since the value of D is different , then the curves would diverge as λ decreases.

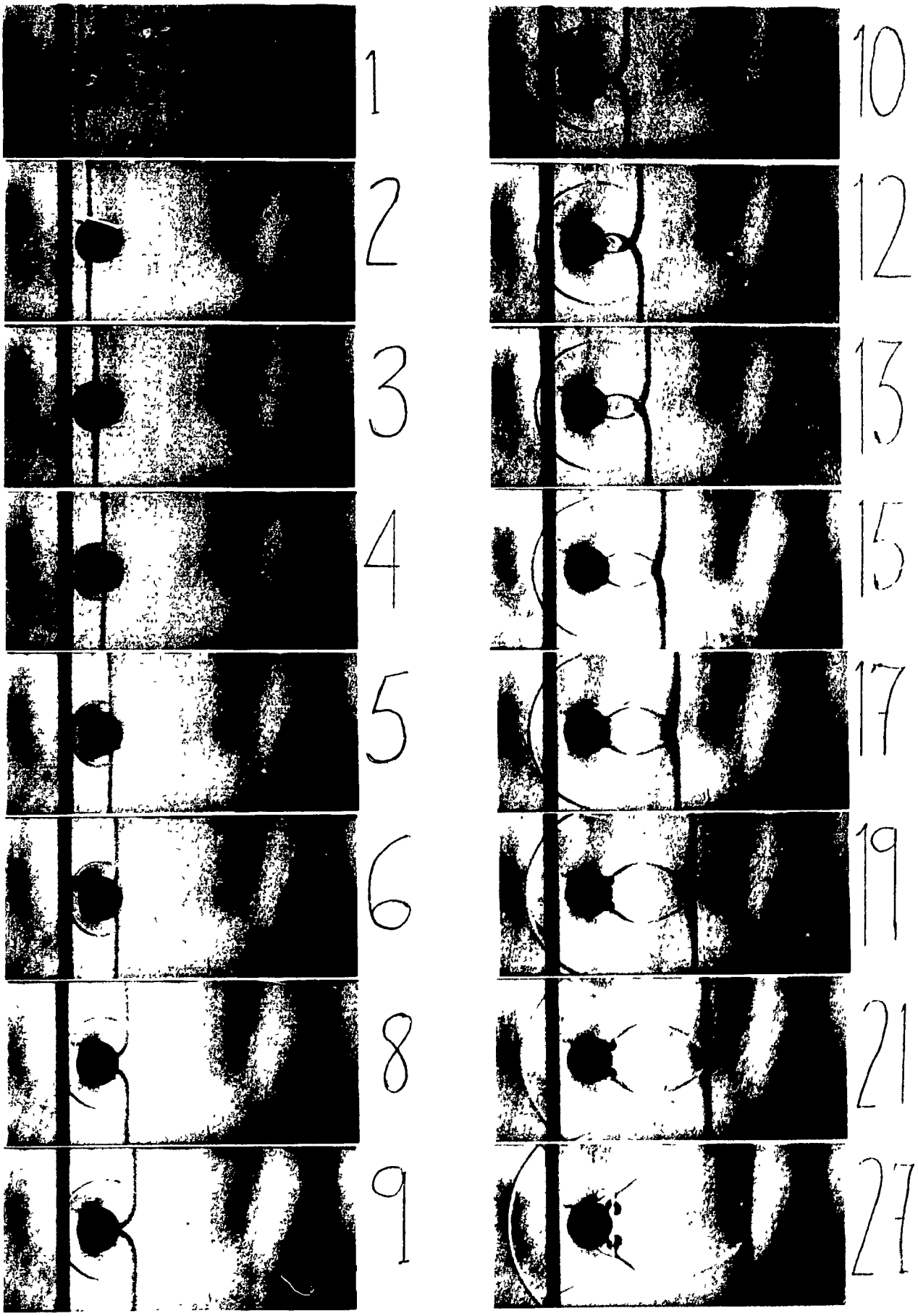

Figure 2.5. Stoich. C_2H_2-O_2, P_o = 90 torr, D=1", $D/\lambda \geq 20$, 1.82 μs between frames

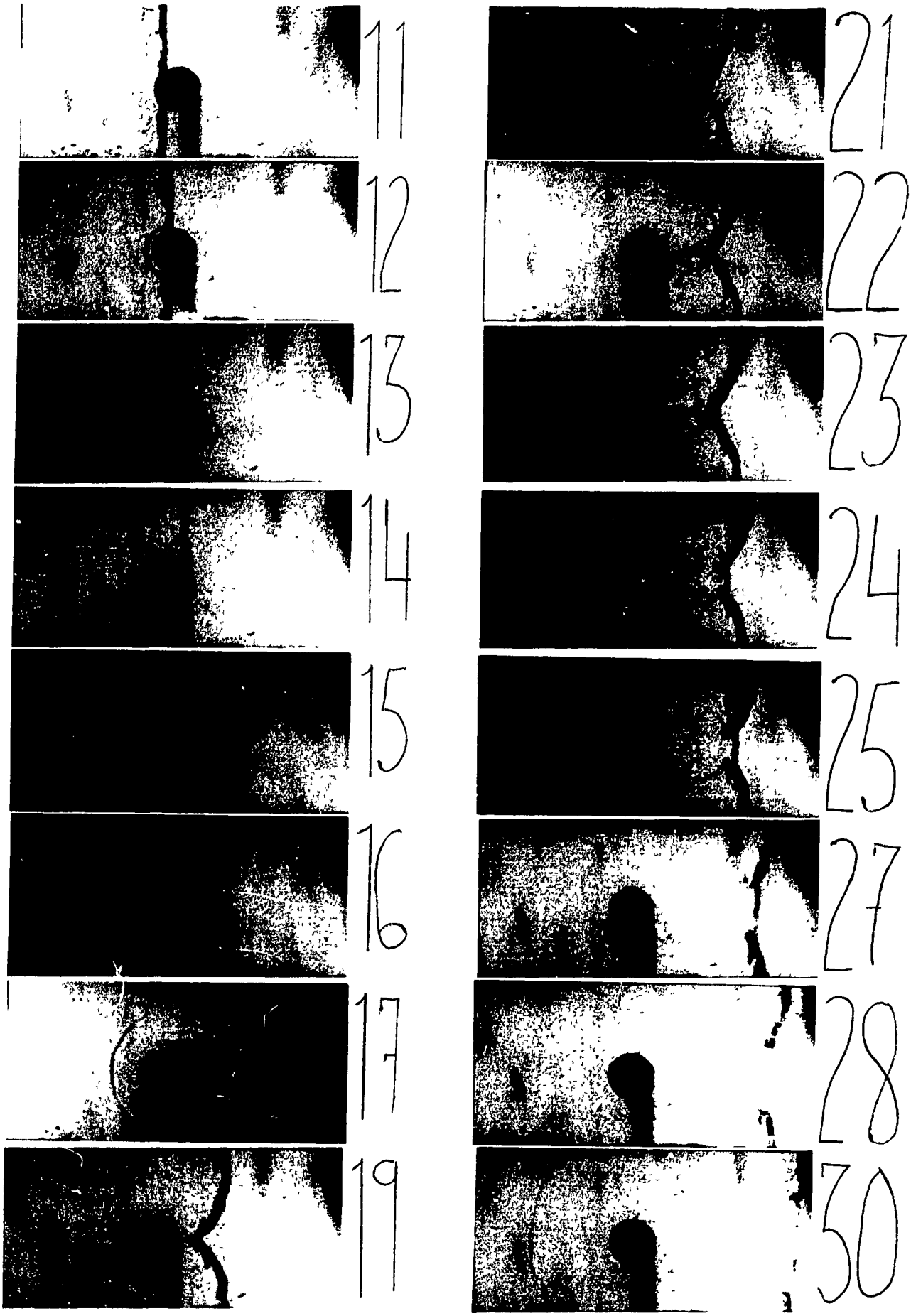

Figure 2.6. Stoich. C_2H_2-O_2, P_o = 10 torr, D=1", D/λ > 2, 3 μs between frames

Figure 2.7. Smoke foil record of $0.75Ar + 0.25(C_2H_2 + 2.5\ O_2)$, P_0= 50 torr, D=1/2 , $D/D_{CJ} \leq 1$

Figure 2.8. Smoke foil record of $0.75Ar + 0.25(C_2H_2 + 2.5\ O_2)$, P_O= 30 torr, D=1/2", $D/\lambda \approx 1/2$

Figure 2.9. Smoke foil record of $0.75Ar + 0.25(C_2H_2 + 2.5\ O_2)$, P_O= 20 torr, D=1/2"

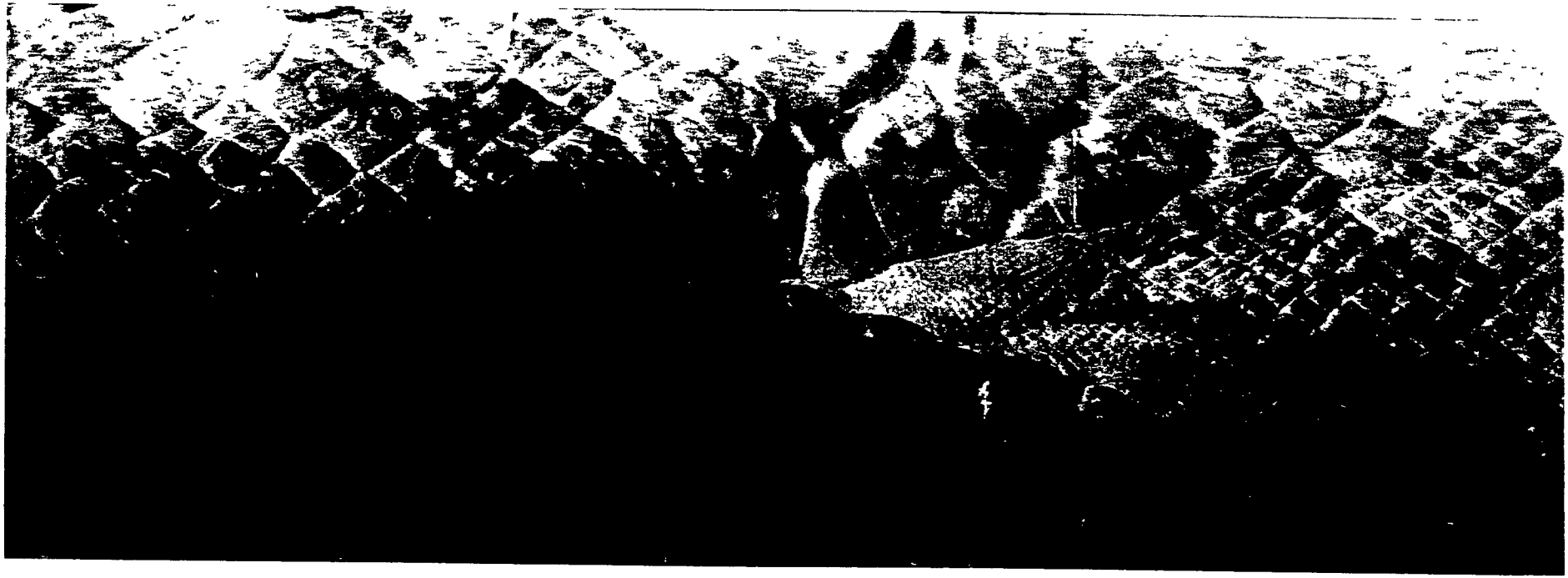

Figure 2.10. Smoke foil record of $0.4Ar + 0.6(C_2H_2 + 2.5\ O_2)$, P_O= 30 torr, D=1.25", $D/\lambda \approx$ 4-6

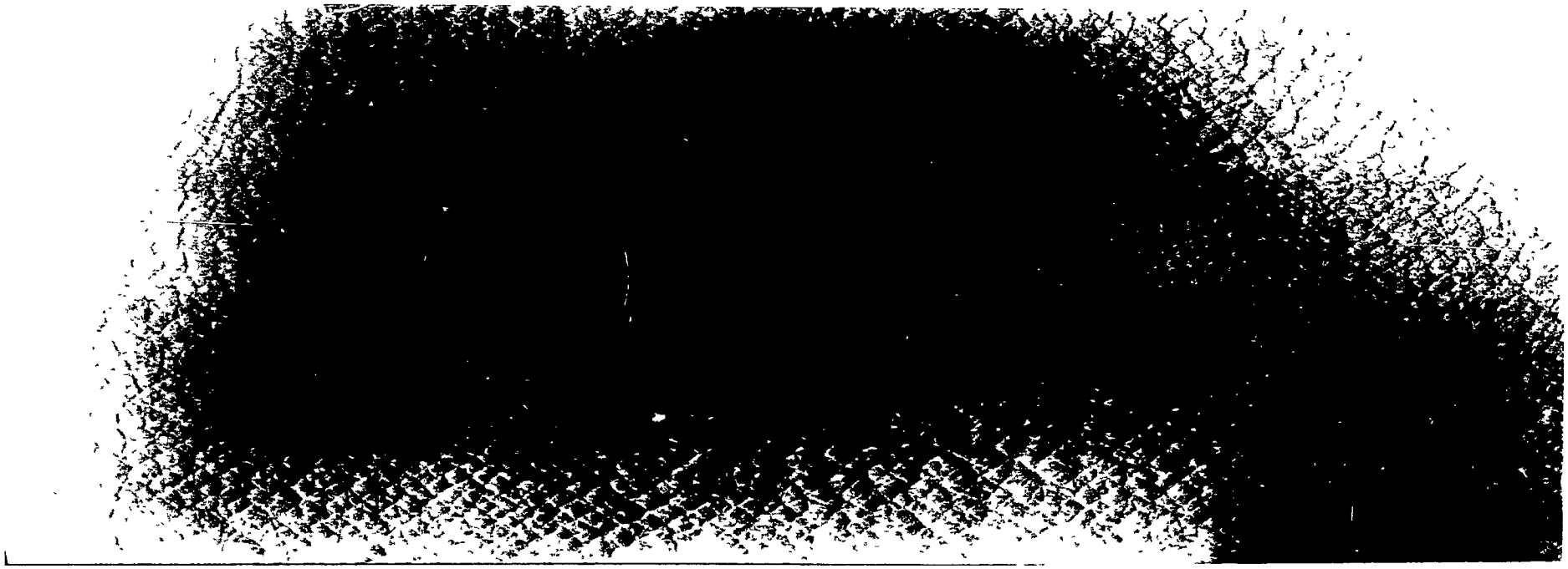

Figure 2.11. Smoke foil record of C_2H_2 - O_2, P_O= 20 torr, D=1.25", $D/\lambda \approx 8$-10

Figure 2.12. Smoke foil record of C_2H_2 - O_2, P_O= 20 torr, D=2.35", D/$\lambda \approx 16$

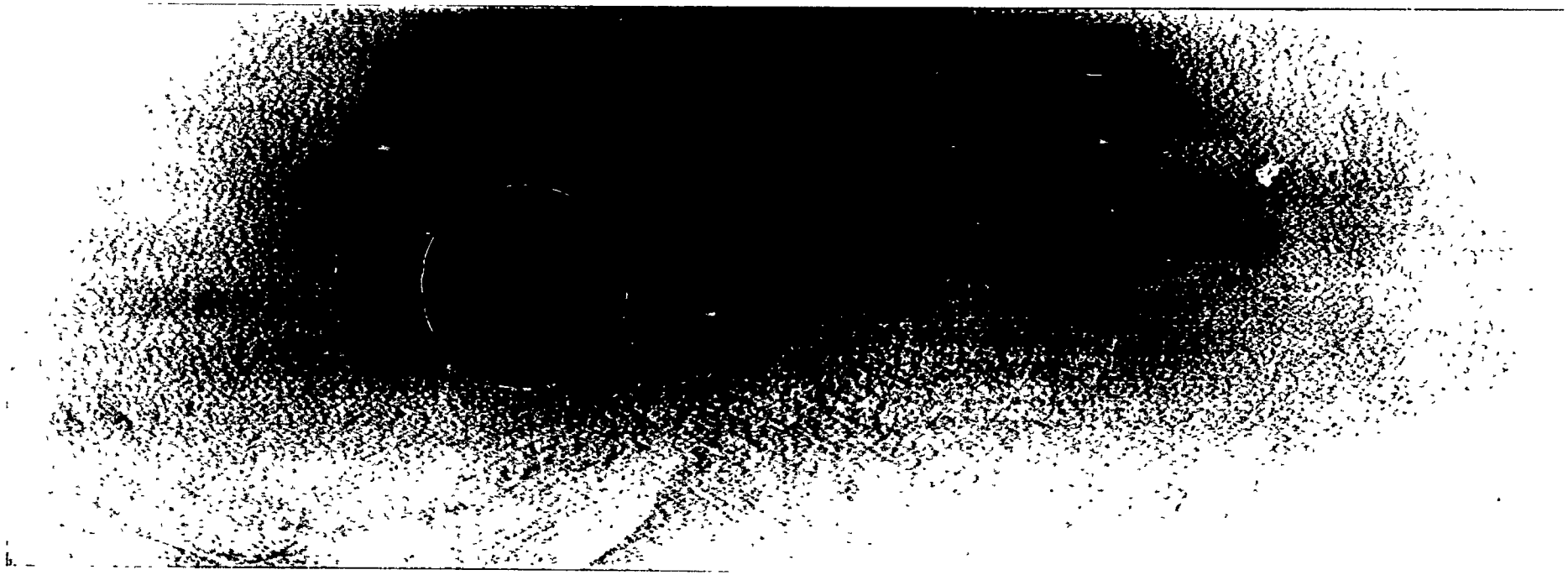

Figure 2.13. Smoke foil record of C_2H_2 - O_2, P_O= 60 torr, D=1.25", $D/\lambda \geq 25$

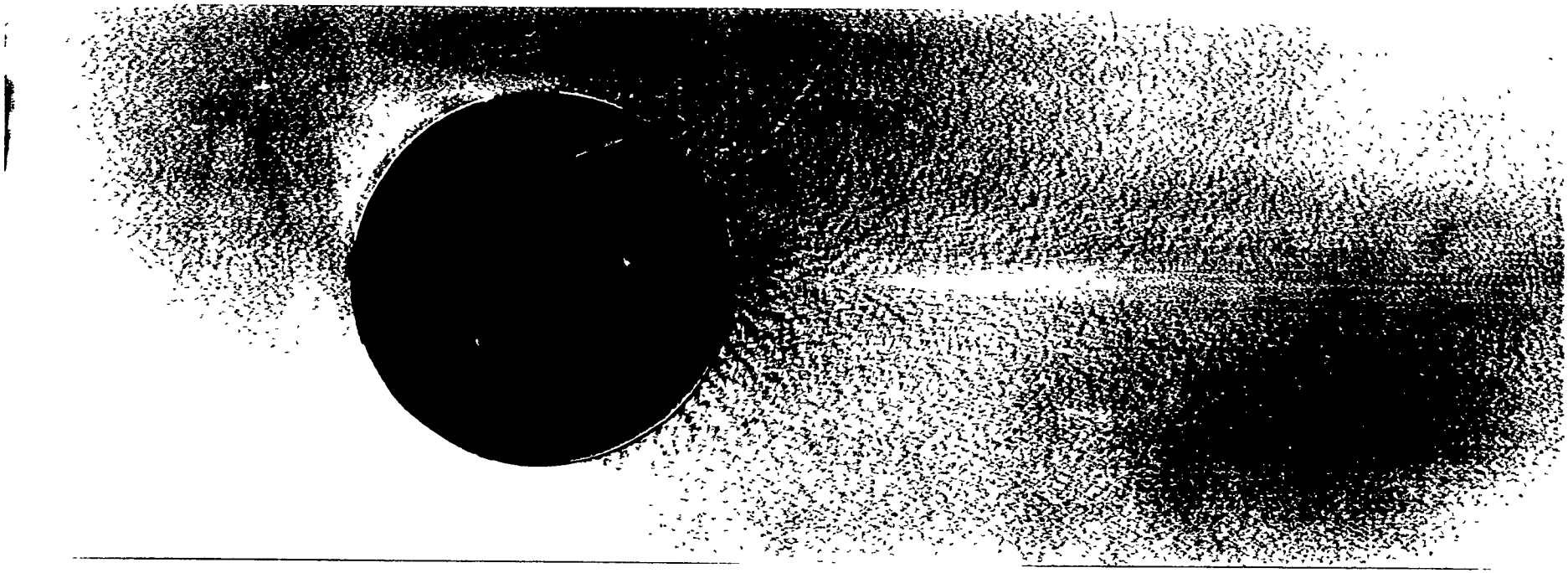

Figure 2.14. Smoke foil record of C_2H_2 - O_2, P_O= 70 torr, D=2.35", $D/\lambda \geq 55$

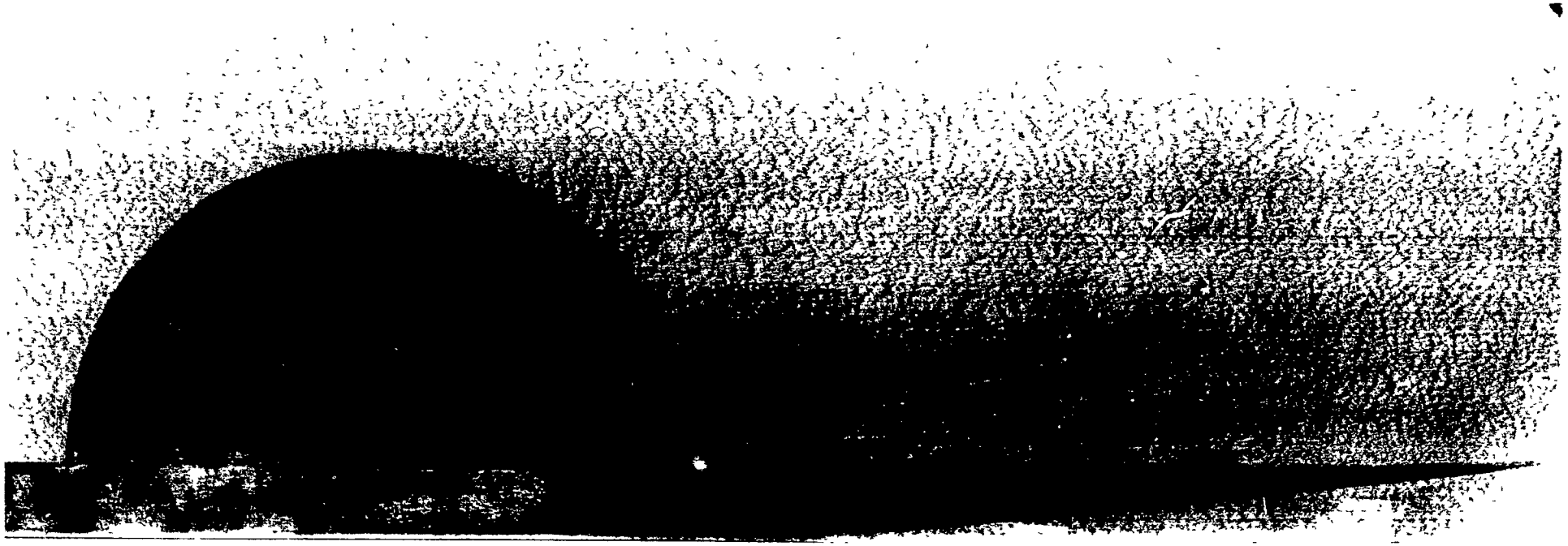

Figure 2.15. Smoke foil record of $C_2H_2 + 2.5O_2$, P_O= 70 торт. D=4". $D/\lambda \geq 65$

Figure 2.16a

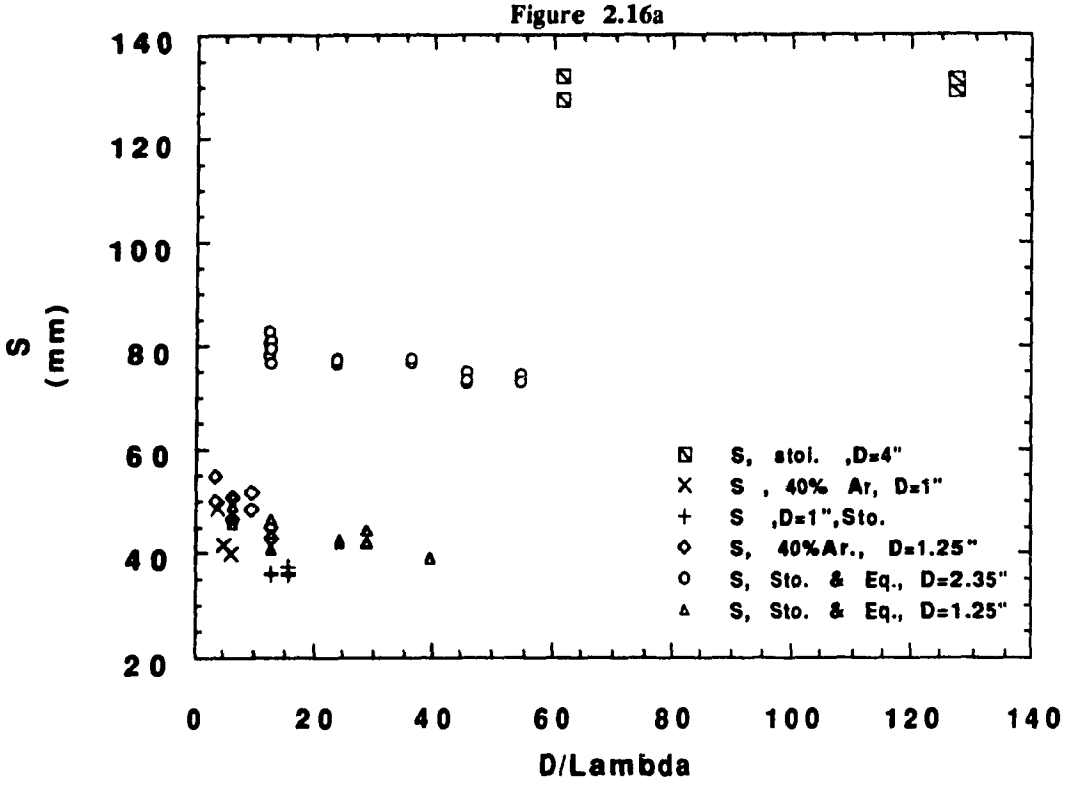

Figure 2.16b

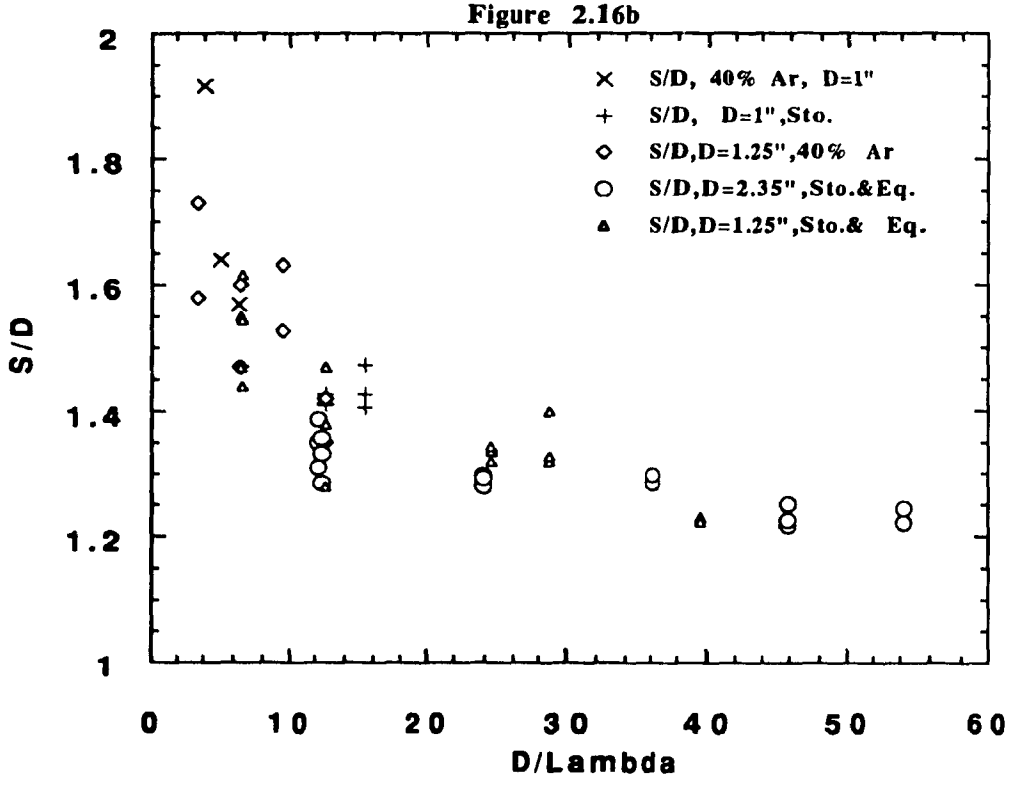

Figure 2.17a

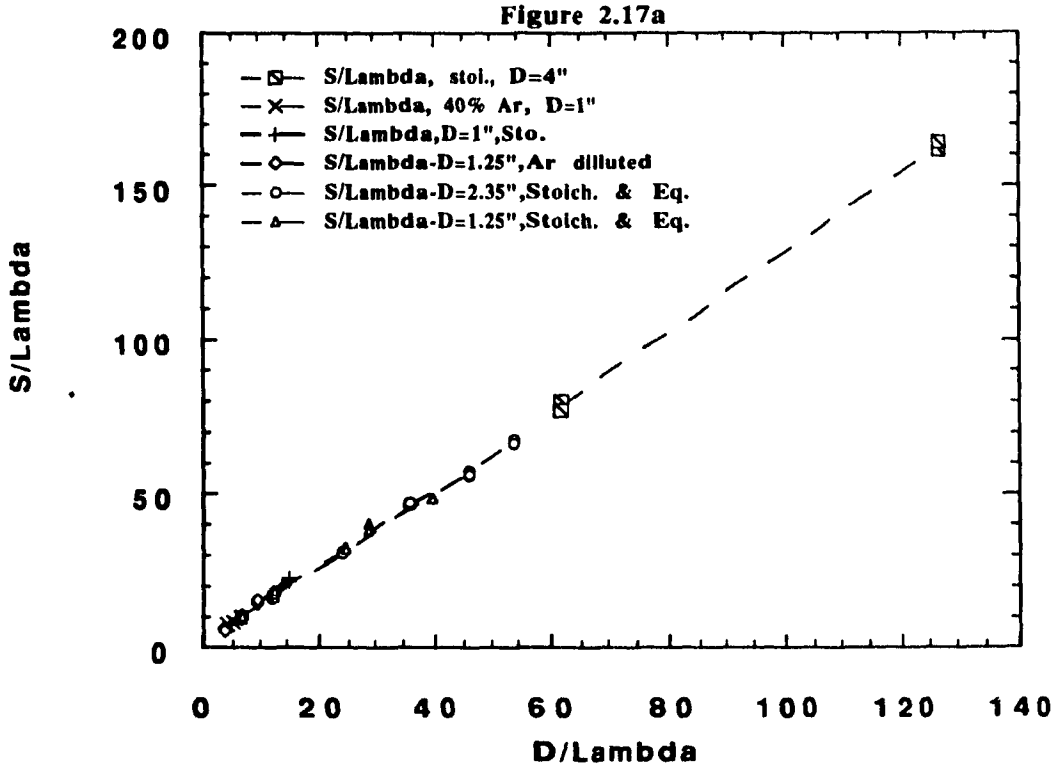

Figure 2.17b

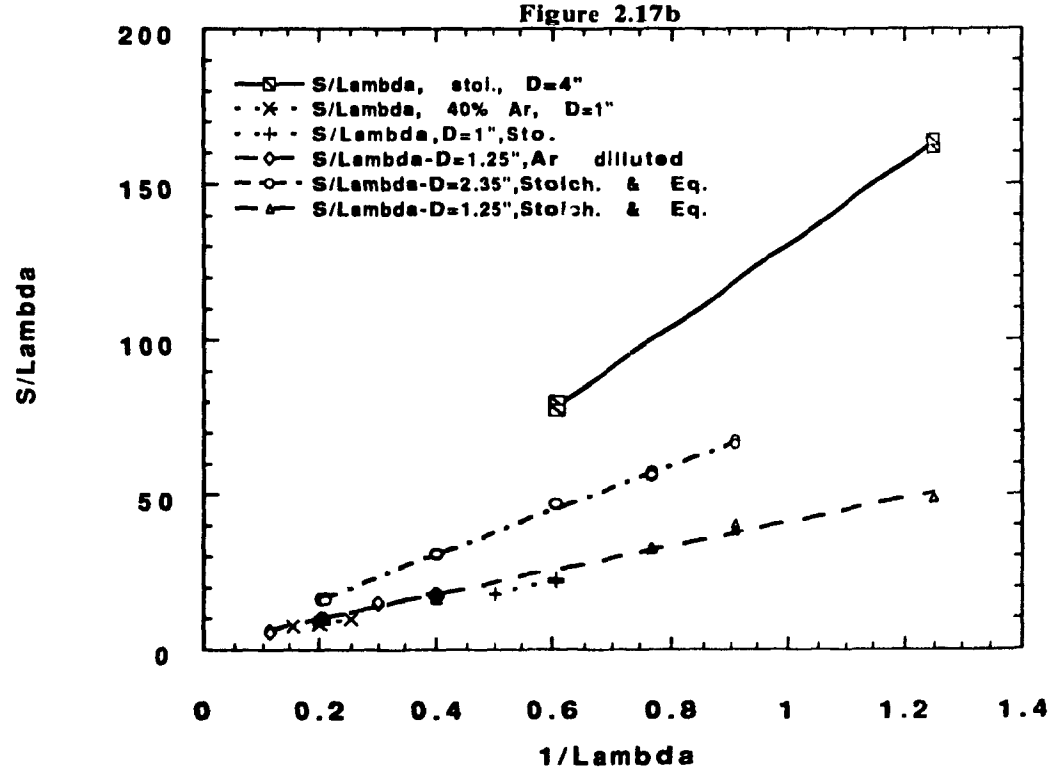

Chapter 3

Theoretical Investigation

The experimental investigation presented in chapter 2 has revealed that for high D/λ values, the cellular structure of the detonation does not influence much the diffraction process. The detonation front then behaves more like a discontinuity. In the theoretical investigation, a model is sought that can give good quantitative predictions about the diffraction process.

For the case of cylinders, two different approaches have to be used for the upstream and downstream half. Along the upstream half, the detonation undergoes a compression, and an approach based on Whitham's ray shock theory can be used. Past the upstream half, that approach cannot be used anymore. The area-Mach number relation used for overdriven detonations has an asymptote at $M=M_{CJ}$. Along the downstream half, the detonation wave is undergoing an expansion, and its velocity drops below M_{CJ}. Hence a new approach is needed to solve for attenuated waves. A two-front model for the propagation of two dimensional detonations in channels of diverging cross-sections is suggested. It is based on analyses by Fay and Murray on velocity deficit of detonations due to an area change between the shock and CJ plane. The model has been implemented in a computer code based on Dr. D. Schwendeman's code for shock wave diffractions.

The standard case of overdriven detonations is briefly described first, and its limitations are pointed out. A quasi one dimensional model for attenuated detonation waves is then presented. This one dimensional model is used as a building block for the modelling of 2-D detonations. The computer code is then presented, along with computer results for the diffraction past cylinders and wedges.

3.1 Theory for Accelerated Detonations

A detonation will tend to accelerate when it goes through a decreasing area change, such as along a wedge or a ramp, or down a converging channel. In previous studies for this case, an approach based on Whitham's ray shock theory has been used.

In his theory, Whitham (1957) defined a suitable set of orthogonal coordinates α & β , where α=constant represents the shock position and β=constant are rays orthogonal to the shock position. Whitham chose $\alpha=a_o t$, where a_o is the sound speed in the uniform gas ahead of the shock.

From geometrical considerations, he proved that

$$\frac{\delta\theta}{\delta\beta} = \frac{\delta A}{M\delta\alpha} \quad \text{and} \quad \frac{\delta\theta}{\delta\alpha} = \frac{-\delta M}{A\delta\beta}$$

if A = A(M) then

$$\frac{\delta\theta}{\delta\beta} - \frac{A'(M)}{M}\frac{\delta M}{\delta\alpha} = 0 \quad \text{and} \quad \frac{\delta\theta}{\delta\alpha} + \frac{1}{A(M)}\frac{\delta M}{\delta\beta} = 0$$

these equations are like the equations of non-linear sound waves and can be treated in the same way. Writing the above equations in characteristic form, Whitham obtained:

$$\left(\frac{\delta}{\delta\alpha} \pm c\frac{\delta}{\delta\beta}\right)\left(\theta \pm \omega(M)\right) = 0$$

where

$$c^2 = \frac{-M}{AA'} \quad , \quad \omega(M) = \int_1^M \frac{dM}{Ac}$$

which shows that $\theta \pm \omega(M)$ = constant on characteristics $c\pm$: $\delta\beta/\delta\alpha = \pm c$

The characteristics defined by $c \pm$ are curves on which information (θ and M) propagate along the shock.

For the relation A=A(M), Whitham used Chester's equation in its integrated form suggested by Chisnell for the motion of shocks in channels of slowly varying cross-sections.

In the application of Whitham's theory for detonations, it is enough to derive an area Mach number relation which holds true for detonations. Using the Chapman Jouget model for a detonation wave, the jump conditions for P, ρ, and u can be found across the discontinuity. The basic conservation equation across the detonation can be written in characteristic equations (similar to the shock wave case), where :

$$C+: \quad dP + \rho u a_2 du = -\rho_2 \frac{a_2^2 u_2}{(u_2 + a_2) A_0} dA + F(x - (u_2 + a_2))$$

F is an arbitrary function which can be set to zero without much error [10] . For M >>1, and a dimensional value of heat liberated per unit mass, Q, Bartlmä obtained the following expression:

$$\frac{dA}{A} = -H(M)dM \quad , \quad H(M) = \frac{1}{(\gamma_2 + 1)} \frac{\left(\frac{u}{c_0} + \frac{c}{c_0}\right)}{\frac{P u}{P c_0}} \left[M\left(1 + \Omega^{1/2}\right) + \frac{\rho c}{\rho_0 c_0} \right] \frac{(1 + \Omega)^{1/2}}{\Omega^{1/2}}$$

where

$$\Omega = 1 - 2\left[\frac{\gamma_2}{\gamma_1} + (\gamma_2 + 1)Q\right]\frac{1}{M^2} \quad , \quad Q = \left[\frac{\gamma_2 - 1}{\gamma_1 + 1}(1 + Q_0) - \frac{\gamma_2}{\gamma_1}\right] \quad , \quad Q = \frac{q}{C_{p_1} T_0}$$

and as $M \rightarrow M_{CJ}$, $\Omega \rightarrow 0$, $H(M) \rightarrow \infty$

Bartlmä's area-Mach number relation H(M), just as the ones used by Bergeron (1978) and Akbar (1991), has an asymptote at $M=M_{CJ}$, as seen in figure 3.1. Hence, it can only be used for overdriven detonations, and does not apply in situations where detonations waves are attenuated. Some other relation between the velocity deficit of a detonation wave (M goes below M_{CJ}) and area change (diverging area) has to be used.

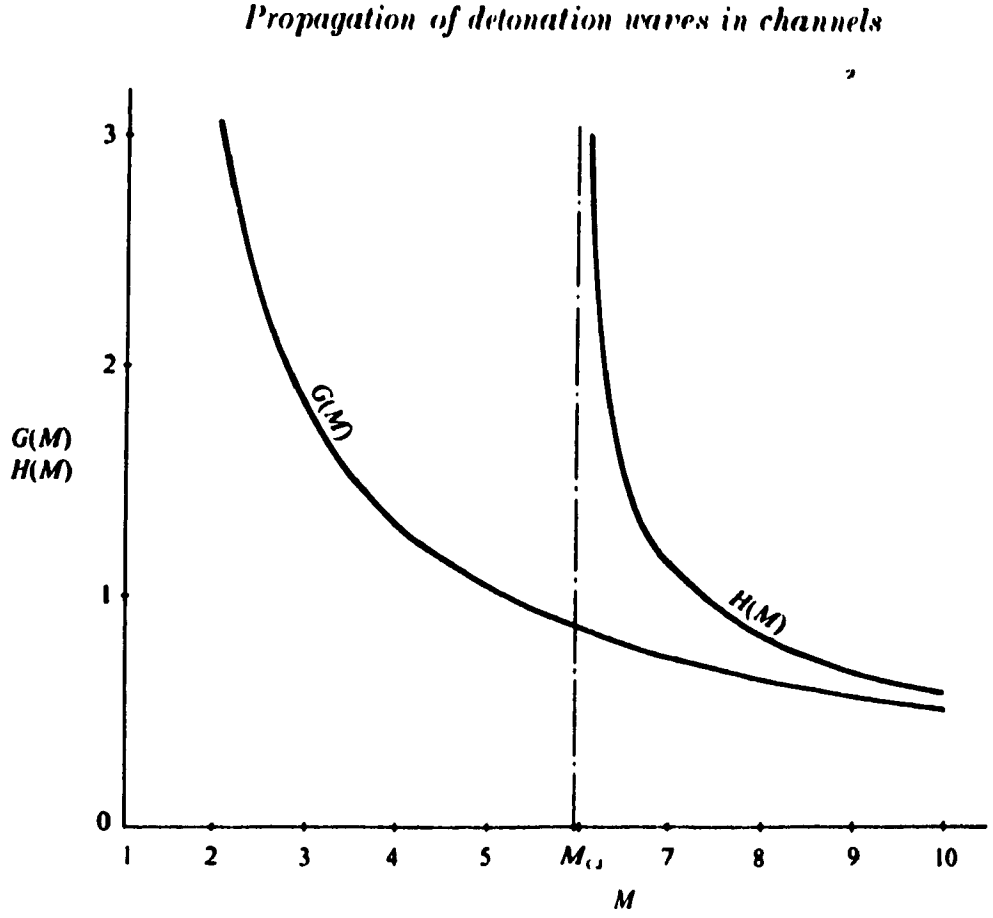

Figure 3.1. Area-Mach number plot for reactive , H(M), and non-reactive shocks, G(M). (Bartlmä 1990)

3.2 Detonations in Diverging Channels.

When a detonation propagates into a diverging area, the thickness of the detonation increases and the wave front decelerates. The increase in thickness is due to the fact that a weaker shock front results in lower post shock temperatures, hence a longer time for the compressed particles to ignite. In such cases, a single front model for decelerated detonations cannot be used anymore. Instead a two front model is used which takes into account the distance between the shock and CJ plane.

The question remains of how to relate the area change to the wave front's velocity in such cases. Bartlmä considered that for detonation waves where the chemical reaction zone is separated from the shock plane, then the shock propagates independently of that zone. This might be true, but only for decoupled detonations. Detonations are in many cases decelerated due to an area divergence, but without any decoupling occurring between the shock and burning plane.

The same two front model used by Bartlmä (1990) is used again here but with the shock and reaction zone remaining coupled. Eventually, as the induction time increases, decoupling might occur and the leading shock will propagate as an independent shock.

3.2.1 *1-D Detonation Diffraction*

As a building block for further 2-D analyses of the problem, consider a quasi-one dimensional case of a detonation propagating in a channel with an infinitesimally small divergence, An equation is sought which relates the change in area dA to the wave's Mach number M_1, similar to Chester's equation for inert shocks. Reference is made to the works of Fay and Murray, on a similar problem.

Fay related the flow divergence due to negative boundary layer displacement within the reaction zone to account for the velocity deficit of a detonation wave propagating in a tube. In a fixed shock coordinate system, the wall has a constant velocity U_1 equal to the velocity of the

unburned gas upstream of the shock, figure 3.2. The partially reacted gas in the combustion zone would have a lesser velocity because of its increased density. Hence, downstream of the shock, the tube wall has a velocity higher than that of the bulk of the gas. Because of its higher velocity, the fluid in the boundary layer seems to have a greater mass flow per unit area than that in the main stream, and it thus appears to the main flow that some fluid is 'leaking' through the wall, or that the wall has an enlarged cross section.

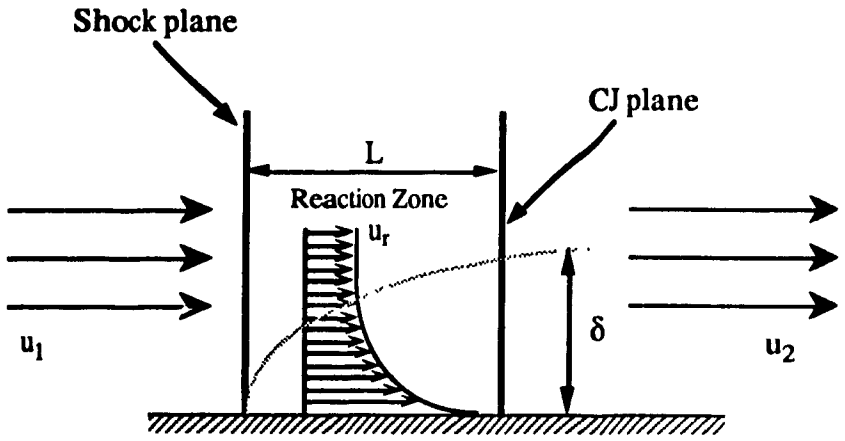

Figure 3.2. Boundary layer and velocity distribution in reaction zone

Fay denoted by ξ the fractional increase in area of the tube. He incorporated the ξ in the differential equations of continuity, momentum, and energy. He then integrated and solved these equations numerically to obtain an explicit expression for velocity deficit in terms of ξ : $\Delta U_1/U_1 = 0.53\,\varepsilon\xi$ for $\xi << 1$ where $1 < \varepsilon < 2$. ξ was related to the displacement thickness δ^* through the expression : $\xi = 4\delta^*/D$, where δ^* is the displacement thickness evaluated at the CJ plane. To determine δ^* at the CJ plane, the position of that plane had to be determined first.

In doing so, Fay considered a case where only one reaction coordinate (α) is needed to describe the reaction composition of the reacting gases. Values of α would be such that it is zero for

unreacted mixtures, and 1 for completely reacted ones (at CJ plane). The enthalpy of the gas would then be a function of pressure, density, and α:

$h=h(p,\rho,\alpha)$. Expressing the enthalpy in differential form he obtained:

$$dh = \left(\frac{\partial h}{\partial p}\right)_{\rho,\alpha} dp + \left(\frac{\partial h}{\partial \rho}\right)_{p,\alpha} d\rho + \left(\frac{\partial h}{\partial \alpha}\right)_{p,\rho} d\alpha$$

Using the above equation, along with the conservation equations in differential form, he solved for dp. For the pressure gradient (dp) to remain finite when $u^2 = \left(\frac{\partial p}{\partial \rho}\right)_{s,\alpha}$

i.e. when the flow velocity equals the speed of sound (at CJ plane), he showed that

$$\left(\frac{d\alpha}{dx}\right)_{x=t} = \frac{\xi}{t}\left(\frac{C_p T_2}{h^0}\right) = \frac{4\delta^*}{Dt}\left(\frac{C_p T_2}{h^0}\right) \quad \text{where } \delta^* = 0.22 t^{0.8}\left(\frac{\mu_e}{\rho_1 u_1}\right)^{0.2}$$

Since $d\alpha/dx$ could not be determined as a function of position behind the shock front, α was assumed to approach some constant equilibrium value exponentially with distance from shock wave: $\alpha = \alpha_e[1-\exp(-x/\lambda)]$.

That expression for α was substituted in the previous equation to obtain:

$$\exp\left(\frac{-t}{\lambda}\right) = 0.88\left(\frac{\lambda}{D}\right)\left(\frac{C_p T_2}{\alpha_e h^0}\right)\left(\frac{\mu_e}{\rho_1 u_1 t}\right)^{0.2}$$

where C_p is the frozen heat capacity, T is the absolute temperature, h^0 is the heat of reaction, μ_e is the viscosity of the gas in the combustion zone at the outer edge of the boundary layer, λ is a relaxation length estimated from measurements of the density profile within a detonation front, and t is the thickness of the detonation wave.

Hence, the above equation was used to determine t, knowing all the other parameters. After calculating the value of t, the value of δ^* could be found, and thus the corresponding value of ζ and the velocity deficit was calculated.

Fay compared his theoretical predictions for the velocity deficit of detonations in tubes to experimental results reported in previous works. The agreement between the calculated and experimental velocity deficit was judged quite reasonable considering the uncertainties involved.

Murray later used the integral form of Fay's equations to find an explicit expression for the value of the Mach number of the wave as a function of divergence between shock and CJ plane. Again , with ξ defined as $\xi = A_{CJ}/A_S - 1$ the conservation equations were written as

mass: $\rho_1 = \rho_2 u_2 (1 + \xi)$

momentum: $\rho_1 u_1^2 + p_1 = (\rho_2 u_2^2 + p_2)(1+\xi) - \int_0^\xi p \, d\xi$

energy: $\frac{u_1^2}{2} + h_1 + q = \frac{u_2^2}{2} + h_2$

As in Fay's case, since the exact pressure distribution along the boundary within the reaction zone was not known, the integral in the momentum equation was defined as

$$\int_0^\xi p \, d\xi = p_2 \varepsilon \xi \text{ where } 1 < \varepsilon < 2$$

The above equations along with the definition of the speed of sound, were combined to give:

$$2\left[1 + \frac{q}{C_p T_1}\right] = \left[\frac{\gamma_2}{\gamma_1}\right]^2 \left[\frac{\gamma_1 - 1}{\gamma_2^2 - 1}\right] \left\{\frac{1}{1 - \frac{\xi t}{(1 + \gamma_2)(1 + \xi)}}\right\}^2 \frac{(\gamma_1 M_f^2 + 1)^2}{M_f^2} - (\gamma_1 - 1) M_f^2$$

Murray introduced a new function defined by

$$1 + \Psi = \left\{\frac{1}{1 - \frac{\varepsilon \xi}{(1 + \gamma_2)(1 + \xi)}}\right\}^2$$

Hence the previous equation reduced to

$$2\left\{\frac{q}{C_{p_1} T_1} - \frac{\gamma_1 - \gamma_2}{\gamma_1(\gamma_2 - 1)}\right\} \frac{\gamma_2^2 - 1}{\gamma_1 - 1} = \frac{\left(M_f^2 - \frac{\gamma_2}{\gamma_1}\right)^2}{M_f^2} + \frac{\Psi \gamma_2^2 \left(M_f^2 + \frac{1}{\gamma_1}\right)^2}{M_f^2}$$

For large M_1, the equation reduced to

$$2\left\{\frac{q}{C_{p_1} T_1} - \frac{\gamma_1 - \gamma_2}{\gamma_1(\gamma_2 - 1)}\right\} \frac{\gamma_2^2 - 1}{\gamma_1 - 1} = M_f^2 (1 + \Psi \gamma_2^2)$$

If the heat release is assumed constant, then the left hand side of the equation has a constant value. Hence the right hand side is equal to a constant:

$$M_f^2 (1 + \Psi \gamma_2^2) = \text{cst}$$

Murray justified his assumption of a constant heat release by saying that an area increase would decrease both pressure and temperature of CJ plane. If the heat release is controlled by dissociation at that point, then the effect of the pressure and temperature drop will tend to cancel each other. Finally, since $\Psi = 0$ when $\xi = 0$, then

$$\frac{\Delta M_1}{M_{1_{\xi=0}}} = 1 - \sqrt{\frac{1}{1 + \gamma_2^2 \Psi}} \qquad \text{where} \quad \frac{\Delta M_1}{M_{1_{\xi=0}}} = \frac{M_{1_{\xi=0}} - M_1}{M_{1_{\xi=0}}}$$

Now consider the schematics in figure 4a. In the steady state case if the shock plane is at Shk1, then the corresponding CJ plane would be some distance downstream. Assuming that the reaction zone length is negligible compared to the induction zone length, then most of the burning takes place at the CJ plane. The distance between the CJ plane and the shock plane is then the induction zone length, and the time a particle takes from the instant it is shocked to the instant it reaches the CJ plane is the induction time τ.

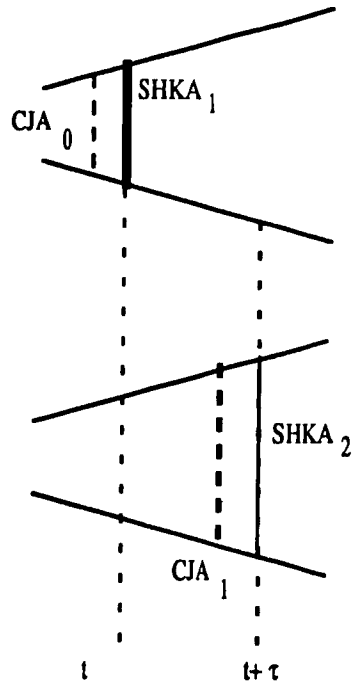

Figure 3.3. Two front model.

Consider the schematic of figure 3.3 showing the two front detonation model at two time instants τ seconds apart. A particle shocked at position Shk1 (of shock area ShkA1) will reach the CJ plane τ seconds later. Assuming the particle travels at a constant speed given in the lab frame by the post shock velocity U_1, then it will cover a total distance of $U_1\tau$.

During the time τ, the shock front moves from position Shk1 to Shk2. If the velocity of the shock is assumed to remain constant during that time interval, then Shk2 is a distance of $M_1 a_0 \tau$ downstream of Shk1. The two front model has thus been propagated for a time interval τ. The area CJA1 of the CJ plane at the new position is then calculated, and the value of ξ is given by

$$\xi = \text{CJA1/ShkA1} - 1 .$$

Using Murray's equation, corresponding Mach number deficit of the shock front is determined. The shock front now has a new Mach number M_2, where $M_2 < M_1$. Consequently, the shocked fluid particles have a new post shock velocity U_1, and a new higher value for τ has to be used. The new detonation front composed of Shk2 and CJ1 can now be propagated for another time interval τ_2 following the same procedure, with the shock propagating with a velocity $M_2 a_0$.

3.2.2 *Change in Induction Time*

An expression for the change in induction time, $\Delta\tau_i$, was given by Edwards et al. (1979). τ_i was expressed as $\tau_i = A\,\rho^{-1}\exp(E/RT)$, where ρ and T are the post shock density and temperature respectively, A is a kinetic rate factor, and E is the activation energy. By combining this expression with the Rankine-Hugoniot relations for a normal shock wave the following was obtained

$$\frac{\Delta\tau_i}{\tau_i} = -2\,\frac{\Delta M_s}{M_s}\,\frac{2 + (\gamma - 1)M_\xi^2\,\dfrac{E}{RT}}{2 + (\gamma - 1)M_\xi^2}$$

Therefore each time the detonation front is propagated, a value for $\Delta\tau_i$ can be calculated once ΔM_i has been determined. The initial value for τ_i can be found using empirical relations for different mixtures, such as the ones used by Edwards et al. :

$$\log_{10}\left\{[O_2]^{\frac{1}{3}}[C_2H_2]^{\frac{2}{3}}\tau_i\right\} = -10.81 + \frac{17\,300}{4.58\,T} \qquad \text{for oxyactylene mixtures.}$$

The quasi 1-D model is thus completed, and will be used as a building block for 2-D detonation propagation in diverging channels.

3.2.3 *2-D Detonation Propagation*

An orthogonal system similar to the one defined by Whitham is used in the study of 2-D diffractions. As in Whitham's approach, every two adjacent rays approximate a stream tube in which the detonation propagates. In each stream tube, a method similar to the one for quasi 1-D detonation described earlier is applied.

3.2.4 *Implementation of the Theory*

The implementation of the above theory for 2-D detonation diffraction is based on Schwendeman's (1986) code for the propagation of shock waves. The code was originally designed to apply Whitham's theory for shock wave propagation. To ensure the validity of the code and to learn its proper usage, it is first applied for the diffraction of inert shocks around cylinders. The results obtained are identical to the ones shown by Bryson and Gross, and are shown in figure 5.

The main modifications made on Schwendeman's original code, is the use of a two front model for the wave instead of the single front model used by Schwendeman for inert shocks. Also, Schwendeman used Chester's equation to relate the velocity deficit between to successive shocks to the area divergence between them. However, in the present code, the velocity deficit is a measure of the area divergence between the shock and its CJ plane, rather than between two successive shock positions.

The code follows the following algorithm:

The initial wave front is divided into a discrete set of points with the end points being on the boundary walls. The interior points of the shock front are at first advanced along the normal to the wave with a post shock velocity U_1, and for a time increment τ_1. The position of the endpoints is determined by satisfying the condition that the wave remains perpendicular to the boundary walls. The new position thus determined is actually the CJ plane CJ2, as described in the 1-D approach. With the discrete set of points at their new position, the equation of the front is taken to be that of a spline curve fit through the points. The area of the new CJ plane can now be determined and the value of ξ for each stream tube calculated and substituted in Murray's equation to determine the new velocity.

Before proceeding, the discrete points of the initial wave front are again advanced, this time with velocity equal to M_2a_0, and for the same time increment τ_1. Again a spline curve is fitted through the advanced set of points, and a new position of the shock plane, Shk2, is thus determined.

With the velocity deficit found for each steam tube, the respective values for $\Delta\tau$ and the post shock velocity are also found. The front Shk2 is now propagated forward for a fixed time $t = \tau_0$. Note that the wave's velocity, the post shock velocity, and the induction time now vary along the wave front. Again, the discrete points (xi,yi) along the front are propagated twice, the first time with a velocity Ui to determine the position of the CJ plane and subsequently the value of ξ_1 for each stream tube. The points (xi,yi) are propagated a second time from their initial position at Shk2 and with a velocity distribution along the front given by $M_{2i}a_0$ to determine the third shock position Shk3. This process is repeated until the detonation propagates past the divergence.

As the leading shock's strength decreases, the corresponding induction time increases. Schelkin's instability criterion states that for a 1-D wavefront, if increases in $\Delta\tau_i$ is such that $\Delta\tau_i/\tau_i \geq 1$, then the wave front can be considered to be decoupled. Upon decoupling, the present model

can still be used but with the shock wave now propagated using Chester's equation as was done by Bartlmä.

3.2.5 *Sample Output*

Dr. D. Schwendeman's code is first used and the results obtained by Bryson and Gross are reproduced. The case of shock wave diffraction by a cylinder is shown in figure 3.4

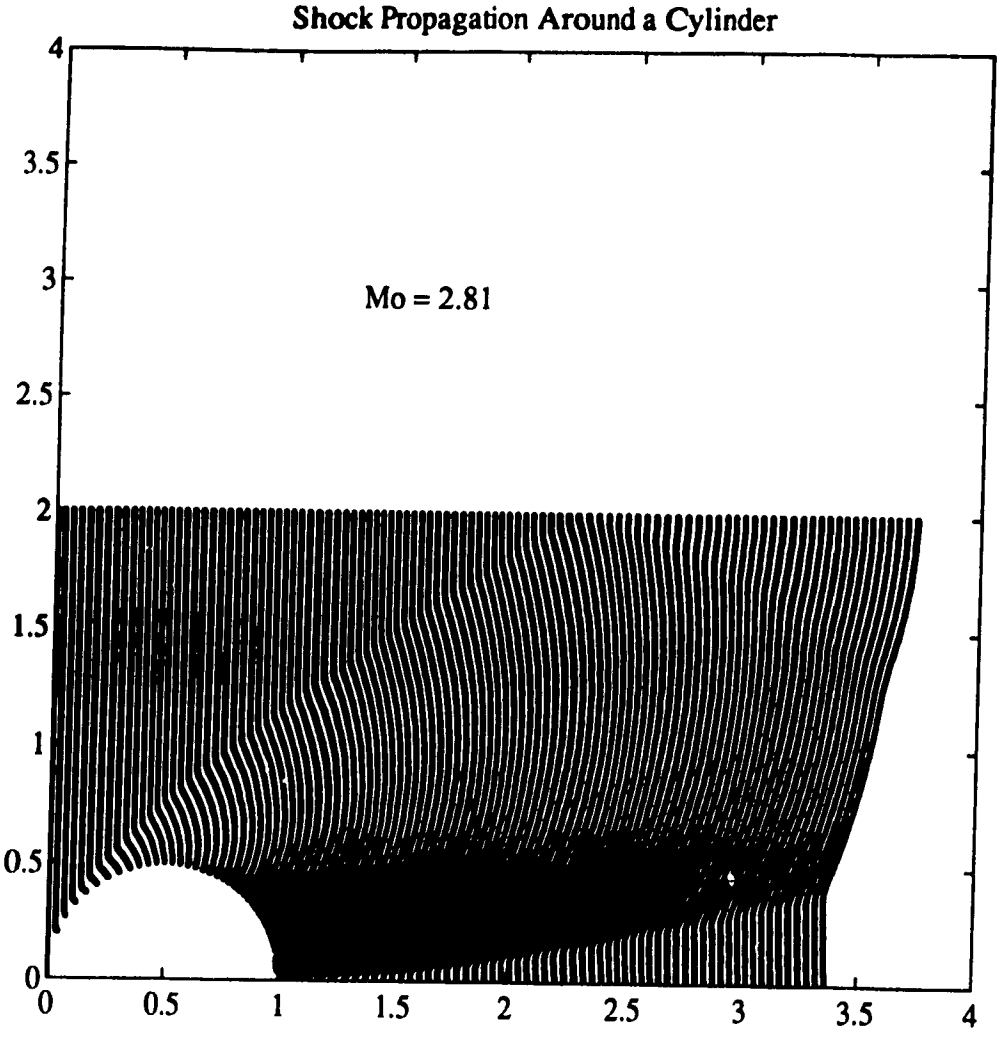

Figure 3.4. Output of Schwendeman's code for shock wave diffraction by a cylinder

The code developped for detonations only applies for detonation propagation in channels of diverging cross sections. Hence, it can only be applied for detonation propagation along the downstream half of the cylinder. The experiments performed in the work of this thesis all used complete cylinders and thus the results cannot be compared to the code's output. It is suggested that specific experiments be done to evaluate the output of the code and determine the most suitable numerical value for the parameters used in the code.

Consider the plot in figure 3.5 of a detonation diffracting along the downsteam half of a cylinder. It simulates a detonation diffracting along a radius of curvature of 0.25, where the total channel width is 1. The initial detonation wave front is devided into a discrete set of 100 points, and the intial induction time is considered to be 5e-06 seconds, with an intial Mach number of 7.0. Figure 3.6a and 3.6b show respectively the Mach number history and the induction time history for that case. Keeping the same wall radius of curvature and initial detonation's Mach number, but varying the number of discrete set of points (25) and initial induction time (1e-06) changes the output considerably. Figures 3.7a and 3.7b show respectively the Mach number and induction time history for the second case. Thus, experiments are needed to determine which number of discrete points would give the best results for different cases of detonation diffraction in diverging channels.

Neverthleless, the Mach number history for inert shocks is compared to the first case mentioned above and the detonation's Mach number are higher, as expected, figure 3.8.

The results from the code are judged satisfactory, and even though they might not be quantitatively correct. The results make sense, with the velocity steadily decreasing more and more as the wave propagates downstream the diverging wall. This is expected since the area divergence of the channel's cross section increases exponentially from x=0 to x=0.25, to reach a maximum at x=0.25, as seen in figure 3.5. The induction time also increases exponentially.

As described above, the code uses Murray's equation relating velocity deficit to area divergence between the shock and CJ plane. However, it can be easily modified to use other equations, such as ones relating the wave's velocity to its curvature. An example of such equations

is Bdzil's (1988) equation, which relates the velocity deficit of a shock to its local curvature for the propagation of a detonation into a rate stick (pipe filled with explosive).

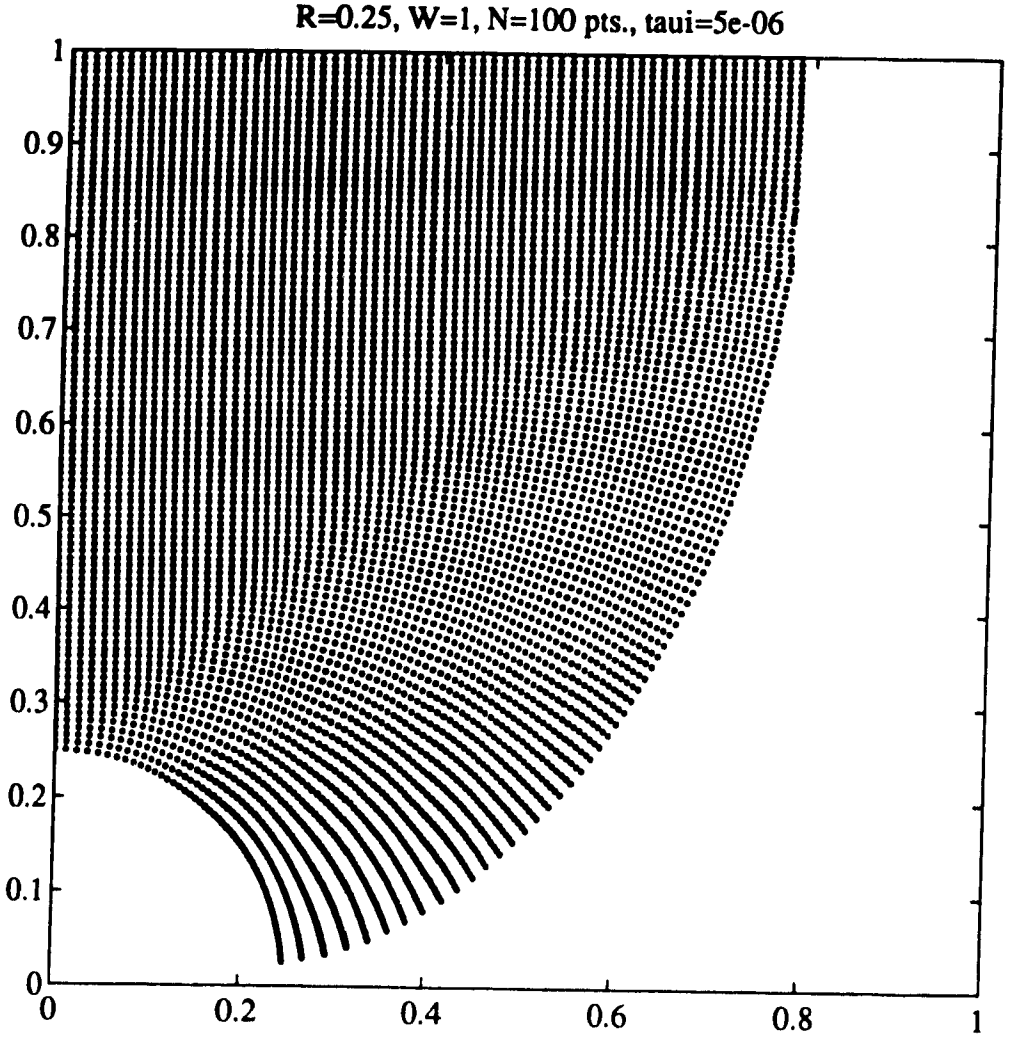

Figure 3.5. Detonation propagation in a diverging channel of radius of curvature 0.25 and width 1.

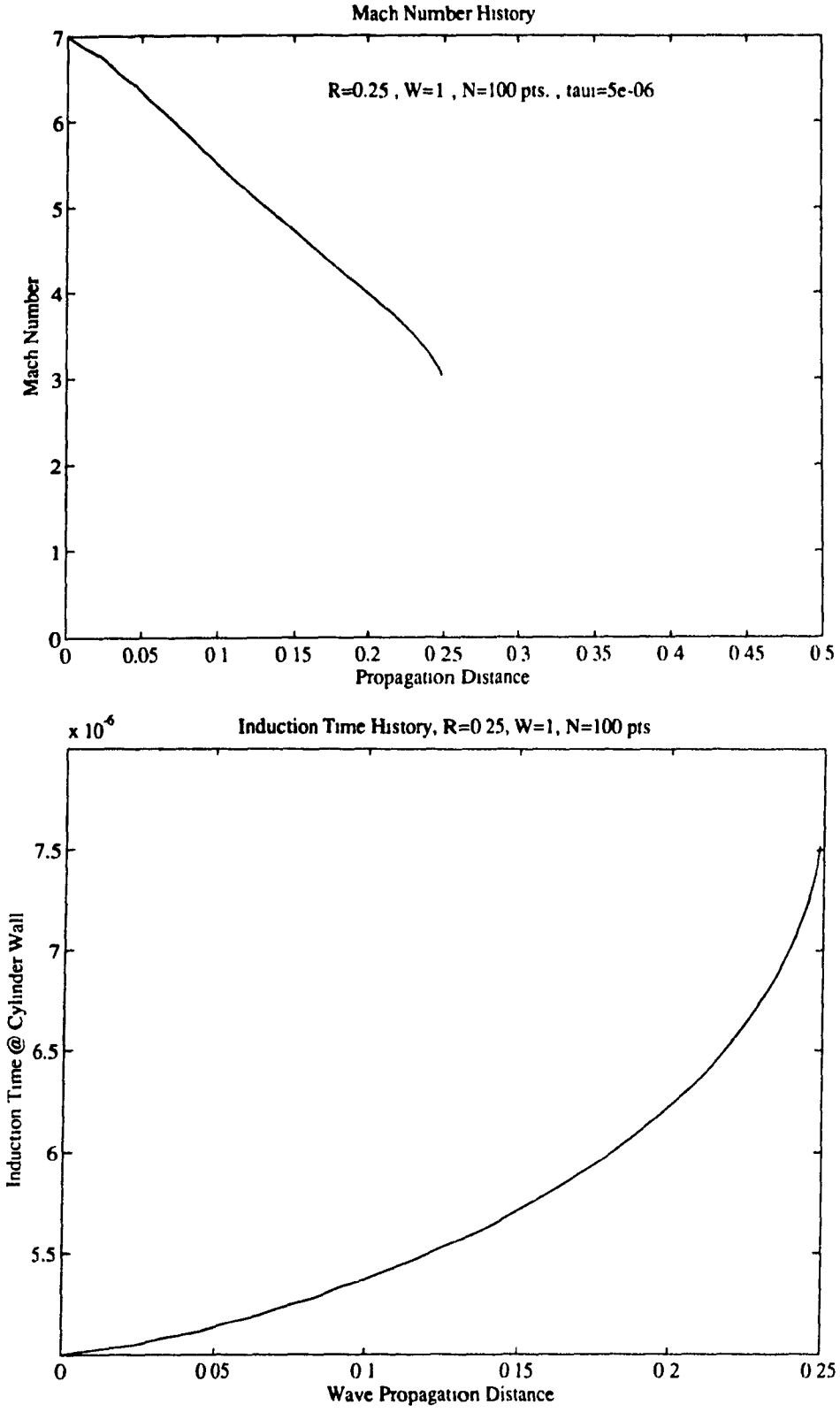

Figure 3.6. Mach number and induction time histories at cylinder wall.

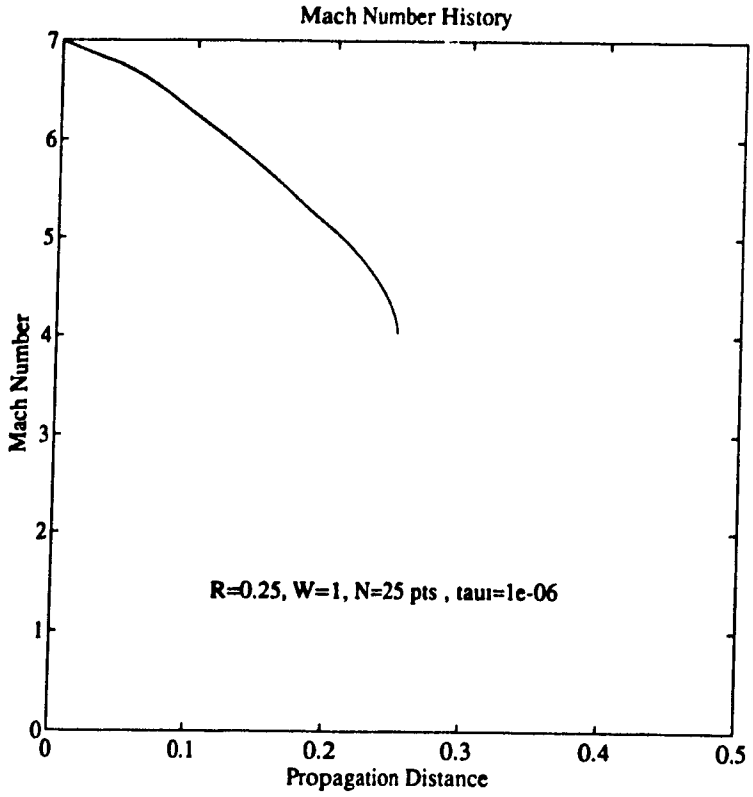

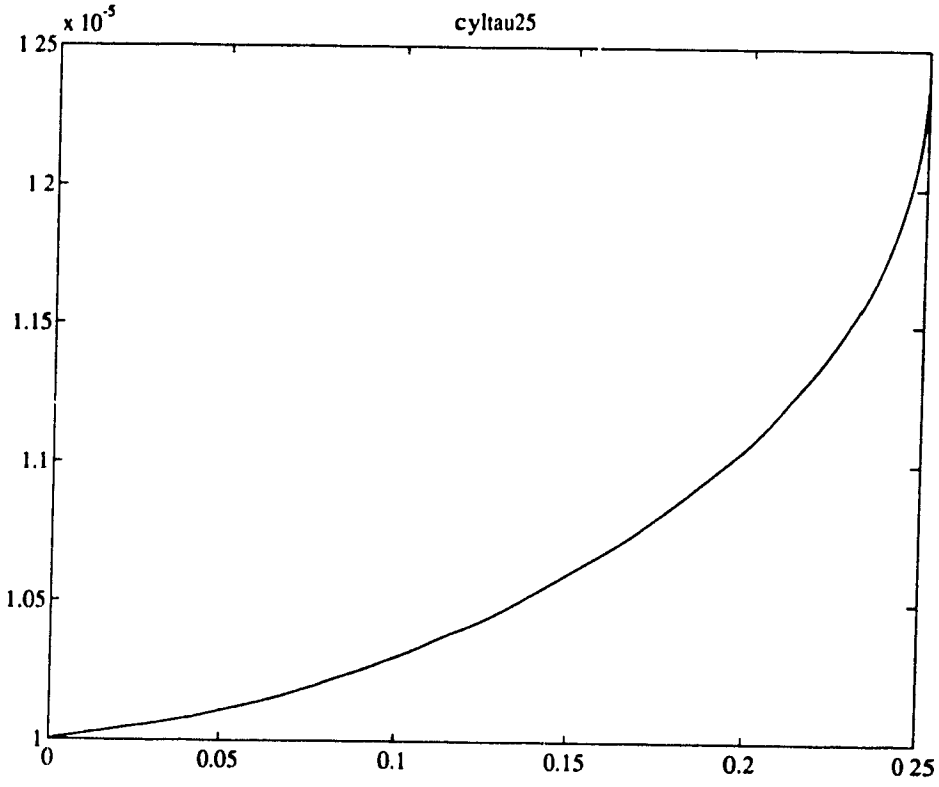

Figure 3.7. Mach number and induction time history at cylinder wall: case II.

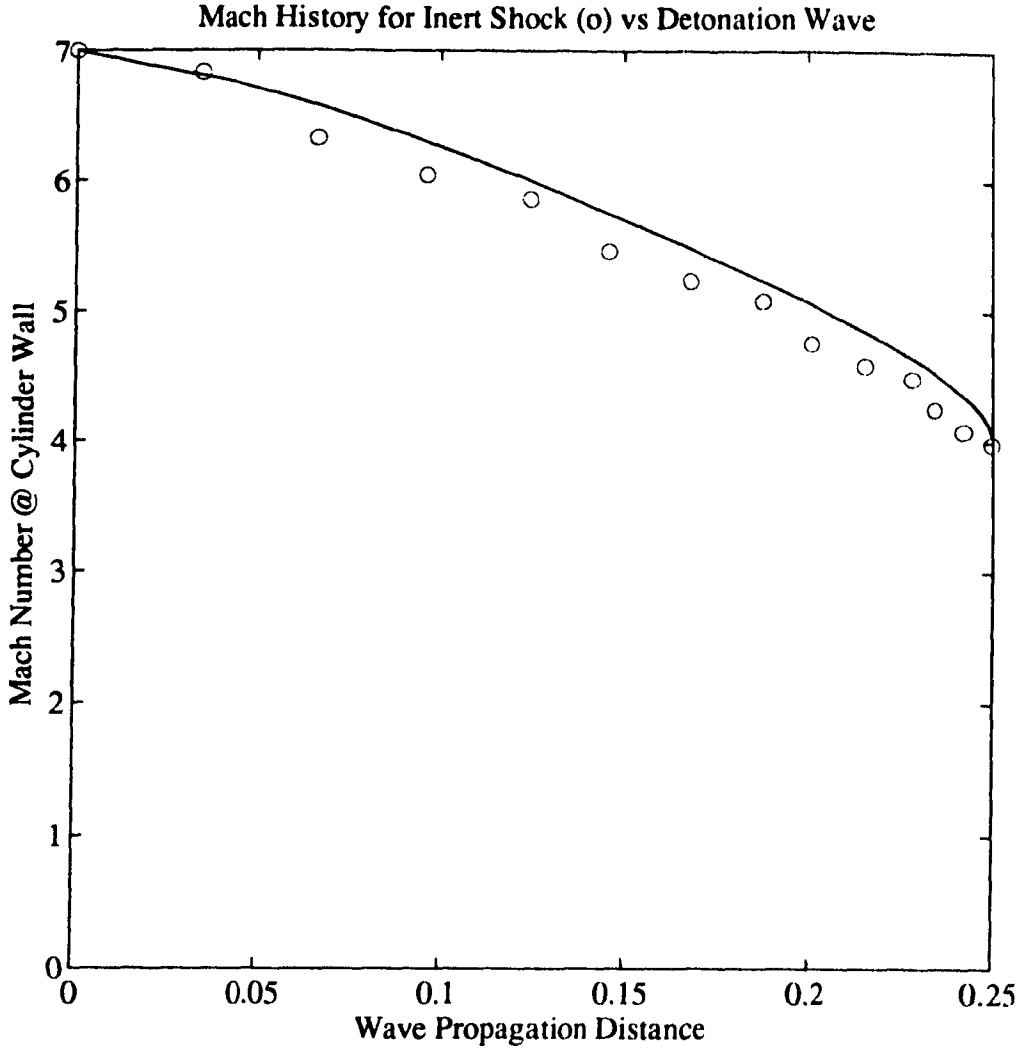

Figure 3.8. Comparison of Mach number history at cylinder wall for inert and reactive shocks.

Chapter 4

Summarizing Remarks and Conclusion

In the previous two chapters, the results of experimental and theoretical investigation of detonation diffraction around cylinders are presented and discussed. The experimental investigation reveals a correlation between the D/λ ratio and the distance of re-initiation behind the cylinder. As the D/λ ratio is increased, the distance of re-initiation behind the cylinder normalized with respect to the cylinder diameter decreases asymptotically to a value of about 1.2. At high D/λ values, the cellular structure around the cylinder never fails although a slight increase in size is noticed for the cells along the cylinder wall. In that range of D/λ, the tests are very repeatable and any discrepancies in the results are attributed to measurement error.

Hence, the effect of the diffraction on cell structure of a detonation wave is minimal for high D/λ values. Also, the S/D value stays around 1.2 as D/λ increases beyond 40, implying that the re-initiation mechanism for such cases becomes independent of cell size and dependent only on the geometry of the flow. Another feature of experiments with high D/λ values is that the first loci of triple points is detectable. Hence, the diffraction process of a detonation exhibits all the features of that of a shock wave, leading to believe that the detonation behaves as a discontinuity.

In contrast, for D/λ values between one and twenty, the effect of the diffraction on the cell structure is more pronounced. Also, the re-initiation distance exhibits more randomness even though the S/D value tends to decrease as D/λ increases from 1 to 20. Expansion heads can be traced out on both sides of the line of symmetry behind the cylinder, beyond which no cells exist until re-initiation. The re-initiation itself seems to be due to the collision of opposite transverse wave crossing both expansion heads towards the line of symmetry. The reflection of these transverse waves off each other create hot spots which cause re-initiation. It is also noted that the curvature of the diffracted waves for small D/λ values is larger than for high D/λ values. Also the angle subtended by the re-initiated wave (with the point of re-initiation as its vertex) gets larger as the D/λ ratio is decreased. At the limit the angle approaches the vertex angle of individual cells.

In this chapter a physical explanation to the observations made above is given. The problem of detonation diffraction around a cylinder is subdivided into four cases: $D/\lambda < 1$, $1 \leq D/\lambda \leq 20$, $20 < D/\lambda \leq 40$, $D/\lambda > 40$. The theoretical analyses of chapter 3 is applicable only when $D/\lambda > 40$.

From the smoke foil records presented in chapter 2 the following is confirmed. Each cell is initiated by the collisions of two transverse waves traveling in opposite directions. The traces left on the smoke foils are those of the triple points formed by the intersection of the transverse wave and the leading shock front. The initiated cell itself is bounded by two transverse waves which will eventually collide with other ones and initiate new cells. This cycle is continuously repeated and cell initiation provides the mechanism for the sustainablity of the detonation, figure 4.1. When a detonation wave undergoes a diffraction, this mechanism is perturbed. The diffraction amounts to changing the boundary conditions of the cells along the walls, hence they are the first to be affected. In chapter 2 it was concluded that the diffraction pattern of detonations by cylinders is related to the ratio of the cylinder diameter to the cell size. It is believed that this ratio is a measure of the diffraction within each cell. For D/λ larger than unity, the larger its value the smaller is the diffraction within each cell. Hence the smaller is the effect of the actual cell size. This is illustrated by the fact that as the D/λ increases from unity to a value of about 40, the distance of re-initiation behind the cylinder decreases. For D/λ higher than 40, the distance of re-initiation is constant at about 1.2D, implying that the actual cell size does not influence much the diffraction process beyond $D/\lambda = 40$. Also for small D/λ, the diffraction is so severe that the cells along the wall of the cylinder cease to exist. As D/λ increases beyond 20, the cell structure never fails, although the cells along the cylinder wall do increase in size. How a change in the boundary condition of a detonation affects its cell structure is explained in the next section.

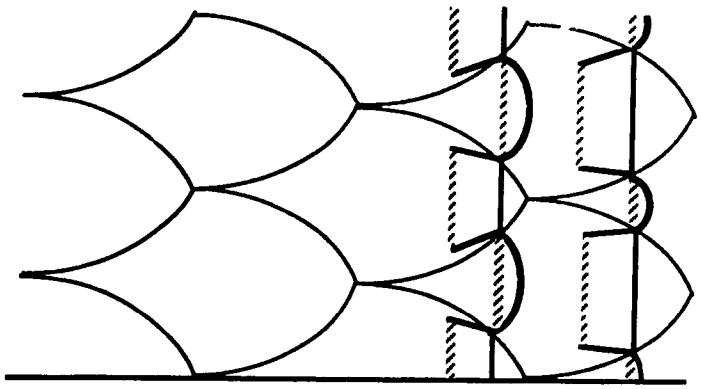

Figure 4.1. Cellular structure of a detonation wave.

4.1 Effect of Diffraction on Cell Structure

The collisions of transverse waves traveling in opposite directions ensures the continuous re-initiation of cells. If the rate of collisions of the transverse waves is disturbed by the boundary conditions, then the detonation's velocity will change. Should the rate increase, then the detonation will accelerate. If the rate decreases, the detonation is slowed down and in some cases their would be no cell re-initiation, meaning the detonation front has failed.

Consider figure 4.2, point **I** represents the point where two transverse waves reflect off each other. By the time the lower transverse wave, wave *a*, reflects off the wall, the upper transverse wave, wave *b*, has reflected off wave *c* and travels back to meet wave *a*. Ideally, they will meet again at point **II**, where **I** and **II** are at a distance of $\lambda/2$ from the wall. The distance between **I** and **II** is the longitudinal length of a cell, L_C., and is about 1.67λ. If the wall yields away beyond **II**, then the waves of the initiated cell at **II** have to travel a longer distance to reach the wall. Hence both waves *b'* and *a'* have to travel a longer time to collide, which causes a delay in the combustion renewal behind the local shock front. The local shock velocity then drops below the nominal terminal velocity, meaning the next Mach stem generated should be weaker than the preceding one.

Also, the line joining **II** to **III** is now slightly curved. At each cycle, more cells are affected by the wall divergence. It is obvious from such an analysis that the more the wall diverges within one cell length, the more pronounced is the effect of the divergence on the detonation wave. In the limit when the divergence is very large, then the cell structure of the detonation wave close to the wall fails. Such is the case in diffraction around cylinders for low D/λ values.

Another example is the propagation of a detonation from a tube to an unconfined area. The cell structure along the wall fails upon exiting the tube, which eventually leads to separation of the burning zone from the leading shock.

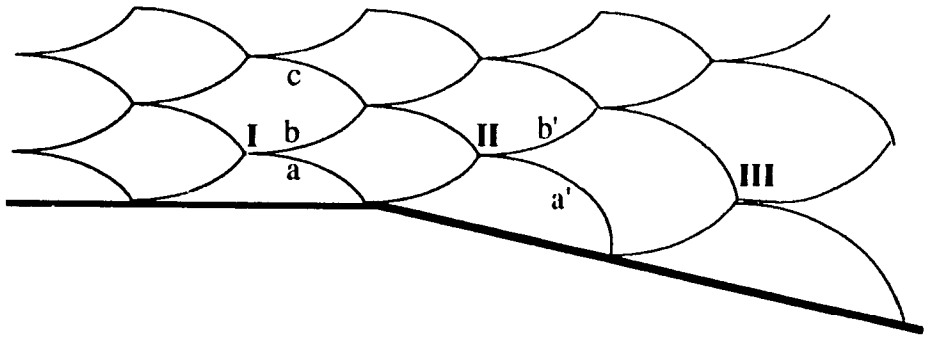

Figure 4.2. Local effect of diffraction on cell structure.

When the divergence is smaller and gradual, Thomas et al. showed that successful propagation can occur where the cell structure of the wave never fails. The wave adapts to the gradual divergence with the initiation of new cells. The criteria of cell size to channel width ratio established by Thomas et al for various divergence angles, can be interpreted as a measure of the limit for the divergence within each cell. Recall that Thomas et al. established that for a given channel width, an increasing divergence required an ever increasing number of cells across the channel. This can be explained by the fact that for a certain channel width and divergence angle, the more cells there are across the channel, the smaller the cell size, hence the smaller the divergence within each cell.

The other limit is when the cell size is very small and the divergence is almost negligible within each cell. Since the hydrodynamic thickness of the detonation is believed to be of the order of the cell size, the divergence within the detonation front would also be negligible. The detonation front can then be approximated as a discontinuity.

The above analyses is also applicable for detonation propagation in converging channels. When the cell size is small relative to the convergence, the discontinuity approximation holds true, as is the case for Ong. However, when the cell size is large, then the cell structure cannot be neglected and the transverse waves have to be accounted for, as is the case for Akbar and Shepherd. A converging wall has the effect of precipitating the transverse wave collisions. The transverse waves close to the wall will reflect off the wave earlier than anticipated, and before they reach their weakest values. Thus the new cells generated at the wall will be stronger ones, causing the average wave front velocity to increase.

4.2 Diffraction Around Cylinders

The problem of detonation diffraction around cylinders in acetylene oxygen mixtures is subdivided into four cases: $D/\lambda < 1$, $1 \leq D/\lambda < 20$, $20 < D/\lambda \leq 40$, $D/\lambda > 40$. The effect of the diffraction on the cell structure is different for each of these cases.

I- $D/\lambda < 1$: When the cell size is larger than the diameter, the cylinder has an intracellular effect on the detonation front and only the local cell is affected. In that case, the cylinder falls between two transverse waves. The diffraction process depends on the stage at which the cell is in its development when it collides with the cylinder. This dependence makes the exact diffraction pattern unpredictable and random, as observed in the experiments. In the limit where $D/\lambda << 1$, experiments show that the diffraction around a cylinder of the wave front between two transverse waves can exhibit similar characteristics as that of shock waves. This is explained by the fact that when the cylinder diameter is much smaller than a cell width, the cell's leading front is relatively

planar compared to the cylinder. Furthermore, if the cell is at its initial stages, then its front is an overdriven Mach stem (Edwards et al.), hence it is not surprising that it behaves as a planar shock wave. In that case, a mach stem is generated downstream the cylinder but does not initiate a new cell. The next cell is only initiated when the transverse waves from adjacent cells first collide downstream the cylinder.

II- $1 \leq D/\lambda \leq 20$: When the cell size is of the order of a few cylinder diameters, the cell pattern is strongly affected by the cylinder. The diffraction which the cells along the cylinder wall undergo is beyond their capacity to adapt to it. Firstly, along the upstream half of the cylinder, no Mach reflection can be noticed from an inspection of the smoke foil records. This is so because the effect of wall convergence is felt only along a few cells' lengths, which apparently is not enough for the generation of overdriven cells. Second, along the downstream half, the divergence which occurs within one cell's length is too large. The wall divergence delays the reflection of the cell's transverse waves off the wall resulting in a more decayed cell front and transverse wave. When the transverse wave finally reflects off the wall, the it might be too weak to generate a new cell upon reflection. Consequently, the adjacent cells will also fail since they have nothing to reflect off along one of their sides. The failure of the cells close to the wall leads to the existence of a region downstream the cylinder where no cell structure exists. The region is comparable to one cylinder's cross-section for values of D/λ close to 1, and decreases as D/λ increases to 20. The region is bordered by areas where the cell structure is unaffected. For D/λ close to 1, lines can be drawn distinguishing these areas, implying that the divergence is such that the cells fail abruptly when they are affected. The lines expand in a V shape behind the cylinder similar to expansion heads, and curve towards each other further downstream. As the D/λ ratio is increased, the lines bounding the region where no cell structure exists come closer to each other, until about $D/\lambda \approx 20$. Above that value, there is no region where the cell structure is nonexistent.

Transverse waves are continuously crossing these lines from the region where the cell structure exists to the region where it is nonexistent. Close to the cylinder, the transverse waves

weaken before reaching the centerline. Further downstream, as the boundary lines are caving towards each other, the transverse waves have to travel a shorter distance before they collide along the centerline. The re-initiation of detonation in the cylinder's wake is noticed to occur almost always at the collision of two transverse waves. At re-initiation, a strong wave is propagated forward. No cell structure is noticed at re-initiation, and it starts to appear only further downstream the re-initiation point.

In the theoretical analyses of detonation diffraction for $D/\lambda < 20$, the detonation cannot be approximated as a discontinuity since its cell structure cannot be neglected. Furthermore, the detonation diffraction still exhibits elements of randomness which are related to the randomness in the initiation of cells. This randomness is illustrated in the scatter of the points on the S/D vs D/λ plot for the range $1 < D/\lambda < 20$. Schlieren photographs of the wave in the cylinder's wake do not show clear decoupling between the shock and the burning zone, although smoke foil records indicate the absence of a complete cell structure. Hence, even an approach similar to Bartlma's is debatable since there is not enough evidence that the leading shock is propagating independent of the burning zone. Also, along the upstream half of the cylinder, the approximation of a detonation as a discontinuity will predict the formation of a detonative Mach stem. This is not the case for $D/\lambda < 20$ as evidenced by the smoke foil records which show no fine cell structure, characteristic of a detonative Mach stem.

$20 < D/\lambda \leq 40$: For detonation diffraction in that region, the cell structure never fails throughout the process. The cell size along the wall does change considerably as the wave diffracts. The wave does not exhibit the full characteristics of a discontinuity, since the cells along the upstream half of the cylinder do not exhibit the characteristics of an overdriven Mach stem. Recall that for shock waves, a strong Mach reflection occurs at about 45° from the forward stagnation point. From the S/D vs D/λ plot, it is noticed that the cell size λ still affects the diffraction pattern. Hence the case

of $20 < D/\lambda \leq 40$ is regarded as a transition stage between that where a detonation is characterized by its cell structure and that where the cell structure can be neglected.

$D/\lambda > 40$: Finally, for cases where $D/\lambda > 40$, the detonation exhibits all the features of a discontinuity, as is concluded from the Schlieren photographs and smoke foil records. The Schlieren photographs shown in chapter 2 show the full characteristics of a discontinuity for values as low as $D/\lambda > 25$. However, smoke foil records only exhibit such characteristics beyond $D/\lambda=40$. A terminal value of 1.2 for S/D is reached in the plot of S/D vs D/λ. In these cases, the incident wave never fails, and it is incorrect to keep defining S as the distance of re-initiation, since their is no wave failure. Recall, that both parts of the diffracted wave reflect off each other downstream the cylinder; S then denotes the distance where the regular reflection turns into a Mach reflection. For $D/\lambda > 40$, S becomes independent of cell size and dependent only on the cylinder diameter. Furthermore, beyond $D/\lambda = 60$, traces on the foils of an overdriven Mach stem could be detected at about 45 to 50° from the forward stagnation point. Therefore it is concluded that for cases where $D/\lambda > 40$, the cell structure can be neglected and the wave generated downstream the cylinder is a Mach stem.

In that range of D/λ values, the pattern of detonation diffraction by single cylinders is identical to that of shock waves. A bow shock is created when the detonation first impinges on the cylinder. The reflection off the cylinder's upstream half is at first regular. At about 45° from the forward stagnation point the reflection becomes a strong one. Two loci of triple points are generated one on each side of the cylinder. As the wave diffracts past the cylinder, the curvature of the diffracted part is much smaller than for small D/λ. When the diffracted part of the wave meet behind the cylinder, the reflection off each other is initially a regular one. At about a distance of 1.2D downstream the cylinder's stagnation point, the reflection becomes a Mach reflection. A new wave then grows and merges quickly with the original wave front which is not affected much by the presence of the cylinder. The reason why the Mach reflection almost always occurs at about

1.2D behind the cylinder is that the detonation behaves as a discontinuity and its cell structure can be neglected. Hence, the only parameter which would influence the diffraction pattern would be the wave's Mach number. In the experiments made, only pure acetylene oxygen mixtures were used to obtain high D/λ. The Mach number of the detonations in each of these mixtures and for the same initial pressure are very close to each other. Furthermore, the Mach number is a function of the square root of the pressure ratio, hence it does not change much in the range of pressures used (40-90 torr). Therefore, the Mach number in all experiments performed at high D/λ values is around 6.9 - 7.0. Consequently, the diffraction pattern is identical for all these tests and Mach reflection always occurs at 1.2D behind the forward stagnation point.

4.3 Suggestions for Further Studies

The experiments performed in the course of this investigation used only pure and Argon diluted acetylene oxygen mixtures. These mixtures have a regular cell structure, and the pure ones are very sensitive also. It would be interesting to repeat the tests using irregular and less sensitive mixtures such as propane oxygen mixtures. It is expected that at high D/λ values, the behavior will be the same in both cases. The cell size being so small relative to the cylinder diameter that it would not affect the diffraction, whether the cell structure is regular or not should not be a factor. The re-initiated wave downstream the cylinder should inevitably occur since in such cases it is governed mainly by geometrical considerations.

However, for low D/λ values, the behavior might be different in both cases. The propane oxygen mixtures being more irregular will have an even more random behavior at D/λ close to unity. The interesting part would be the region downstream the cylinder where the cell structure fails, and whether that region would still exist and be such well defined when irregular mixtures are used. Another question is whether the sensitivity of the mixture affects the re-initiation of the detonation downstream the cylinder.

Separate experiments have to be performed to verify the validity of the model developed in chapter 3 for detonations in channels with diverging cross-sections. The velocity of a diffracting detonation has to be measured experimentally and compared to that predicted using the code based on the model. It is recommended that experiments be performed in diverging channels, where the diffraction is not severe and the angle of divergence can be changed. Pressure transducers should be used to monitor the speed of the detonation. Photodiodes can also be used but are not easy to interpret, especially when dealing with attenuated detonations.

Other analyses can be made by taking a series of Schlieren photographs of a detonation wave propagating in diverging channels, and plotting its non dimensionalised shape. Such analyses was done by Bartlmä and Schröder in their investigation, but they did it for cases of severe diffraction where separation occurred. Hence they ended up plotting the shape of the separated leading shock front only. To test the model of chapter 3, the detonation has to be approximated as a discontinuity, therefore the use of very sensitive mixtures at high pressures is recommended. The detonation will be less prone to decoupling under these conditions. The shape of the non dimensionalised wave can then be compared to that predicted by the code.

Finally, should the model prove to be correct, a new code would have to be written which merges both models: that for a converging area change using an approach similar to Whitham's and that for diverging area change developed in chapter 3 and based on Fay and Murray's theories. Such a code can then be used to predict the complete diffraction pattern of detonation waves around cylinders.

4.4 Conclusion

The diffraction of detonations in acetylene oxygen mixtures has been investigated. From the experimental investigation it was concluded that the ratio of cylinder diameter to cell size of the mixture is a critical parameter in determining the diffraction pattern. When the D/λ value is less than one, the effect of the cylinder is intracellular and the overall detonation front is not affected. The cylinder at most causes one cell cycle to be skipped. Re-initiation occurs downstream the cylinder and is in fact nothing more than a new cell being initiated. It is due to the collision of a the transverse waves from the cells next to the one being intercepted. The pattern is very random due to the randomness of the cell cycle.

For values of D/λ above 1, there is a general linear relation between the distance of re-initiation behind the cylinder and the cylinder diameter. That linear relation was illustrated by the straight line obtained in the plot of S/λ vs D/λ values for all the tests made. The agreement between the actual experiments and the straight line fitted between the experiments increases with increasing value of D/λ . It was concluded that for D/λ between 1 and 20, the actual cell size could not be neglected. The experimental results were still random in that range. The randomness was attributed to the relatively large cells which themselves have a random behavior. It was concluded that the re-initiation in those cases is due to the collision of transverse waves downstream the cylinder in the region where the cell structure ceases to exist.

For values of D/λ greater than 40, the diffraction pattern became independent of cell size, and dependent only on the cylinder diameter. Schlieren photographs show that detonations in that range exhibit the same characteristics as that of shock wave diffraction around single cylinders. Smoke foil records show that the cell structure never fails upon diffraction, and the cell size remains very small relative to the cylinder diameter. Therefore, it was concluded that for oxyacetylene mixtures in the range of $D/\lambda > 40$, the cell structure of a detonation can be neglected and the detonation approximated as a discontinuity. There is no re-initiated wave as such, since the incident wave never fails. The phenomena observed is that of the regular reflection between the two parts of the

diffracted wave off each other, turning into a Mach reflection. It was concluded that the pattern is entirely governed by geometrical considerations and the cell structure can be neglected.

Two dimensional models can then be applied, which use the discontinuity approximation for a detonation to solve for the diffraction pattern. An approach similar to Whitham's theory can be used along the upstream half of the cylinder. Along the downstream half, a two front model was developed based on Fay and Murray's theories for velocity deficit due to an area increase between the shock and the CJ plane. The model was implemented in a computer code, and the numerical results obtained were judged qualitatively good but still have to be compared to experiments.

For further studies, it was suggested to experiment with an irregular and less sensitive mixture such as propane. The behavior of the detonation as it diffracts by the cylinder can then be compared to that of regular and sensitive mixtures. Also, specific experiments have to be made to test the validity of the model developed.

References

Akbar, R, and Shepherd, J.E., "Analysis of Mach Reflection of Gaseous Detonation", *submitted for consideration of presentation at the 14th ICDERS*, 1993.

Akbar, R., "On The Application Of Whitham Theory To Gaseous Detonations" , Masters Thesis, Rensselaer Polytechnic Institute, New York, 1991.

Bartlmä, F., "The Propagation of Detonation Waves in Channels of Varying Cross-section", *Journal of Fluid Mechanics*, Vol. 218, pp. 225-238, 1990.

Bartlmä, F., and Schröder, K., "The Diffraction of a Plane Detonation Wave at a Convex Corner", *Combustion and Flame*, Vol. 66, pp. 237-248, 1986.

Bdzil, J.B., and Stewart S.D., "The Shock Dynamics of Stable Multidimensional Detonation", *Combustion and Flame*, Vol. 72, pp. 311-323, 1988.

Bergeron, M.-A., "Investigation Of Focusing Of Gaseous Detonation Waves" , Masters Thesis, McGill University, Montreal, 1978

Bryson, A.E., and Gross, R.W.F., "Diffraction of Strong Shocks by Cones, Cylinders, and Spheres", *Journal of Fluid Mechanics*, Vol. 10, pp.1-16, 1961.

Edwards, D.H., Thomas, G.O., and Nettleton, M.A., "The diffraction of a planar detonation wave at an abrupt area change", *Journal of Fluid Mechanics*, Vol. 95, part 1, pp. 79-96, 1979.

Fay, J.A., 'Two-Dimensional Gaseous Detonations: Velocity Deficit" , *Physics of Fluids*, Vol. 2, 1959, pp. 283-289.

Gavrilenko, T.P., and Prokhorov, E.S., "Overdriven Gaseous Detonations", *Proceedings of the 8th ICOGER*, pp. 244-250, 1983.

Knystautas, R., and Lee, J.H.S., and Guirao, C., "The Critical Tube Diameter for Detonation Failure in Hydrocarbon-Air Mixtures" , *Combustion and Flame*, Vol. 48, 1982, pp.63-83.

Lee, J.H.S. and Lee, B.H.K., "Cylindrically Imploding Shock Waves", *The Physics of Fluids*, pp. 2148-2152, 1965.

Murray, S.B., "The Influence of Initial and Boundary Conditions on Gaseous Detonation Waves" , Ph.D. Thesis, McGill University, 1984.

Ong, R.S.B., "On The Interaction Of A Chapman Jouget Detonation Wave With A Wedge", Ph.D. Thesis, University Of Michigan, 1955.

Schwendeman, D.W., "Numerical Shock Propagation Using Geometrical Shock Dynamics" , Ph.D. Thesis, California Institute of Technology, 1986.

Thomas, G.O., Edwards, D.H., Lee, J.H.S., Knystautas, R., Moen, I.O., and Wei, Y.M., "Detonation Diffraction by Divergent Channels", *Proceedings of the 10th ICDERS*, pp. 144-154, 1985.

Whitham, G.B., "A New Approach to Problems of Shock Dynamics. Part I. Two Dimensional Problems", *Journal of Fluid Mechanics*, Vol. 2, pp. 146-171, 1957.

Whitham, G.B., "Linear And Non-Linear Waves" , *Wiley Interscience*, New York, 1974.

Appendix I

Experimental Set-up

The following sections detail the components used in the experiments, such as the main channel, ignition system, photographic equipment, etc. ... A sketch of the overall experimental apparatus is shown in figure I.1.

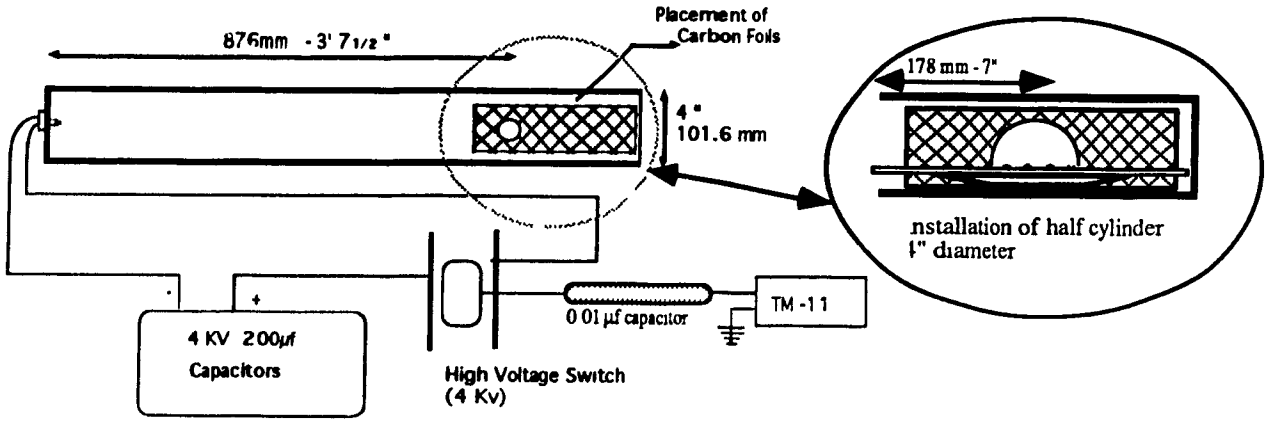

Figure I.1a. Set-up for smoke foil experiments, high Argon dilution

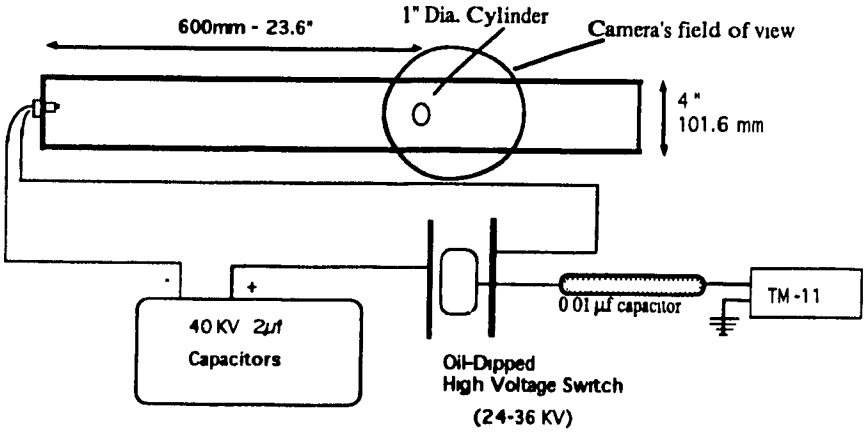

Figure I.b. Set-up for Schlieren photography

Figure I.1. Experimental Apparatus

I.1 Detonation Channel

The main component of the experimental set-up is a two dimensional rectangular channel. The test section is 1085 mm long, 101 mm wide, and 25.4 mm thick. The channel consists of a rectangular aluminum piece with an empty core of the test section's dimensions. This central aluminum piece is bound by two rectangular optical quality glass (1/2" thick) enclosed in a metallic frame. A total of 10 bolts around the periphery hold together the two frames, the glasses, and the aluminum core. Two O-rings are laid in special grooves on each side of the aluminum core to ensure smooth and tight contact between the glass pieces and the aluminum piece. An exploded view of the channel is shown in figure I.2.

At one end of the channel, an inlet/outlet valve is installed in the aluminum core. At the other end, three holes are drilled and tapped to accommodate the home made spark plugs. Along the two long walls of the channel, holes are drilled and tapped to accommodate pressure, and temperature probes, and photodiodes. These are not used in the present experiments and remain plugged.

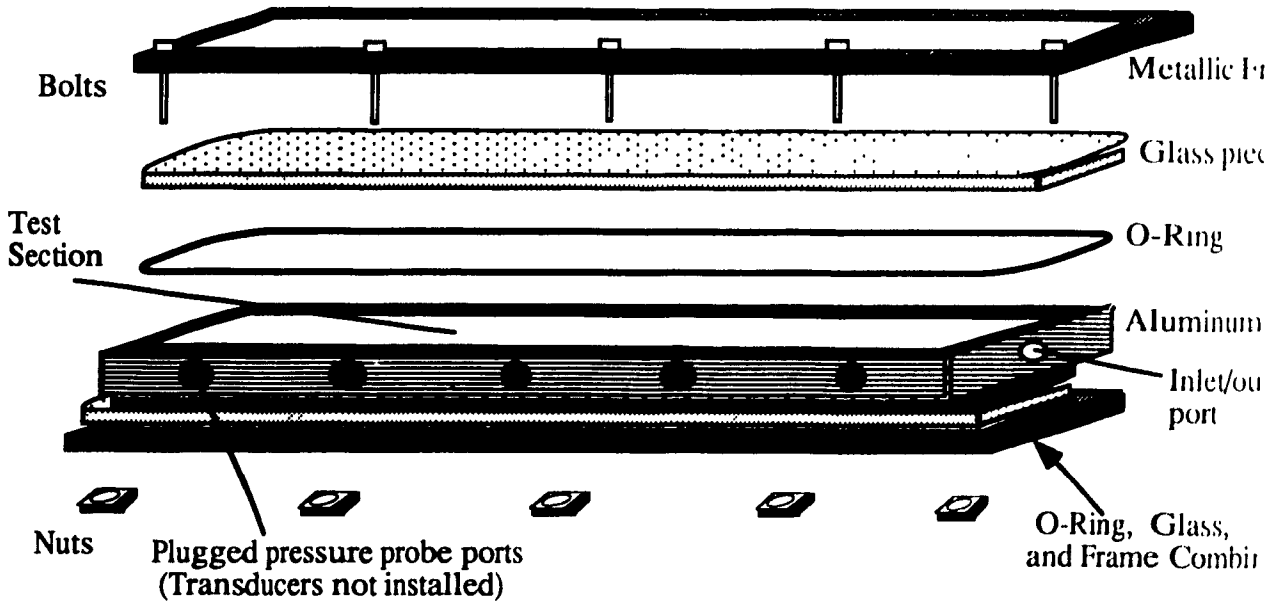

Figure I.2. Exploded view of channel

I.2 Ignition Plugs

A sketch of an ignition plug is shown in figure I.3. These plugs are easily machined in the machine tool lab at McGill. A hole is drilled first into a threaded Delrin plug. Two metallic needles are then slidden in the hole and fixed in position with epoxy. The plug is also fitted with an O-ring groove to provide a good seal At the spark end of the plug, the needles are sharpened and brought close together to ensure that the spark will occur at two points and not along the whole exposed needle part.

At the outer end of the plug, the needles are connected to the switch terminal and the ground. Adequate insulation should be placed around the needles to avoid any spark occurring outside the channel. Although Milar sheets are used for that purpose in the present apparatus, a thick layer of Teflon is more suitable for high voltages.

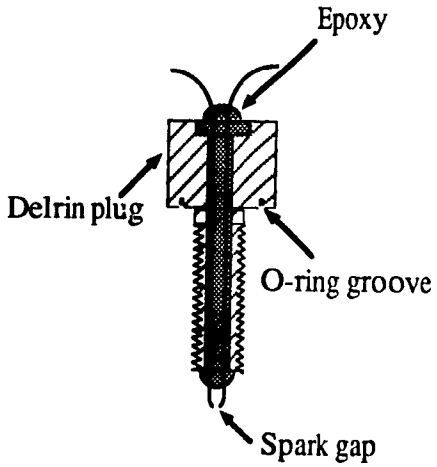

Figure I.3. Ignition spark plug

I.3 Ignition System

Two types of ignition systems are used:

I) A high voltage, fast discharge, and low capacitance system.

II) A low voltage, slow discharge, and high capacitance system.

The first type of system uses a pair of 1μf, 40 Kv capacitors connected in parallel. A high voltage switch (***EG&G*** , GP-148) rated between 24 and 36 KV is used. A *Hipotronics* high voltage DC power supply is used to charge the two capacitors to the required voltage. The capacitors are charged to 32 Kv in most tests to stay within both operating ranges: that of the capacitors and that of the switch. That system is used for stoichiometric, and equi-molar oxyacetylene mixtures, and oxyacetylene mixtures with up to 40% Argon dilution.

The system is characterized by a very fast discharge, hence it can be used in tests where accurate synchronization is required, e.g. for Schlieren photography. The discharge and the noise associated with the ignition occurs in less than 10μs. An ***EG&G*** TM-11A trigger module is used for triggering. A wire from the TM-11A is connected to the high voltage switch through a 0.0001 μf, 30 Kv capacitor. The capacitor prevents an accidental transmission of current from the switch back to the TM-11A. Another wire from the TM-11A is connected to the ground. The TM-11A can be triggered manually by pressing the fire button on it, or externally from a pulse generator through a BNC connection.

When the TM-11A is triggered, it sends a 30 Kv, very low capacitance charge to the high voltage (HV) switch. The HV switch in itself consists of two terminals separated by a gap filed with inert gas. The gap is such that at the switch's rated voltage, the change will not jump from the high potential terminal to the low potential one. The rated voltage should not be exceeded to avoid pre-ignition. The charge from the TM-11A is used to create a spark inside the gap which ionizes the gas and makes it conductive. The charge is then conducted from the high potential terminal to the other. The spark plug then has 32 KV across its electrodes, which it discharges as a spark. Note

that the capacitor-switch combination is dipped in an insulating oil, Voltesso 35, to prevent HV dissipation in humid air.

The second type of ignition system has the same set-up as the first. However, it uses a pair of 100 μf, 4 Kv capacitors connected in parallel. Consequently an ***EG&G*** HV switch with an operating range 2-6 Kv has to be used. This system takes considerably longer to discharge. The slow discharge is needed for mixtures with high activation energies, such as 75% Argon diluted oxyacetylene mixtures. The discharge in the first type of ignition system resembles a sharp pulse, while that of the second type is like a square wave.

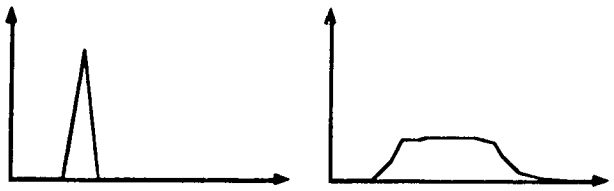

Pulse discharge Square wave discharge

Theoretically, both ignition systems supply the same amount of energy (1600J). However the energy is dumped so fast in the first type that it does not initiate detonations in mixtures with high activation energies. The use of the second type of ignition system is not recommended for two reasons when accurate synchronization is needed.

Firstly, because the discharge time is long, it is not known at which instant detonation initiation occurs. Initiation does not always occur at the same time interval after the fire button is pressed, and differences of about 15 μs are recorded between trials. Using the framing Schlieren camera, such a time difference can lead to several blank frames at the beginning or at the end of the film strip. Second, the long charging time is a disadvantage as it comes at the expense of keeping the mixture a longer time inside the channel before firing. This can lead to some dilution if the channel is not perfectly sealed.

I.4 Photodiode Box

A photodiode box consisting of two photodiodes placed at 13 cm from each other is used to probe the time of arrival of the detonation wave before the cylinder, and its average velocity between the two photodiodes. The circuit of the photodiode box is shown in figure 4. The capacitor and 1000 Ω resistance act as a low pass filter, eliminating the low frequency noise from the signal.

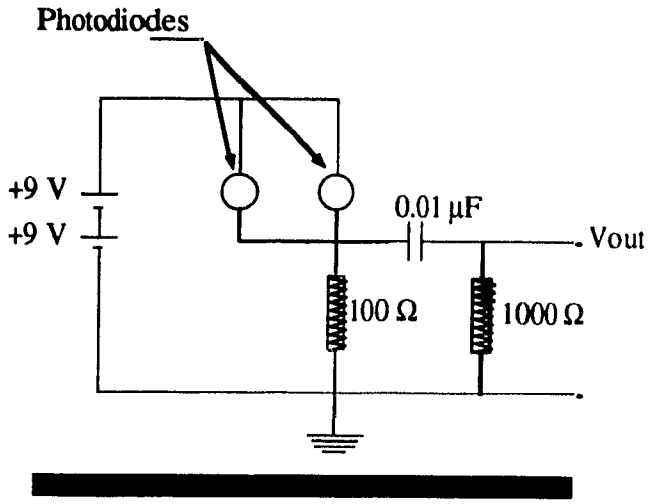

Figure I.4. Circuit of photodiode box

I.5 Bar and Stroud Schlieren Camera

The Bar and Stroud Camera is a double pass Schlieren system employing mirrors (double pass as opposed to single pass where the light rays pass through the test section only once). A system that uses mirrors is much cheaper than one which uses lenses, and less light is lost from the desired optical paths. Figure 5 shows the schematic diagram of the system used with the Bar and Stroud camera at McGill.

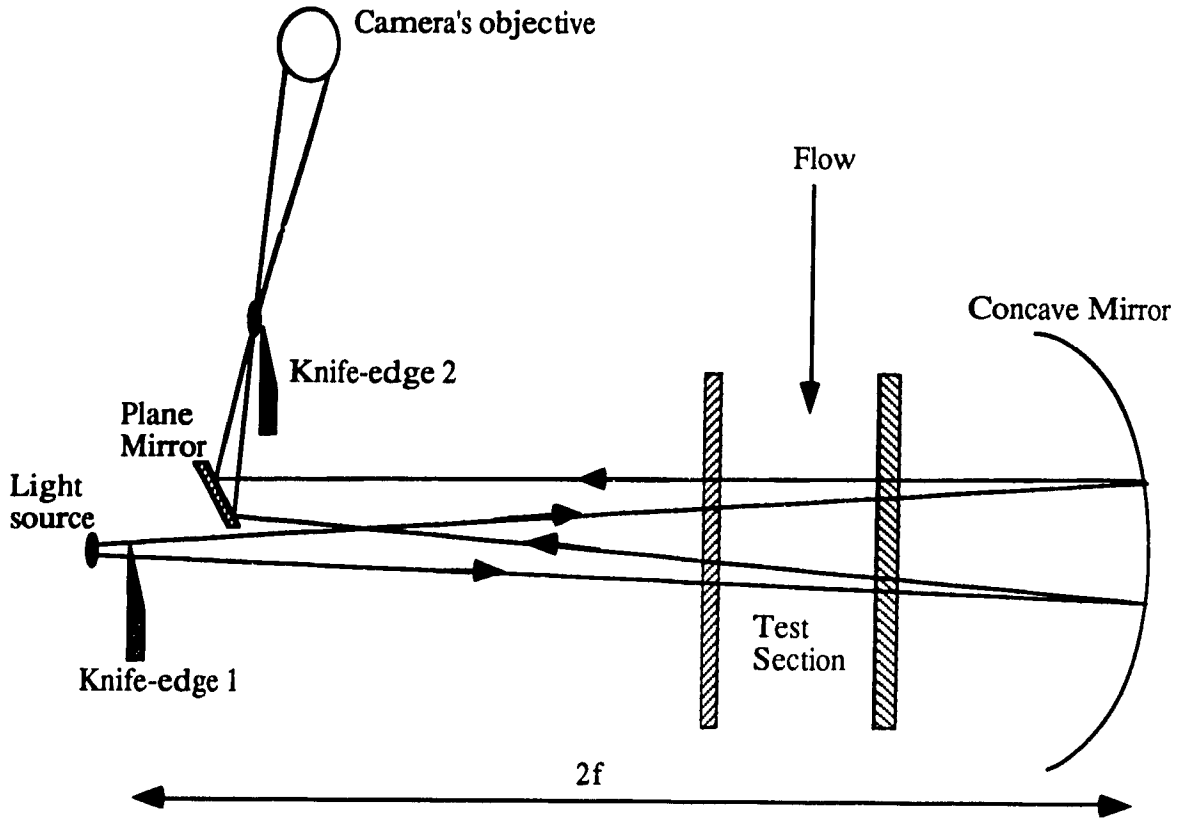

Figure I.5. Double pass Schlieren system employing mirrors.

Half of the light is intercepted by knife-edge 1, thereby defining the light beam more sharply. Knife-edge 1 is positioned such that light from the illuminated line source is focused in its plane, and the image of the source is parallel to the knife-edge. The first knife edge is placed in the center of the concave mirror, and acts as a sharp source of light to the system. The light rays pass through the test section before reflecting off the concave mirror. Upon reflection, the rays pass through the test section a second time, and will form an image at the center plane. On their way to the center plane, the light rays are intercepted by a planar mirror which reflects them towards the camera's objective. The image now forms in another plane called the cut-off plane. The knife-edge controlling the Schlieren effect is then placed at that cut-off plane where it intercepts part of the light deflected by the flowing gas. Therefore, when the beam finally reaches the screen, this part of

the test section appears darker. The brightness of the image on the screen thus depends on the orientation of the knife-edge as well as the magnitude and direction of the density gradient.

If the knife-edge is positioned to cut off half the light when there is no flow in the test section, the following will be observed when gas flows:

1.- If the density gradient decreases in the positive y-direction, the light rays will be bent towards the negative y-direction (i.e. towards the knife-edge), thus more light will be intercepted. The image on the viewing screen will then be darker than the rest of the image of the test Section.

2.- On the other hand, if the density gradient increases in the negative y-direction, more light will bypass the knife-edge thus giving a brighter image.

Micrometers are used to adjust the position of the knife-edge.

I.5.1 *Mechanical equipment*

The Bar and Stroud camera consists of a mirror connected to a blade of an air-driven turbine, with the mirror enclosed in a vacuum chamber. Just like a regular camera, this camera has an objective lens, a shutter, a shutter operator and uses 38 mm film.

However, the operation of individual elements, and how they are used differs drastically from a regular camera. The two main differentiating features of this camera are the following.

1.- The film strip remains fixed while the image of the event being filmed moves across it.

2.- The camera initiates the event to be filmed.

By inspection of the schematic of the inside of the camera as seen from the front with the door open, given in Fig. 6., one can deduce the following:

The image beam goes through the objective lens, passes through another lens and is reflected upon the rotating mirror. The image is then focused by another strip of lenses, and projected on the laid out film strip. The challenge when operating the camera, arises in synchronizing the time at which we wish to start filming the event, and the position of the image beam being on the first frame. Considering that the total duration of the event ranges between about 80-140 μs, and that the mirror rotates at frequencies up to a maximum of 5500 Hz, this task does not seem easy

However, as will be discussed next, the use of photodiodes, and electronic synchronization equipment simplifies the operation.

I.5.2 *Monitoring of Mirror position*

The mirror has to be regularly monitored to calculate its rev/sec, and to determine the position of the image w.r.t. the film strip. Two photodiodes are used for this purpose. An infrared emitter, as shown in Fig. 6 emits a beam of infrared light in a direction parallel to the image beam. The infrared beam is made to reflect off the rotating mirror, in the same manner the image beam is being reflected. The infrared red beam is however intercepted by the two photodiodes placed just outside the mirror chamber The second diode is placed such that it is struck when the infrared beam is in the same direction as the beam from the mirror to the first frame position. The first diode is placed such that it is struck when the beam is at -14° (i.e. CW) relative to the first frame position. Hence, by amplifying the photodiode outputs and connecting them to an oscilloscope, we are able to tell when the mirror is at 14° from the first frame, and when it is exactly at the first frame position.

Having two diodes, the mirror's frequency can be easily determined. Note from the Geometry of the set up, the image frequency is twice the mirror frequency, but has same sense.

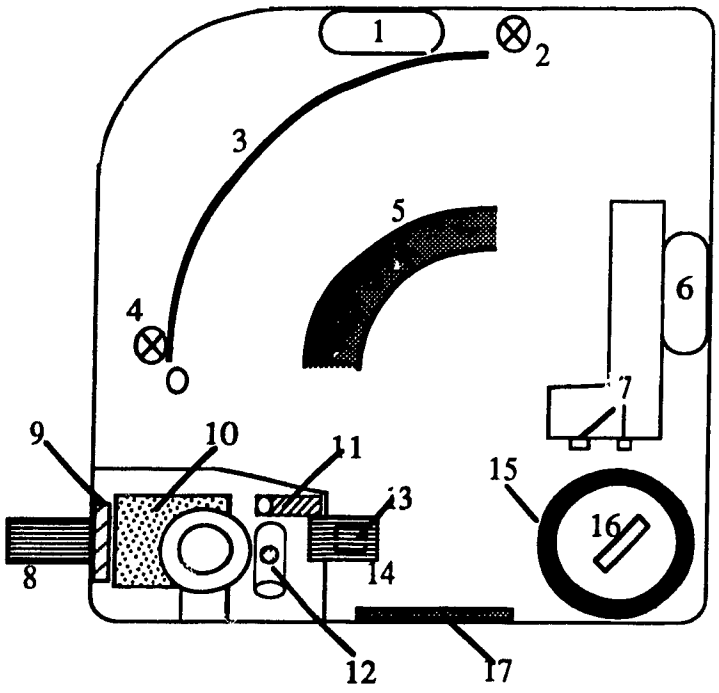

1- photodiode #2, preamplifier
2- unexposed film canister
3- film track
4- film take up canister
5- lens bank
6- photodiode #1 preamplifier
7- photodiodes
8- camera's objective lens
9- shutter
10- shutter solenoid
11- viewer mirror
12- viewer
13- infrared emitter
14- lens
15- mirror chamber
16- rotating mirror
17- connector strip

Figure I.6. Interior components of the camera.

Finally, the outputs from the two diodes are connected to a frequency counter through a synchronization unit, that synchronization unit calculates the frequency of the rotating mirror which then appears on the frequency counter.

I.5.3 *The flash*

The flash used in the set up is made up of a xenon flash tube charged by a Maser power supply. The power supply is usually set a 2.5 Kv. Before using it in an experiment, the flash intensity histogram has to be traced, so as to calculate how much time the flash needs to reach its peak intensity. A photodiode placed anywhere in front of the flash could be used for that purpose, and its response monitored on an oscilloscope. For a 2.5 Kv initial charge, the flash needed about 500μs to reach its peak, after which the light intensity decreases again.

I.5.4 *Timing*

Notation Used:

f_m = Mirror frequency (rev/sec)

w_m = Angular velocity of mirror = 360 * f_m

w_i = Angular velocity of image beam = 2 * wm =720 * f_m

T_m = Period of mirror rotation = $1/f_m$

$T_{14°}$ = Time for beam to sweep through 14°

T_{d1} = Time delay 1, as set on first delay generator

T_{d2} = Time delay 2= setting of second delay generator

T_f = Time for flash to reach a usable intensity

T_e = Time that the detonation wave takes to reach the section of interest (where it will be filmed), from the time it has been triggered.

The lens bank between the mirror and the film contains 30 lenses, placed side by side, which span a total angle of 58° with a 2° separation between them.

Fig. 7 shows a schematic of the experimental set up of the system. It could be seen that T_{d1} controls the flash while T_{d2} controls the ignition system. Frequency counter 1 continuously monitors the rotating speed of the mirror, while frequency counter 2 records the mirror's frequency when the camera first starts filming.

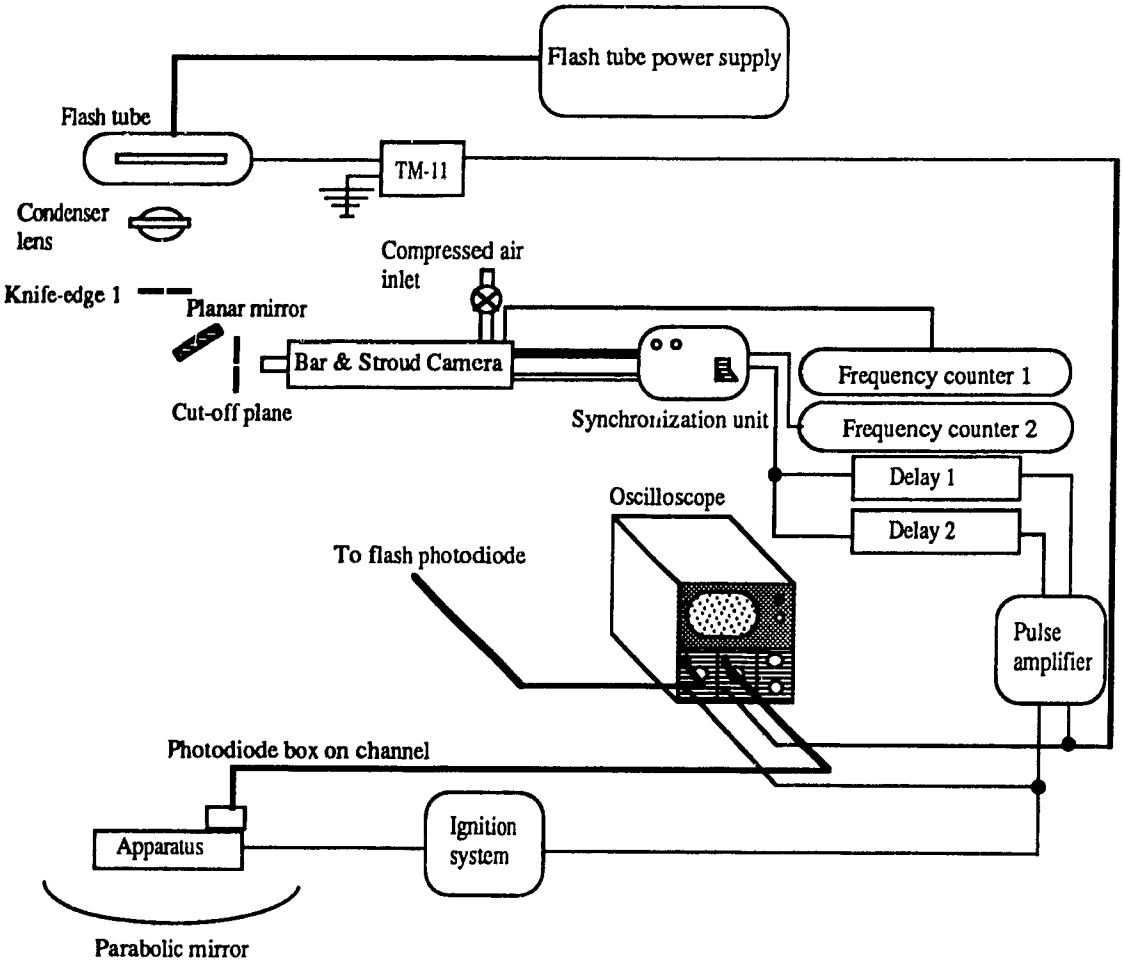

Figure I.7. Experimental set-up of system.

Setting the Time Delays.

The time delays are calculated according to the following scheme.

The framing rate (frame/sec) = (30 frames/a span of 58°) * w_i

$$= 30 * 360 * 2/58 * f_m$$

time elapsed between frames = 1/framing rate

= exposure time of one frame

T_{30} = Time to film 30 frames

= Total filming time = 30 * exposure time

= 30/framing rate

T_{14} = Time for beam to sweep through 14°

= $14/w_i$

After pressing the red fire button on the synchronization unit, and at the next instant the image beam is at the -14° position, both delays are triggered by the synchronization unit. The mirror will keep on rotating, and return to the 0° position after a Time = T14 + Tm (Fig. 8). Hence, when the mirror is back at the 0° position, the detonation wave should be at the beginning of the filming section, and the flash light should have reached its desired level of intensity.

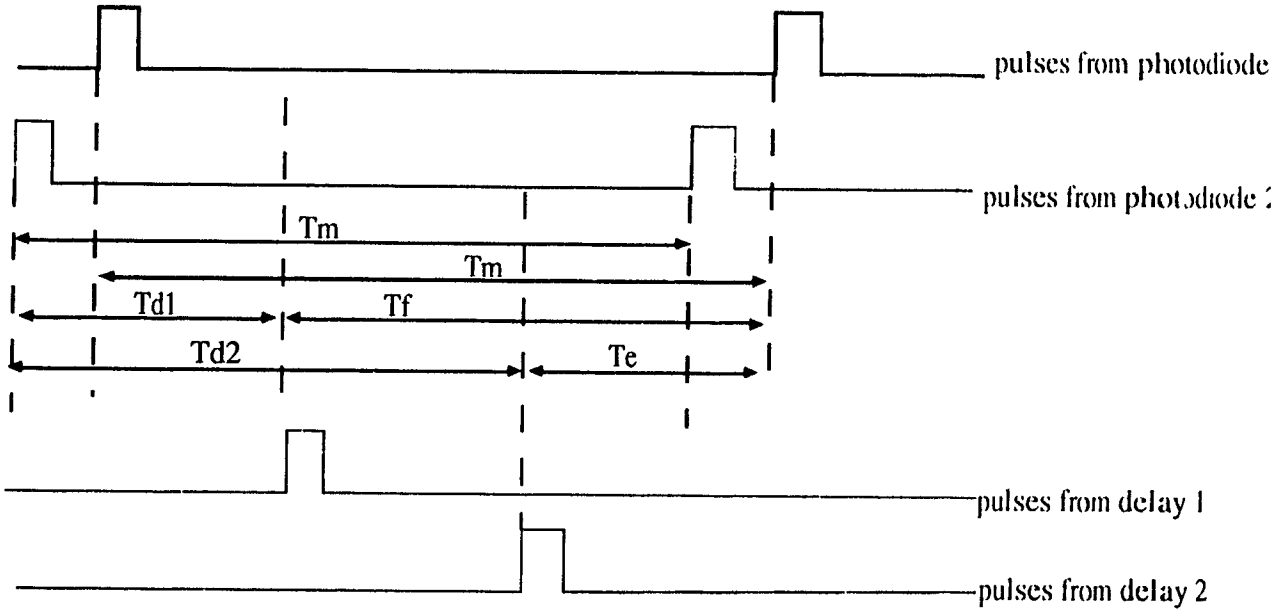

Figure I.8. Time delay distribution

Thus, $T_m + T_{14} = T_{d2} + T_e$

$T_m + T_{14} = T_{d1} + T_f$

knowing T_e, T_f, T_m and T_{14}, we can calculate T_{d1} and T_{d2}.

I.5.5 *Maintenance*

If used properly and carefully, the Bar and Stroud camera should not require a lot of maintenance. Proper operation consists, among others, of using clean and dry air to drive the turbine, because dust and moist will cause the bearings to seize up and break. The camera should only be run when the mirror chamber is evacuated (below 8-10 mmHg) otherwise air friction will reduce the life of the bearings and the oil would not be induced into the mirror bearing.

Furthermore, the level of the oil on the rear wall of the camera has to be regularly checked to avoid the mirror turning with no oil in the bearings. This problem is further accentuated in our case because of the oil leaks. They have been attributed to the old age of the camera, and the fact that the bearings started to wear out thus causing air leaks into the mirror chamber and oil leaks into the chamber and also to the surrounding of the camera.

Special shell Corena 100 oil has to be used, or a mixture of 7 parts shell Clavus 40 (SAE 30) and 1 part Bardahl motor oil (SAE 10).

The glass window of the mirror chamber and the chamber itself, have to be cleaned when needed, with special lens cleaner. However, the mirror surface should never be touched.

Finally, also because of its old age, it should be avoided to let the camera running for a long time (i.e. more than 1 minute).

It should also be mentioned that the camera shutter does not work, which required the installment of a manual air-shutter, controlled by the operator.

Also, the viewer section which is intended to facilitate the focusing of the image entering the camera, cuts off part of the image and makes the focus imperfect. This means that one must position the rotating mirror, by trial and error, such that an image is visible on the film, and use this image for focusing purposes. This procedure is time consuming and frustrating but thankfully does not have to be done often.

The problems mentioned above, if accounted for, do not affect much the functioning of the camera.

I.6 Experimental Procedure

The two mirrors are aligned w.r.t. the knife-edges, each other, and the objective of the Bar and Stroud before the start of the experiments and never moved afterwards. When the rectangular channel is mounted in front of the first mirror, it has to be perpendicular to the light beam coming from the light source towards the mirror. To ensure this, we hold a plane mirror flat on the back side (the one closest to the parabolic mirror) of the apparatus, and check where its reflection will appear. If the reflection appears to be superimposed on the source, i.e. the rectangular channel's walls are perpendicular to the incoming beam. Hence our test section is perpendicular to the light rays, and we can proceed with the experiment. If the reflection is far from the light source, the channel has to be rotated sideways and/or vertically such that the reflection falls on the light source.

As discussed above, focusing the camera is now a matter of trial and error, where the camera is operated and then turned off. If, when the mirror stops rotating, the image happens to fall on one of the frames, then we can proceed with the focusing. If such is not the case, we have to repeat the procedure until the mirror stops at a favorable position.

Once the optical alignment is completed, and after the choice of mixture and initial conditions is done, the time delays are calculated. The camera's vacuum pump is turned on, its oil level is checked, the delays are set, and the channel is evacuated. The film take-up counter on the camera does not work properly and thus is not used. Instead, the film is cut (in total darkness) into strips of about 90 cm and manually installed in its rail. The synchronization unit is then turned on, the frequency counters reset, and the flash power supply turned on and set to 2.5 KV, and its trigger module switched on.

The mixture is finally loaded, and the air inlet valve is opened gradually until the camera's mirror reaches its desired frequency. The voltage is then loaded, the ignition trigger module is switched on, the lights turned off, the shutter opened, and the fire button is pressed when the reading on

frequency counter 1 corresponds to the required frequency The shutter is then closed, the ignition trigger module and the voltage loader are switched off. The flash power supply is put in the OFF position, and its trigger module turned off. The capacitor is then discharged with the grounded bar so as to avoid any accidents with the residual voltage which is left across the capacitor's terminals. The reading on the frequency counter 2 is recorded, the camera turned off, and all vacuum pumps turned off. The film is then retrieved in complete darkness to be developed and, if necessary, printed.

Appendix II

Outline of Numerical Scheme

Two flowcharts are presented in this appendix. The first explains Dr. Schwendeman's code for the propagation of shock waves, while the second outlines the code developed in chapter 3. A good understanding of Dr. Schwendeman's scheme will help in the understanding of the present one, and in pointing out the differences between the two codes.

II.1 Flowchart of Schwendeman's code

The following flowchart has been drawn by the present author for the purpose of simplifying the understanding of Schwendeman's code for future users. It shows the order in which the main subroutines are called. Several other necessary subroutines are used but are not shown here for simplicity. Among these are subroutines used to calculate the boundary conditions, the cubic spline curve fit through the points, the plotting and printing subroutines, etc. ... The numbered paragraphs below correspond to the bolded letters shown on the flowchart, and provide some explanations on the purpose of the respective subroutine call.

1- SHKDFN is the name of the main program. Only a work dimension of 4000 is specified here, and SHKSUB is immediately called afterwards. SHKSUB calls SHKPRM to set the initial parameters.

2- In SHKPRM the following is specified. This is a 2-D problem (IAX=0), and the normal to the shock front is to be calculated using the cubic spline curve fitted through the discrete set of points on the shock front (INOR=0). The initial velocity is constant along the shock (IVC=1). The user has the choice of using the strong shock approximation, the weak shock one, or the true relation in solving the area-Mach number relation. In these calculations, the strong shock approximation is used, i.e. IVEL=0. The minimum and maximum velocities are set to 1.0001 and 20.0 respectively. The unacceptable error in velocity is set to 0.0001 and the maximum number of iterations in calculating the integral in the routine ROM (Romberg scheme) is set to 3 (IMAX=3).

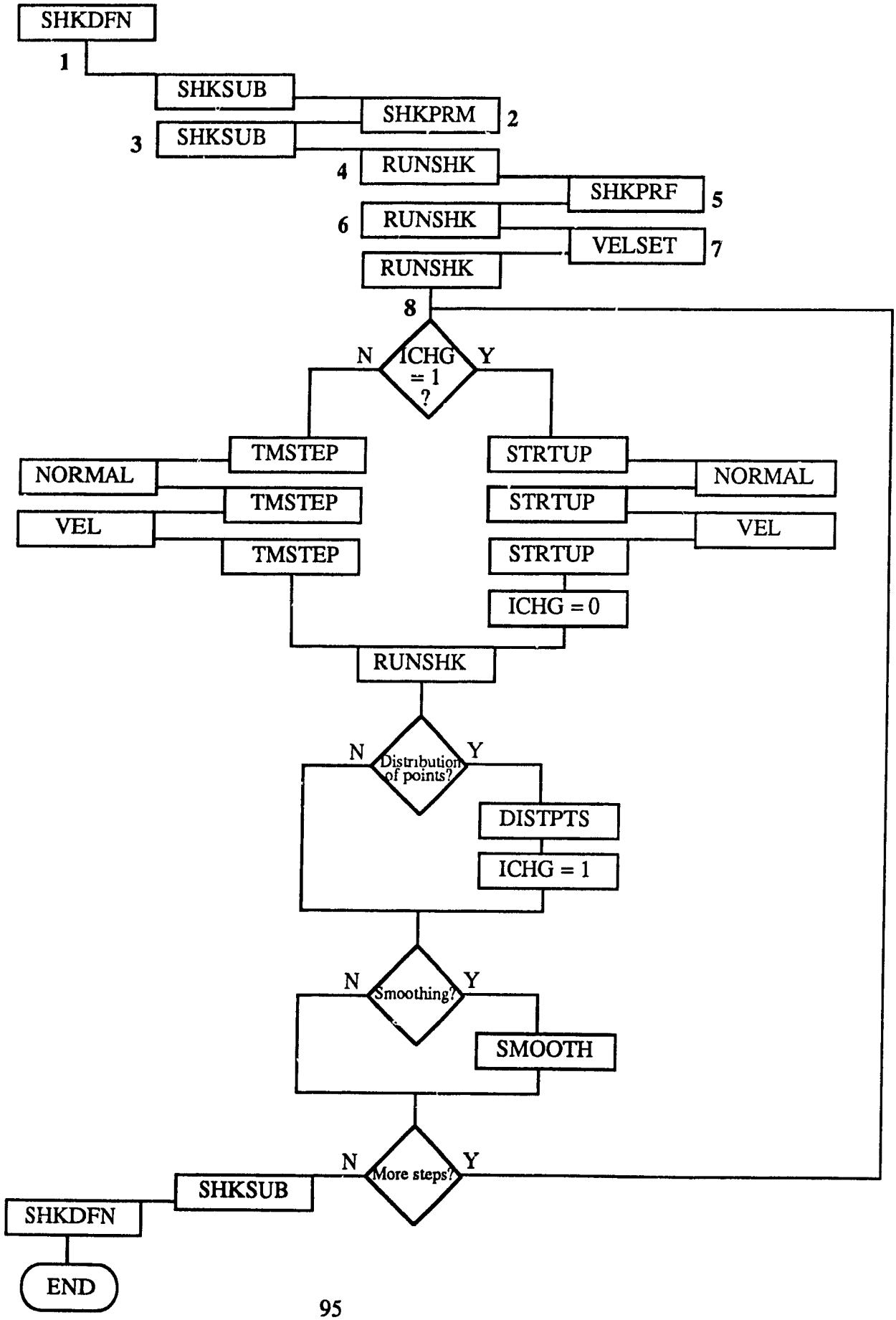
SHKDFN
1
SHKSUB
SHKPRM
2
3
SHKSUB
4
RUNSHK
SHKPRF
5
6
RUNSHK
VELSET
7
RUNSHK
8
N
ICHG = 1 ?
Y
TMSTEP
NORMAL
TMSTEP
VEL
TMSTEP
STRTUP
NORMAL
STRTUP
VEL
STRTUP
ICHG = 0
RUNSHK
N
Distribution of points?
Y
DISTPTS
ICHG = 1
N
Smoothing?
Y
SMOOTH
N
More steps?
Y
SHKSUB
SHKDFN
END

The maximum number of velocities VT and integral values AI for the table to be created in routine VELSET is set to 150 (MMAX=150). The minimum allowable distance between points is set to $0.5D_{avg}$ and the maximum one is set to $1.5D_{avg}$ (DSMIN=0.5, DSMAX=1.5). The minimum allowable angle between the rays $(X_{i+1} - X_i, Y_{i+1} - Y_i)$ and $(X_{i-1} - X_i, Y_{i+1} - Y_1)$ is set to 45° (used when deleting and inserting points) (ANGMIN = 45.0). Finally the maximum number of points allowed is 200 (NMAX=200).

After initialization the user is prompted to enter values for the number of time steps to be computed (IBCH), the number of steps after which smoothing is to be performed (ISMD), and the number of steps after every which redistribution of points is to be performed (IDST). The user also specifies every how many steps are the plot data (IPDT), the Mach number data (IMDAT), and the monitor data (IMON) to be printed on their respective units (units 2, 3, and 1).

3- Back to SHKSUB, the real work space is now split depending on whether or not the weak shock approximation is used, and whether the initial velocity is constant or not. A check is made to make sure that the dimension required is less than the dimension specified. If everything is fine, the program proceeds in calculating the successive shock positions, and RUNSHK is called.

4- In RUNSHK, a check is first made to determine whether this is a new problem or whether some restart data has to be retrieved from unit 4. In the case of a new problem, subroutine SHKPRF is called.

5- SHKPRF sets the initial shock profile and wall parameters. The time coordinate and the velocity of the medium in which the shock travels are set to zero (T,Vext). The user is prompted to enter the number of points along the shock, the initial Mach number, and time spacing (N, VI, TAU). The wall parameters are set such that there is a wall at S=0 and S=N (IW0=1, IW1=1), where S=distance along the shock. The initial profile of the shock is then set, i.e. S0(I) is calculated for I=1,..,N where S0 is the distance along the shock (arc length) at T=0 .

6- After exiting SHKPRF, subroutine VELSET is called for general initializing and to get VT and AI for later velocities. Here VT(j) is the Mach number value in the table of integrals, and AI(j) is the value of the integral of f(M) at the point VT(j).

7- The main purpose of VELSET is to create a table of integral values for the function f(M) in the area-Mach number relation. Once this table is created the Mach numbers may be found quickly given the area ratio using Newton's method and a nearby VT(j) as an initial guess. If a strong or weak shock approximation is used, then there is no need to create a table of integrals. VELSET uses the function ROM, which is a real function based on the Romberg integration scheme, where the value of ROM (V1,V0,ERR,ITER) is the approximate integration of G(M) between V1 and V). ERR is the absolute error tolerance, and ITER is the number of iterations required for convergence within ERR. G(x) is a real function which is the value of the integrand in the function f(M) in the area-Mach number relation. The Gamma value used by Schwendeman is 1.4. After creating the table of integrals, the program goes back to RUNSHK.

8- The counters are now reset to zero, and a flag parameter ICHG is set to 1. ICHG is used to determine which time step marching scheme is to be used. All printing of initial data is done now before the time stepping loop is started.

A time step of TAU is used to increase T, the number of steps are counted with ISTEP. If ICHG is equal to 1, then STRTUP is called, in which the shock front is advanced from T to T+TAU using an improved Euler step. ICHG is then set to zero, and TMSTEP is thus used in the next time loop. TMSTEP is a leap-frog marching scheme and needs two previous data points to move the shock for a time interval TAU, thus it cannot be used for start up conditions. TMSTEP and STRTUP use the real functions VEL and subroutine NORMAL to calculate the velocities of and the normals to the shock front at the discrete points assumed. The area ratio is then calculated in both TMSTEP and STRTUP, before being used in VEL to determine the corresponding Mach number. VEL uses the table created by VELSET to find the Mach number corresponding to the given R, the area ratio).

The point spacing is checked at the required intervals, and if some points are added or deleted (using DSTPTS) then ICHG is set to 1 again. That is done because after the redistribution of points along the shock front, the previous shock position cannot be used in conjunction with the present one, since they both no longer have the same number of discrete points describing them.

The shock has to be advanced based on one shock position, hence STRTUP has to be used. Smoothing of the shock front is performed in subroutine SMOOTH if requested. The time loop goes on until the number of steps required is reached. The data to be stored in the different units is written at every run, and if there is no terminal error in Romberg convergence and ISTEP ≠ total steps requested, then the loop goes on.

II.2 Code for detonations:

Most subroutines are basically the same as the ones developed by Schwendeman for his code. Some modifications have been made to TMSTEP and STRTUP so that they can be used to propagate both the CJ and shock plane at different times. One of the parameters sent to the subroutine indicates whether STRTUP (or TMSTEP) is to use the CJ plane data or that of the Shock plane, hence advancing one or the other. Also the subroutine which calculates the velocity of the wave front has been changed. VELSET is not required anymore, since no table of integrals for Chester's equation needs to be made. Instead, other subroutines have been written to perform that function. The printing subroutines have also to be modified for the two front data.

The flowchart below describes the numerical scheme developed to apply the algorithm explained in chapter III. Several other necessary subroutines are used but not shown below for simplicity. Among these are the subroutines used to calculate the boundary conditions, the cubic spline curve fit through the points, the printing subroutines, etc... .

Again, the numbered paragraphs below correspond to the bold numbers on the flowchart, and provide some explanations:

1- The first few subroutine calls, DETDFN through RUNDET, are similar to the ones in Schwendeman's code. They have been modified to initialize the shock front of the two front model, and define the parameters relevant to the two front model. Many new parameters are introduced defining the induction time, induction length, CJ plane area, etc.. .

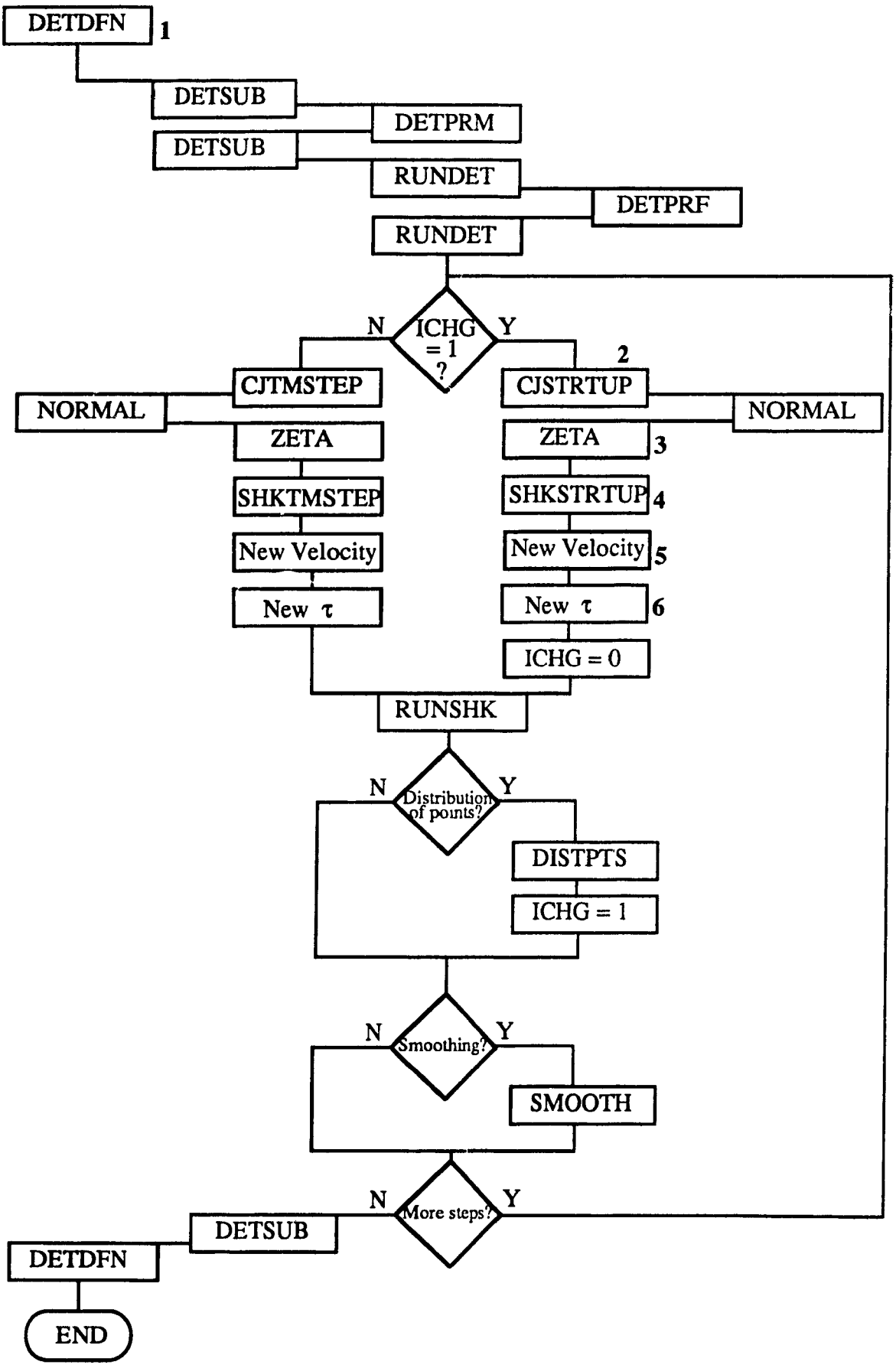
DETDFN
1
DETSUB
DETPRM
DETSUB
RUNDET
DETPRF
RUNDET
N
ICHG = 1 ?
Y
2
CJTMSTEP
CJSTRTUP
NORMAL
NORMAL
ZETA
ZETA
3
SHKTMSTEP
SHKSTRTUP
4
New Velocity
New Velocity
5
New τ
New τ
6
ICHG = 0
RUNSHK
N
Distribution of points?
Y
DISTPTS
ICHG = 1
N
Smoothing?
Y
SMOOTH
N
More steps?
Y
DETSUB
DETDFN
END

2, 4- CJSTRTUP and SHKSTRTUP are both the same subroutine STRTUP used differently twice. The first time, it is used to advance the CJ plane and calculate its new area. The second time it is used to advance the shock plane and calculate its new area. Basically, STRTUP will advance any front by one time step using an improved Euler scheme. The coordinates of the front has to be sent, along with the time step required.

3- ZETA calculates the divergence factor defined as the area of the CJ plane over the area of its shock plane.

5,6 - The new velocities and induction times along the wave front are found based on the value of zeta calculated in subroutine ZETA. These values will be used the next time the fronts are advanced. Notice that for the next time step, subroutine TMSTEP will be used to advance the front if no point redistribution has occurred. The algorithm is the same as that described in chapter III, and is repeated at every time step.